UNIVERSITY OF COPENHAGEN
FACULTY OF SCIENCE

Properties of Proximitized 2DEGs

Master's Thesis in Condensed Matter Theory

Bjarke Rasmus Nicolaisen

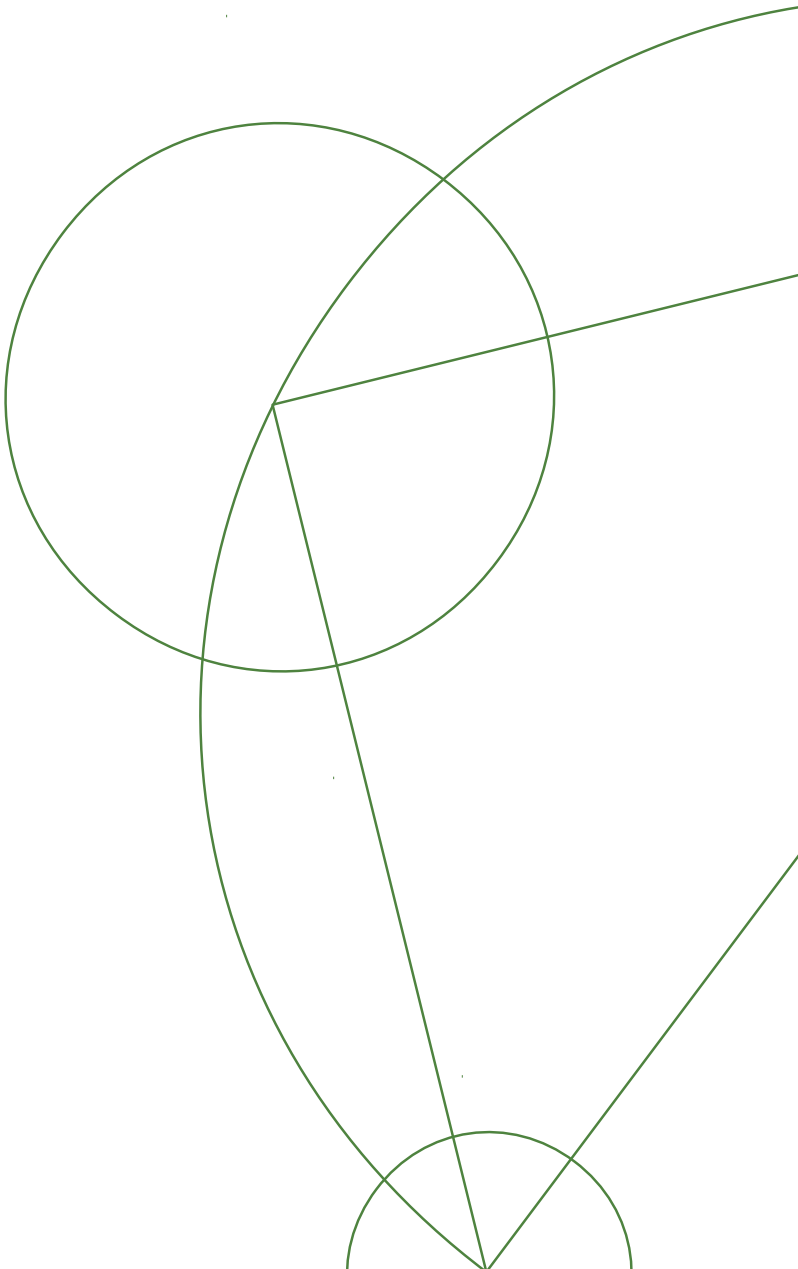

Niels Bohr Institute
Supervisor: Prof. Karsten Flensberg
Submitted: January 15, 2017

UNIVERSITY OF
COPENHAGEN

Faculty:	Science
Institute:	Niels Bohr Institute
Author:	Bjarke Rasmus Nicolaisen
Email:	*jqm470@alumni.ku.dk*

Title and Subtitle:	Properties of Proximitized 2DEGs - Master's Thesis in Condensed Matter Theory
Supervisor:	Prof. Karsten Flensberg
Handed in:	January 15, 2017
Defended:	February 6, 2017

Name _____

Signature _____

Date _____

Abstract

In this thesis we theoretically analyze the proximity effect of a superconductor on a two-dimensional electron gas (2DEG) with Rashba spin-orbit interaction (SOI) in the presence of a magnetic field and its corresponding fingerprints in tunneling spectroscopy through a contriction in the 2DEG. We first analyze the junction without SOI via two different models, one in a wave-function approach and one in a Green's function approach in the tunneling regime. We establish that when the wavenumber in the 2DEG can be approximated by the ground-state wavenumber in the infinite square well there is a correspondence between the two models, and study the induced gap and effective g-factor in this approximation. The induced gap rises as a function of coupling between the 2DEG and superconductor, while the effective g-factor moves from the g-factor in the 2DEG towards that of the superconductor with increased coupling.
We then analyze tunneling spectroscopy through a constriction in a proximitized 2DEG driven into the tunneling regime via a quantum point contact (QPC). We derive analytically and study numerically some properties of the density of states (DOS) in the 2DEG with proximity-induced superconductivity without SOI. Here we find two peaks, one at the induced gap and one at the superconductor-gap, and also find that a finite chemical potential introduces an asymmetry in the DOS, which is important for the conductance. Finally we study the system numerically including Rashba SOI, comparing our results to experimental data. We present results that resemble experiment in that we get an induced gap of the right size and get a qualitative match with the other conductance feature in experiment. These results have the drawback that the effective g-factor needed to get a correspondence between experiment and theory is too large compared to measurements on similar designs. The understanding of the proximitized 2DEG structure with Rashba SOI and Zeeman field is important for research in topological superconductivity.

Acknowledgments

Producing this thesis was no easy feat for me, and I am very grateful for the big help I got from all of the wonderful faculty in the CMT group at the Niels Bohr Institute. First and foremost a big thanks to my supervisor prof. Karsten Flensberg, not only for providing me with such an interesting topic to write about, but also to find the time week in and week out to discuss my progress (or lack thereof), which with such a busy schedule is quite amazing. I was not always steering my boat towards land, but due to your guidance I found my way to shore and I will always be grateful for that.
Also a big thanks goes out to Michael Hell, who almost became my collaborator in the last months of my thesis work, which was not only a great help but also a very enjoyable experience. Thank you also for revising parts of this thesis with me.
Then there are all the students in the CMT group who made the long days at the institute fun and inspired me to work even harder. I am grateful to all of you - you know who you are.
A special thanks to Asbjørn Rasmussen for his collaboration along the way not only during my thesis work, but through all my university years. It has been a pleasure.
Also I would like to acknowledge the 2DEG-team at the Center for Quantum Devices for supplying the experimental data, and for having me at the group meetings so that I could get an idea of what is actually going on in the devices I am modelling. Also a thanks to Stephan Plugge for giving me the idea to attend these group meetings, which was a big help for me. A special thanks also goes out to Asbjørn Drachmann for his help with explaining the experimental side of things to me.

Contents

List of Figures

Chapter 1

Introduction

Realizing a useful quantum computer seems to move closer to reality in recent years. The basic idea of a quantum computer is one where instead of an ordinary bit, which can take two values, 0 or 1, a quantum bit, *qubit*, is in a superposition of two quantum states, $|\psi\rangle = a|0\rangle + b|1\rangle$. Such a qubit-based computer has been shown to hold certain advantages over classical computers [1], and at the present point in research there is a lot of focus on trying to realize a quantum computer.
One problem with constructing a qubit is quantum decoherence, which works to alter the qubit state on time-scales faster than what is needed to perform computations with the qubit. As explained in ref. [2] it has been shown that quasiparticle states in systems involving superconductivity called Majorana bound states possess the required properties to be robust against such quantum decoherence.
Over the last years there have been several promising experimental observations that suggest that Majorana bound states have been observed in nanowire-designs [3, 4]. A good indication of the community buzz is that articles on the topic of quantum computers has begun to hit mainstream media [5]. With the belief growing in the community that Majoranas have now been realized, attention begins to shift from realizing isolated systems containing only a few Majorana bound states to designing scalable networks of Majoranas useful for actual quantum computation.
Some proposed designs for scalable designs that could feature in such networks can be found in e.g. ref. [6]. It should be clear that these designs involve large numbers of topological nanowires placed in a well-defined geometry. This however turns out to be a big experimental obstacle since producing hundreds or more nanowires with the desired characteristics is challenging enough in itself; now linking them and placing them accurately on such small length scales as is relevant here is a demoralizing thought. Therefore there is now some investigation into using 2-dimensional electron gases (2DEGs) as a platform for quantum computation [7, 8]. As this is a relatively recent effort there are still unanswered questions about these designs, not all involving Majoranas. This thesis' aim is to provide better understanding of a superconductor-2DEG junction with infinite planar extension, which means we do not expect Majorana bound states to appear; rather the theoretical investigation serves to build a material understanding which is important in order to design 2DEG-based junctions that contain Majoranas.

In this thesis we first outline in chpt. 2 the basic theory that underlines the motivation to study the system in question and explain the methods we are going to employ throughout the thesis. We then go on to model a 2DEG proximitized by a semi-infinite superconductor by two different models: A wave-function approach including an effective quasiparticle mass, effective g-factor and BCS superconductivity in chpt. 3; and by a Green's function approach in the tunneling approximation in chpt. 4. We then derive a correspondence between the two models in chpt. 5. Then we study tunneling spectroscopy of proximitized 2DEGs in chpt. 6, both finding the local density of states (DOS) and eventually obtaining numerical conductance results including Rashba spin-orbit interaction.

Chapter 2

Fundamental Concepts and Theory

Here we review some fundamental theory that may be useful for readers who are unacquainted with some of the subjects. Readers with experience in solid state physics may want to skip parts of this chapter.

2.1 Semiconductor properties

2.1.1 Effective Mass in Semiconductors

Many of the semiconductor properties can be explained by electrons moving in an energy band. Since the group velocity is by definition $\frac{d\omega}{dk}$, and the energy ϵ is $\omega = \epsilon$, we see that

$$\mathbf{v}(\mathbf{k}) = \boldsymbol{\nabla}_k \epsilon(\mathbf{k}). \tag{2.1}$$

The effects of the crystal on the electron motion are contained in the dispersion relation $\epsilon(\mathbf{k})$. This is important with regards to the effective mass-approximation. From looking at the usual free electron dispersion relation:

$$\epsilon(\mathbf{k}) \sim \frac{k^2}{2m}, \tag{2.2}$$

we see that the curvature is determined by m^{-1}, which for a free electron would be constant. However we know that in a crystalline potential the energy bands can have many different shapes as a function of k. This of course means that the usual free electron energy dispersion as a function of k is not applicable anymore. However, we can usually model the energy dispersion as having the same form, but now with an effective mass, m^*:

$$\epsilon(\mathbf{k}) \sim \frac{k^2}{2m^*}. \tag{2.3}$$

This effect is most pronounced in semiconductors. As an example of this we have included a simple derivation in Appendix A, concluding that close to the Brillouin zone boundary we can indeed model the dispersion with an effective mass that depends directly on the size of the band-gap, U, and the bandwidth, λ; in this rather simple calculation we get:

$$\frac{m^*}{m} = \frac{1}{2\lambda/U \pm 1}, \tag{2.4}$$

where the $\pm$ refers to holes and electrons respectively. Since semiconductors have almost filled valence bonds or only slightly filled conduction bands the excitations in semiconductors will lie close to energy gaps in semiconductors, which makes the above formula applicable, whereas the excitations in metals happen around half-filling of the conductions bands where the dispersion is simply like free electrons.

Note that all of this analysis in Appendix 8.1 was done in k-space, assuming translational invariance.

Thus the effective mass approximation is a bulk property and the approximation will not necessarily hold close to the edge of a sample. Nevertheless, our model in this thesis will assume an effective mass uniform everywhere in the semiconductor, which changes discontinuously at the boundary to the superconducting metal where the mass is again the free electron mass.

2.1.2 Zeeman Field in Semiconductors

It is an important and well-known result of quantum field theory that in the non-relativistic limit the Dirac equation reduces to the Schrödinger equation, with a term $-\mu\cdot\mathbf{B}$ added to the Hamiltonian. (see ref. [9] chpt. 8 for a thorough derivation.) We will call this term the *Zeeman* term. Particles placed in an electromagnetic field can in this limit be independently described by the eigenvalue equation:

$$\left[\frac{\tilde{\mathbf{p}}^2}{2m} - \mu\cdot\mathbf{B}\right]u = Eu, \tag{2.5}$$

where $\tilde{\mathbf{p}} \equiv \mathbf{p} - e\mathbf{A}$, $\mu = g\frac{e}{2m}\mathbf{S}$, $\mathbf{S} = \frac{\sigma}{2}$ (we set $\hbar \equiv 1$), and where this theory predicts $g = 2$.

When you treat particles in solids, this effect can be changed due to the electromagnetic fields from ions and other electrons. Here we will not even present a toy-model calculation of this effect, but rather refer to ref. [10] chpt. 6, in which the magnitude of the spin-orbit interaction (SOI) and its effect on the Zeeman energy is calculated. It turns out that in analogy with the effective mass we can also model the response of the electrons in a semiconductor with SOI to an external magnetic field by replacing the g-factor for a free electron by an effective g-factor, g^*.

It is important here to note that the renormalization of the g-factor and Rashba SOI (which we will discuss in the next section) are in general independent effects that can coexist as well as exist exclusively on their own. This justifies that we in this thesis focus a lot on the parameter regime where we have an effective g-factor in the 2DEG with zero Rashba SOI.

2.1.3 Spin-Orbit Interaction

For many effects observed in solids, relativistic effects are not important. However, under certain circumstances they can become relevant and as we will touch upon later, it seems they are very influential in the systems under consideration in this thesis. Therefore we will present a derivation for a free charged particle in an electromagnetic field and see how relativistic effects couple the orbital motion and the spin. The full derivation of how to go from free particle SOI effects to SOI effects in solids is rather involved, and I refer the reader to ref. [10] for a well-renowned treatment of SOI in solids. Rather we will present a toy model-calculation to get some intuition about the effects.

The SOI is a relativistic effect. An electron moving with velocity $\mathbf{v}$ in an electric field $\mathbf{E}$ will in its own rest frame experience a magnetic field given by:

$$\mathbf{B} = -\gamma(\mathbf{v}\times\mathbf{E})/c^2, \tag{2.6}$$

where γ is the Lorentz factor known from special relativity. Now assume that we have a central electric field given by $\mathbf{E} = |E|\hat{\mathbf{r}}$, which corresponds to the situation for an electron in a simple atom. Also assuming weak relativity, i.e. $\gamma \approx 1$ we get a magnetic field given by:

$$\mathbf{B} = \frac{\mathbf{r}\times\mathbf{p}}{m_e c^2}\left|\frac{E}{r}\right|. \tag{2.7}$$

Now we write the electric field as the gradient of the potential, $\mathbf{E} = -\boldsymbol{\nabla}\tilde{V}$. Assuming the central approximation, i.e. that the potential is centrally symmetric, we can write this gradient as:

$$|E| = \frac{\partial \tilde{V}}{\partial r} = \frac{1}{e}\frac{\partial V}{\partial r}, \tag{2.8}$$

where V is the potential energy of the electron and e is the elementary charge. Now inserting the definition of the angular momentum $\mathbf{L} = \mathbf{r} \times \mathbf{p}$ we get:

$$\mathbf{B} = \frac{1}{m_e e c^2}\frac{1}{r}\frac{\partial V(r)}{\partial r}\mathbf{L}. \tag{2.9}$$

Through the Zeeman-coupling, this magnetic field will couple to the electron's spin and give an energy contribution corresponding to the following term in the Hamiltonian:

$$H_{SOI} = -\mu \cdot \mathbf{B} = g\frac{e}{2m_e}\mathbf{S} \cdot \mathbf{B} = \frac{g}{4(m_e c)^2}\frac{1}{r}\frac{\partial V(r)}{\partial r}\sigma \cdot \mathbf{L}, \tag{2.10}$$

where again $\hbar \equiv 1$. Now this derivation is actually fundamentally flawed in that the accelerated rest frame of the electron is actually not inertial; the correction is calculated in e.g. [11] pp. 548-552, and is called the *Thomas correction*. The result is:

$$H_{SOI} = \frac{(g-1)}{4(m_e c)^2}\frac{1}{r}\frac{\partial V(r)}{\partial r}\sigma \cdot \mathbf{L}. \tag{2.11}$$

2.1.4 Qualitative Rashba spin-orbit coupling derivation

For electrons moving in a crystalline potential the angular momentum is altered. Depending on the solid the resulting SOI effect changes a lot, both in magnitude and in functional form. We will focus on Rashba SOI, since this is the effect that is relevant for this thesis. As explained in ref. [10] chpt. 6 the Rashba SOI stems from an inversion symmetry breaking in the direction orthogonal to the 2-dimensional plane. This is for example present at the edges of a material, be that either a 2DEG which will then be characterized by this inversion symmetry breaking throughout the plane, or can be seen only as a surface effect as was done in for example ref. [12] when looking at the gold surface. As suggested by ref. [12] one first try to derive the SOI effect at such a surface would be to assume free electrons moving in the planar surface. The only potential affecting the free electrons at the surface would be the confining potential keeping the electrons confined in the solid; thus:

$$-\boldsymbol{\nabla} V = -\frac{dV_z}{dz}\mathbf{e}_z, \tag{2.12}$$

when z denotes the out-of-plane direction. The corresponding SOI term in the Hamiltonian becomes:

$$H_{Rashba} = \alpha_R \sigma \cdot (\mathbf{e}_z \times \mathbf{v}) = \alpha_R(\sigma \times \mathbf{v}) \cdot \mathbf{e}_z, \tag{2.13}$$

where α_R is the Rashba SOI strength, which is proportional to the gradient of the potential. This term is the famous Rashba SOI term, which we will focus on in this thesis.

The above procedure produces the correct type of term in the Hamiltonian, but with a much-too-weak coupling strength α_R compared with experimental results. To get the real magnitude of the Rashba SOI people have invoked $\mathbf{k} \cdot \mathbf{p}$-theory as in ref. [10] or tight-binding calculations as in ref. [12], but the calculations are somewhat lengthy and will not be reproduced here. Instead we will in this thesis try to assume some values of the Rashba SOI strength based on typical experimental results and see what effect different SOI strengths have on the results of our model.

2.2 Superconductor Properties

2.2.1 BCS Superconductivity

The Bardeen-Cooper-Schrieffer (BCS) theory of superconductivity from 1957 was the first succesful theory that from a microscopic viewpoint explained the phenoma in some solid state systems today known broadly as *conventional superconductivity*. Cooper in 1956 showed the important instability of the Fermi sea in the presence of an attractive interaction due to the formation of so-called *Cooper pairs*. Bascially an electron combining with its time-reversed state of zero net momentum and spin can lower the energy of the total state compared to the two electrons just occupying states at the Fermi energy (see e.g. ref. [13] exercise 17.1 for a guided derivation).

The energy gain of the system by forming such a Cooper-pair is called the superconducting order parameter Δ. The result of this binding-energy of the Cooper pair, Δ, is that a gap in the superconducting single-particle energy spectrum appears around the fermi level, of order Δ. Therefore we also refer to Δ as the *superconducting gap*.

The BCS Hamiltonian is:

$$H_{BCS} = \sum_{\mathbf{k}\sigma} \xi_{\mathbf{k}} c^\dagger_{\mathbf{k}\sigma} c_{\mathbf{k}\sigma} + \sum_{\mathbf{k}\mathbf{k}'} V_{\mathbf{k}\mathbf{k}'} c^\dagger_{\mathbf{k}\uparrow} c^\dagger_{-\mathbf{k}\downarrow} c_{\mathbf{k}'\downarrow} c_{-\mathbf{k}'\uparrow} \tag{2.14}$$

Now in BCS theory we assume that mean-field theory is applicable around the expectation value $\left\langle c^\dagger_{\mathbf{k}\uparrow} c^\dagger_{-\mathbf{k}\downarrow} \right\rangle \neq 0$. Performing a Hartree-Fock mean field procedure of (2.14) yields:

$$H^{MF}_{BCS} = \sum_{\mathbf{k}\sigma} \xi_{\mathbf{k}} c^\dagger_{\mathbf{k}\sigma} c_{\mathbf{k}\sigma} + \left[\sum_{\mathbf{k}} \Delta_{\mathbf{k}} c^\dagger_{\mathbf{k}\uparrow} c^\dagger_{-\mathbf{k}\downarrow} + h.c. \right] + \text{const.}, \tag{2.15}$$

where:

$$\Delta_{\mathbf{k}} \equiv \sum_{\mathbf{k}'} V_{\mathbf{k}\mathbf{k}'} \left\langle c_{-\mathbf{k}'\downarrow} c_{\mathbf{k}'\uparrow} \right\rangle. \tag{2.16}$$

Now the functional form of $\Delta_{\mathbf{k}}$ in BCS theory can be found by assuming an effective phonon-mediated interaction given by:

$$V_{\mathbf{k}\mathbf{k}'} = \begin{cases} -V \text{ for } |\xi_{\mathbf{k}}| < \omega_D \\ 0 \quad \text{otherwise} \end{cases}, \tag{2.17}$$

where ω_D is the Debye frequency (see ref. [13] chpt. 17+18 for more details). By self-consistent analysis the above leads to a superconducting pairing that is constant as a function of $\mathbf{k}$:

$$\Delta^{BCS}_{\mathbf{k}} = \Delta_0. \tag{2.18}$$

Fourier-transforming this to real space yields a point-like interaction:

$$\Delta(\mathbf{r}, \mathbf{r}') = \Delta_0 \delta(\mathbf{r} - \mathbf{r}'). \tag{2.19}$$

Because it is uniform as a function of $\mathbf{k}$ we call this an *s-wave pairing*, referring to the spatially uniform *s-orbital* of electrons in atoms. We will in our analysis only consider the BCS, mean-field type pairing.

2.2.2 BCS quasiparticle density of states

It will be worthwile to show the derivation of the BCS quasiparticle density of states, since the steps in doing this are similar when you include the Zeeman field and Rashba SOI. Here we will follow closely ref. [13] pp. 334-335.

We can interpret the following as the density of states:

$$d_s(\omega) \equiv \frac{1}{2\pi V}\sum_{\mathbf{k}\sigma} A(\mathbf{k}\sigma,\omega) = \frac{-1}{\pi V}\sum_{\mathbf{k}\sigma} \mathrm{Im}G^R_{\sigma\sigma}(\mathbf{k},\omega) = \frac{-1}{\pi V}\sum_{\mathbf{k}\sigma} \mathrm{Im}\mathcal{G}_{\sigma\sigma}(\mathbf{k},\omega+i\eta), \tag{2.20}$$

where we have introduced the retarded Green's function G^R, the spectral function $A = -2\mathrm{Im}G^R$ and the Matsubara Green's function $\mathcal{G}$. The Matsubara Green's function for the BCS superconductor follows from ref. [13] sec. 18.4. If we plug this in and define $E_k^2 \equiv \xi_k^2 + \Delta^2$ we get:

$$d_s(\omega) = -\frac{1}{\pi V}\sum_{\mathbf{k}\sigma} \mathrm{Im}\frac{\omega+i\eta+\xi_{\mathbf{k}}}{(\omega+i\eta)^2 - E_{\mathbf{k}}^2} = -\frac{1}{\pi V}\sum_{\mathbf{k}\sigma} \mathrm{Im}\left\{\frac{1}{\omega - E_{\mathbf{k}} + i\eta} - \frac{1}{\omega + E_{\mathbf{k}} + i\eta}\right\}\frac{\omega+\xi_{\mathbf{k}}}{2E_{\mathbf{k}}} \tag{2.21}$$

$$= \frac{1}{V}\sum_{\mathbf{k}\sigma}\{\delta(\omega - E_{\mathbf{k}}) - \delta(\omega + E_{\mathbf{k}})\}\frac{\omega+\xi_{\mathbf{k}}}{2E_{\mathbf{k}}}, \tag{2.22}$$

where we used that $\frac{1}{x+i\eta} = \mathcal{P}\frac{1}{x} - i\pi\delta(x)$, where $\mathcal{P}f(x)$ means the Cauchy principle part of an arbitrary function $f(x)$ and $\eta = 0^+$. Now we want to change variables from a discrete sum over k to a continuous energy integral via the variable $\xi_{\mathbf{k}} \equiv \frac{k^2}{2m} - \mu$; we do this by introducing the non-superconducting, spin-traced density of states $\nu(\xi)$:

$$\frac{1}{V}\sum_{\mathbf{k}\sigma} f(\mathbf{k}) \equiv \int_{-\mu}^{\infty} \nu(\xi) f(\xi) d\xi. \tag{2.23}$$

Let us now assume that $\nu(\xi)$ varies little on the relevant energy scale. If we also assume that $\mu >> \Delta$ we can extend the integration to all of energy space, which results in:

$$d_s(\omega) \approx \nu(0)\int_{-\infty}^{\infty} d\xi \frac{1}{2}\left\{\left(1+\frac{\xi}{E}\right)\delta(\omega - E) + \left(1-\frac{\xi}{E}\right)\delta(\omega+E)\right\} \tag{2.24}$$

Now under this approximation the odd terms in ξ drop out, and if we only consider for the moment $\omega > 0$ we get:

$$\frac{d_s(\omega)}{\nu(0)} = \int_{-\infty}^{\infty} d\xi \frac{1}{2}\delta(\omega - E) = \int_0^{\infty} d\xi \delta(\omega - E) = \int_{|\Delta|}^{\infty} dE \frac{\partial\xi}{\partial E}\delta(\omega - E) = \int_{|\Delta|}^{\infty} dE \frac{E}{\sqrt{E^2 - |\Delta|^2}}\delta(\omega - E). \tag{2.25}$$

From this we can see that the BCS quasiparticle density of states weighted by the non-superconducting one is:

$$\frac{d_s(\omega)}{\nu(0)} = \frac{\omega}{\sqrt{\omega^2 - |\Delta|^2}}\theta(\omega - |\Delta|). \tag{2.26}$$

It is easy to extend the result to negative energies: $d_s(-\omega) = d_s(\omega)$. We have plotted $d_s(\omega)$ in figure 2.2.1 - here we see clearly the well-known gap of size $2|\Delta|$ in the DOS of the BCS superconductor.

2.2.3 Proximity Effect

If you place a normal conductor next to a superconductor a superconducting gap will appear in the normal conductor. Thus effectively the superconductor 'infects' the normal conductor with superconductivity. This is known as the *Proximity effect*. We will not derive this effect here since we will study this effect in detail later in the concrete example of a 2DEG-superconductor junction.

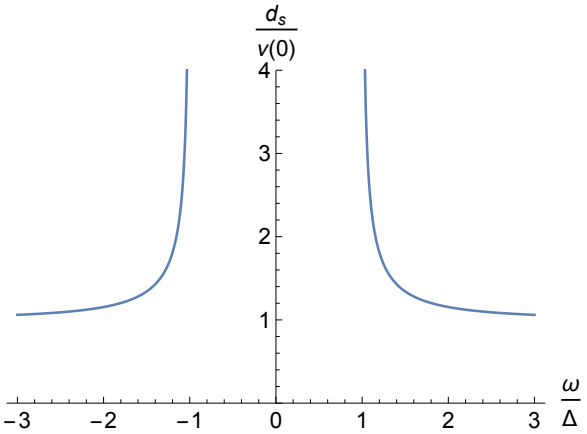

Figure 2.2.1: A typical plot of the BCS superconducting density of states as a function of energy. We see a gap of size $2|\Delta|$ for $|\omega| < \Delta$.

2.3 Bogoliubov-de Gennes Equations

It is well known (see ref. [13] chpt. 1) that if we have a one-particle fermionic operator in second quantization in some arbitrary basis ν:

$$A = \sum_{\nu_i,\nu_j} A_{\nu_i,\nu_j} c^\dagger_{\nu_i} c_{\nu_j} \equiv \sum_{\nu_i,\nu_j} \langle \nu_i | \hat{A} | \nu_j \rangle c^\dagger_{\nu_i} c_{\nu_j} \tag{2.27}$$

we can transform to real space using the quantum field operators $\Psi^\dagger, \Psi$:

$$\Psi^\dagger(\mathbf{r}) \equiv \sum_\nu \langle \mathbf{r} | \nu \rangle^* c^\dagger_\nu; \qquad \Psi(\mathbf{r}) \equiv \sum_\nu \langle \mathbf{r} | \nu \rangle c_\nu. \tag{2.28}$$

This yields:

$$\hat{A} = \sum_{\nu_i,\nu_j} \langle \nu_i | \hat{A} | \nu_j \rangle c^\dagger_{\nu_i} c_{\nu_j} = \sum_{\nu_i,\nu_j} \int \mathrm{d}\mathbf{r} \int \mathrm{d}\mathbf{r}' \langle \nu_i | \mathbf{r} \rangle \langle \mathbf{r} | \hat{A} | \mathbf{r}' \rangle \langle \mathbf{r}' | \nu_j \rangle c^\dagger_{\nu_i} c_{\nu_j} = \tag{2.29}$$

$$\sum_{\nu_i,\nu_j} \int \mathrm{d}\mathbf{r} \langle \nu_i | y \rangle A_{\mathbf{r}} \langle \mathbf{r} | \nu_j \rangle c^\dagger_{\nu_i} c_{\nu_j} = \int \mathrm{d}\mathbf{r} \left(\sum_{\nu_i} \langle \nu_i | \mathbf{r} \rangle c^\dagger_{\nu_i} \right) A_{\mathbf{r}} \left(\sum_{\nu_j} \langle \mathbf{r} | \nu_j \rangle c_{\nu_j} \right) \equiv \int \mathrm{d}\mathbf{r} \Psi^\dagger(\mathbf{r}) A_{\mathbf{r}} \Psi(\mathbf{r}),$$

where we used the locality-condition for single-particle operators in real space: $\langle \mathbf{r} | \hat{f} | \mathbf{r}' \rangle \equiv f(\mathbf{r}) \delta(\mathbf{r} - \mathbf{r}')$. In this manner we can incorporate usual effects like the kinetic energy and also Rashba SOI and Zeeman energy if we allow the indices ν_i, ν_j to run over spin-direction also. However, we will also need BCS superconductivity, which we cannot express in this way. We will include this in a mean-field, BCS manner as explained in section 2.2.1. Using the results from equations (2.15) and (2.18) we can Fourier-transform to real space:

$$H_{\text{super}} \equiv \sum_{\mathbf{k}} \Delta_0 c^\dagger_{\mathbf{k}\uparrow} c^\dagger_{-\mathbf{k}\downarrow} + h.c. = \frac{\Delta_0}{V} \sum_{\mathbf{k}} \int d\mathbf{r} \int d\mathbf{r}' e^{i\mathbf{k}\cdot(\mathbf{r}-\mathbf{r}')} \Psi^\dagger_\uparrow(\mathbf{r}) \Psi^\dagger_\downarrow(\mathbf{r}') + h.c. \tag{2.30}$$

$$= \int d\mathbf{r} \int d\mathbf{r}' \Delta_0 \delta(\mathbf{r} - \mathbf{r}') \Psi^\dagger_\uparrow(\mathbf{r}) \Psi^\dagger_\downarrow(\mathbf{r}') + h.c. = \int d\mathbf{r} \Psi^\dagger_\uparrow(\mathbf{r}) \Delta_0 \Psi^\dagger_\downarrow(\mathbf{r}) + h.c. \tag{2.31}$$

Standard procedure is now to introduce the so-called *Nambu spinor*:

$$\alpha \equiv \begin{pmatrix} c_\uparrow \\ c^\dagger_\downarrow \end{pmatrix}, \tag{2.32}$$

this being in real- or k-space. As explained in e.g. ref. [14] this allows for an elegant way to obtain the eigenspectrum in the problem given a mean-field superconducting pairing. However, since we are also going to include magnetic field and SOI with different spin directions we will not be able to capture all of this in this formalism. The way to establish the problem is to then introduce an extended Nambu spinor:

$$\bar{\Psi}(\mathbf{r}) \equiv \begin{pmatrix} \Psi_\uparrow(\mathbf{r}) \\ \Psi_\downarrow(\mathbf{r}) \\ \Psi_\downarrow^\dagger(\mathbf{r}) \\ -\Psi_\uparrow^\dagger(\mathbf{r}) \end{pmatrix} \tag{2.33}$$

Using the anti-commutation relations for the fermionic quantum field operators:

$$\{\Psi(\mathbf{r}), \Psi(\mathbf{r}')\} = 0; \quad \{\Psi^\dagger(\mathbf{r}), \Psi^\dagger(\mathbf{r}')\} = 0; \quad \{\Psi^\dagger(\mathbf{r}), \Psi(\mathbf{r}')\} = \delta(\mathbf{r} - \mathbf{r}'), \tag{2.34}$$

we can rewrite the total Hamiltonian in a smart way to incorporate all the types of terms we need. Let us take the superconducting term as an example:

$$H_{\text{super}} = \int \mathrm{d}\mathbf{r}\Big(\Psi_\uparrow^\dagger(\mathbf{r})\Delta_0\Psi_\downarrow^\dagger(\mathbf{r}) + h.c.\Big) = \frac{1}{2}\int \mathrm{d}\mathbf{r}\Big(\Psi_\uparrow^\dagger(\mathbf{r})\Delta_0\Psi_\downarrow^\dagger(\mathbf{r}) - \Psi_\downarrow^\dagger(\mathbf{r})\Delta_0\Psi_\uparrow^\dagger(\mathbf{r}) + h.c.\Big) \tag{2.35}$$

$$= \frac{1}{2}\int \mathrm{d}\mathbf{r}\bar{\Psi}^\dagger(\mathbf{r}) \begin{pmatrix} 0 & 0 & \Delta_0 & 0 \\ 0 & 0 & 0 & \Delta_0 \\ \Delta_0^* & 0 & 0 & 0 \\ 0 & \Delta_0^* & 0 & 0 \end{pmatrix} \bar{\Psi}(\mathbf{r}). \tag{2.36}$$

Here there was no constant term from commuting $\Psi_\uparrow^\dagger$ and $\Psi_\downarrow^\dagger$, but some of the other terms in the full Hamiltonian will produce a constant term that has to be added. Repeating this procedure for kinetic energy, SOI and Zeeman term yields:

$$H = \frac{1}{2}\int \mathrm{d}\mathbf{r}\bar{\Psi}^\dagger(\mathbf{r})\mathcal{H}\bar{\Psi}(\mathbf{r}) + \text{const}, \tag{2.37}$$

where H is the second quantized Hamiltonian, $\mathcal{H}$ is a 4×4-matrix that we will call the *BdG*-Hamiltonian.

Now we introduce the pauli-matrices in both particle-hole space, τ, and spin-space, σ, such that:

$$\tau_i\sigma_j \equiv \sigma_j\tau_i \equiv \tau_i \otimes \sigma_j; \quad \tau_i \equiv \tau_i \otimes \mathbb{1}; \quad \sigma_j \equiv \mathbb{1} \otimes \sigma_j. \tag{2.38}$$

In our modelling we will model a 2DEG and a superconductor. Starting from the second quantized Hamiltonian, we can derive that the BdG-Hamiltonians in the 2DEG, $\mathcal{H}_n$, and the superconductor, $\mathcal{H}_s$, will have the following form (written here in k-space):

$$\mathcal{H}_n = \xi_n\tau_z + \alpha(k_y\sigma_x - k_x\sigma_y)\tau_z + \frac{1}{2}g_n\mu_B\mathbf{B}\cdot\sigma \tag{2.39}$$

$$\mathcal{H}_s = \xi_s\tau_z + \frac{1}{2}g_s\mu_B\mathbf{B}\cdot\sigma + \Delta\tau_x, \tag{2.40}$$

where ξ_n, ξ_s are kinetic energies in the 2DEG and superconductor respectively, α is the Rashba SOI strength in the $x-y$ plane of the 2DEG, g_n, g_s are the effective g-factors in each material separately, μ_B is the Bohr magnetion, $\mathbf{B}$ is the applied magnetic field and Δ_0 is the mean-field superconducting pairing, assumed in our model to be real.
Now, importantly there is a relation between H and $\mathcal{H}$. This is the so-called *Bogoliubov-de Gennes*-transformation (see ref. [14] pp. 137-145).

Let us move forward by considering the solutions to the so called Bogoliubov-de-Gennes equations (note that the eigenstates are four-component spinors):

$$\mathcal{H}\langle \mathbf{r}|\,\bar{\psi}_n\rangle = E_n\langle \mathbf{r}|\,\bar{\psi}_n\rangle. \tag{2.41}$$

Assuming that these solutions constitute a complete set, we can represent our quantum field operators in this energy-eigenbasis:

$$\bar{\Psi}(\mathbf{r}) = \sum_n \langle \mathbf{r}|\,\bar{\psi}_n\rangle c_n; \quad \bar{\Psi}^\dagger(\mathbf{r}) = \sum_n \langle \mathbf{r}|\,\bar{\psi}_n\rangle^\dagger c_n^\dagger, \tag{2.42}$$

which yields:

$$H = \frac{1}{2}\int \mathrm{d}\mathbf{r}\left(\sum_n \langle \mathbf{r}|\,\bar{\psi}_n\rangle^\dagger c_n^\dagger\right)\mathcal{H}\left(\sum_n \langle \mathbf{r}|\,\bar{\psi}_n\rangle c_n\right) + \text{const.} = \tag{2.43}$$

$$\frac{1}{2}\sum_{n,n'} E_{n'}\int \mathrm{d}\mathbf{r}\langle \bar{\psi}_n|\,\mathbf{r}\rangle\cdot\langle \mathbf{r}|\,\bar{\psi}_{n'}\rangle c_n^\dagger c_{n'} + \text{const.} = \frac{1}{2}\sum_{n,n'} E_{n'}\langle \bar{\psi}_n|\,\bar{\psi}_{n'}\rangle c_n^\dagger c_{n'} + \text{const.} = \frac{1}{2}\sum_n E_n c_n^\dagger c_n + \text{const.},$$

where the c and $c^\dagger$ are given by:

$$c_m = \int \mathrm{d}\mathbf{r}\langle \mathbf{r}|\,\bar{\psi}_m\rangle^\dagger\cdot\bar{\Psi}(\mathbf{r}); \quad c_m^\dagger = \int \mathrm{d}\mathbf{r}\bar{\Psi}^\dagger(\mathbf{r})\cdot\langle \mathbf{r}|\,\bar{\psi}_m\rangle, \tag{2.44}$$

which follows from equation (2.42). Thus in conclusion, the eigenenergies from equation (2.41) are also eigenenergies of the original second-quantized problem. Therefore solving equation (2.41), known as the *Bogoliubov-de-Gennes Equations* (BdG equations), is also solving the original problem.

2.3.1 Symmetries

Here we draw from ref. [2]. The exact choice of Nambu spinor (equation (2.33)) is made such that it highlights that the dynamics of holes in the absence of magnetic field is the same as that of time-reversed electrons. If we study the definition of equation (2.38) we can see that the σ-matrices govern the spin-structure of the terms that appear in the Hamiltonian, while the τ-matrices govern the particle-hole-structure of the problem. We can write out the τ-structure of the BdG-Hamiltonian schematically as:

$$\mathcal{H} \sim \begin{pmatrix} (\text{electron}-\text{sector}) & (\text{electron}-\text{hole coupling}) \\ (\text{hole}-\text{electron coupling}) & (\text{hole}-\text{sector}) \end{pmatrix}, \tag{2.45}$$

where the different sectors are 2×2-matrices. If we compare with equation (2.37) we see that the terms in the electron-sector will produce terms with $\Psi^\dagger$ to the left and Ψ to the right in the second quantized Hamiltonian, i.e. electron-like terms. Likewise the hole-sector will produce hole-like terms. By choosing the Nambu-spinor as in equation (2.33) we ensure for the Hamiltonians under consideration in this thesis that the BdG-Hamiltonian has the following structure in τ-space:

$$\mathcal{H} = \begin{pmatrix} \mathcal{H}_0 & \Delta \\ \Delta & -\sigma_y\mathcal{H}_0^*\sigma_y \end{pmatrix}, \tag{2.46}$$

where the entries are again 2×2-matrices and we have assumed the entries of Δ real. Thus we see that for whichever 2×2-matrix that governs the electron-sector, $\mathcal{H}_0$, the hole-sector will be governed by the time-reversal of $-\mathcal{H}_0$, since we know that:

$$\hat{T}\mathcal{H}_0\hat{T}^\dagger = \sigma_y\mathcal{H}_0^*\sigma_y. \tag{2.47}$$

This way we have built in the time-reversal symmetry into the formalism by our choice of Nambu spinor.

By extending our Nambu spinor from the 2×1 one to 4×1 spinor we "artificially" double the dimension of the Hamiltonian and thus the number of eigenstates. This means there must be some symmetry present to account for this doubling, so that the number of independent solutions stay the same. This symmetry is the particle-hole symmetry, which can be expressed as the following operator:

$$P \equiv \tau_y \sigma_y K = \begin{pmatrix} 0 & 0 & 0 & -1 \\ 0 & 0 & 1 & 0 \\ 0 & 1 & 0 & 0 \\ -1 & 0 & 0 & 0 \end{pmatrix} K, \tag{2.48}$$

where K is the complex conjugate-operator. We can derive that for our Hamiltonian with Rashba SOI, Zeeman field and s-wave superconductivity with the choice of basis (2.33) for the Nambu spinor we have the following relation:

$$\{\mathcal{H}, P\} = 0. \tag{2.49}$$

This means that if we have an eigenstate of $\mathcal{H}$:

$$\mathcal{H}\langle \mathbf{r}| \psi_i \rangle = E_i \langle \mathbf{r}| \psi_i \rangle, \tag{2.50}$$

then necessarily the state $P\psi_i$ is also an eigenstate with the negative eigenvalue:

$$\mathcal{H}(P\langle \mathbf{r}| \psi_i \rangle) = -P(\mathcal{H}\langle \mathbf{r}| \psi_i \rangle) = -E_i(P\langle \mathbf{r}| \psi_i \rangle). \tag{2.51}$$

This *particle-hole symmetry* and its consequences for the energy spectrum will follow us throughout this thesis.

2.4 Tunneling Spectroscopy in the Linear Response Regime

One way to probe the single-particle propagator is to use tunneling spectroscopy. We will derive the formula for the current in the linear response regime where it is evident how the single-particle density of states (DOS) is probed. Throughout this derivation we follow ref. [13] pp. 133-136 closely.

A tunneling experiment usually consists of two materials (materials 1 and 2) brought into contact with an insulating layer in between. The idea with the insulating layer is to establish weak contact between the materials such that the overlap of the wavefunctions is weak, although non-zero. The overlap of the wavefunctions leads to tunneling terms in the Hamiltonian of the form:

$$H_T = \sum_{\mu\nu}\Big(T_{\nu\mu}c^\dagger_{1,\nu}c_{2,\mu} + T^*_{\nu,\mu}c^\dagger_{2,\mu}c_{1,\nu}\Big), \tag{2.52}$$

where:

$$T_{\nu\mu} = \langle\nu|\hat{H}|\mu\rangle = \int d\mathbf{r}\psi^*_\nu(\mathbf{r})H(\mathbf{r})\psi_\mu(\mathbf{r}), \tag{2.53}$$

with $H(\mathbf{r})$ being the single-particle Hamiltonian. Now the current is defined as the rate of change of particles through the constriction, i.e.:

$$I_e = -e\langle I\rangle, \tag{2.54}$$

where:

$$I = \dot{N}_1 = i[H, N_1] = i[H_T, N_1] = i\sum_{\nu\mu}\sum_{\nu'}\Big[\Big(T_{\nu\mu}c^\dagger_{1,\nu}c_{2,\mu} + T^*_{\nu\mu}c^\dagger_{2,\mu}c_{1,\nu}\Big), c^\dagger_{1,\nu'}c_{1,\nu}\Big] \tag{2.55}$$

$$= -i\sum_{\nu\mu}\Big(T_{\nu\mu}c^\dagger_{1,\nu}c_{2,\mu} - T^*_{\nu\mu}c^\dagger_{2,\mu}c_{1,\nu}\Big) \equiv -i(L - L^\dagger). \tag{2.56}$$

Assuming the coupling between the two materials is very weak, it is adequate to calculate the current only to lowest order in the coupling. Therefore we will use the linear response formula which states that, for a Hamiltonian $H = H_0 + H'\theta(t-t_0)$ with some perturbative H', the change in the expectation value of some operator A from the equilibrium vale $\langle A\rangle_0$ is given by:

$$\delta\langle A(t)\rangle \equiv \langle A(t)\rangle - \langle A\rangle_0 = \int_{t_0}^{\infty} dt'\Big(-i\theta(t-t')\Big\langle\Big[\hat{A}(t), \hat{H}'(t')\Big]\Big\rangle_0\Big). \tag{2.57}$$

In our case we have zero current in steady state so that:

$$\langle I\rangle(t) = \int_{-\infty}^{\infty} dt'\Big(-i\theta(t-t')\Big\langle\Big[\hat{I}_p(t), \hat{H}_T(t')\Big]\Big\rangle_0\Big) \equiv \int_{-\infty}^{\infty} dt' C^R_{I_p,H_T}(t,t'), \tag{2.58}$$

where we defied the *current correlation function* $C^R_{I_p,H_T}(t,t')$. Also note that we are in the interaction picture (see e.g. [13]) so that the time evolution is governed by $H = H_1 + H_2$. We can simplify the correlation function as:

$$C^R_{I_p,H_T}(t-t') = -\theta(t-t')\Big\langle\Big[\hat{L}(t) - \hat{L}^\dagger(t), \hat{L}(t') + \hat{L}^\dagger(t')\Big]\Big\rangle_0 \tag{2.59}$$

$$= -\theta(t-t')\Big[\Big\langle\Big[\hat{L}(t), \hat{L}(t')\Big]\Big\rangle_0 - \Big\langle\Big[\hat{L}^\dagger(t), \hat{L}(t')\Big]\Big\rangle_0 + c.c.\Big] \tag{2.60}$$

$$= 2\mathrm{Re}\theta(t-t')\Big\langle\Big[\hat{L}^\dagger(t), \hat{L}(t')\Big]\Big\rangle_0, \tag{2.61}$$

where the last equation sign follows because we will only consider particle-particle current, which does not allow for terms that do not conserve the number of particles in each system (a supercurrent would allow for these terms). Thus we are left with the following formula for the current:

$$I(t) = 2\mathrm{Re}\int_{-\infty}^{\infty} dt'\theta(t-t')\Big\langle\Big[\hat{L}^\dagger(t),\hat{L}(t')\Big]\Big\rangle_0 \tag{2.62}$$

$$= 2\mathrm{Re}\int_{-\infty}^{\infty} dt'\theta(t-t')\sum_{\nu\mu}\sum_{\nu'\mu'}T^*_{\nu\mu}T_{\nu'\mu'}\Bigg(\Big\langle\hat{c}_{1,\nu}(t)\hat{c}^\dagger_{1,\nu'}(t')\Big\rangle_0\Big\langle\hat{c}^\dagger_{2,\mu}(t)\hat{c}_{2,\mu'}(t')\Big\rangle_0 \tag{2.63}$$

$$-\Big\langle\hat{c}^\dagger_{1,\nu'}(t')\hat{c}_{1,\nu}(t)\Big\rangle_0\Big\langle\hat{c}_{2,\mu'}(t')\hat{c}^\dagger_{2,\mu}(t)\Big\rangle_0\Bigg). \tag{2.64}$$

Now we explicitly pull out the time-dependence that stems from the applied voltage difference (which is the real source of the current):

$$\hat{c}_1(t) = \tilde{c}_1(t)e^{-i(-e)V_1t};\qquad \hat{c}_2(t) = \tilde{c}_(t)e^{-i(-e)V_2t}, \tag{2.65}$$

where the time-dependence of the $\tilde{c}$ is given by a Hamiltonian with a common chemical potential μ. Now we introduce the lesser and greater Green's functions:

$$G^>_{\nu\nu'}(t,t') = -i\Big\langle c_\nu(t)c^\dagger_{\nu'}(t')\Big\rangle_0;\qquad G^<_{\nu\nu'}(t,t') = +i\Big\langle c^\dagger_{\nu'}(t')c_\nu(t)\Big\rangle_0. \tag{2.66}$$

With these definitions we get:

$$I = 2\mathrm{Re}\int_{-\infty}^{\infty} dt'\theta(t-t')\sum_{\nu\mu}\sum_{\nu'\mu'}T^*_{\mu\nu}T_{\nu'\mu'}e^{i(-e)(V_2-V_1)(t-t')} \tag{2.67}$$

$$\Big(G^>_{1,\nu\nu'}(t,t')G^<_{2,\mu'\mu}(t',t) - G^<_{1,\nu\nu'}(t,t')G^>_{2,\mu'\mu}(t',t)\Big) \tag{2.68}$$

This can be rewritten as a trace over μ,ν:

$$I = 2\mathrm{Re}\int_{-\infty}^{\infty} dt'\theta(t-t')e^{i(-e)(-V)(t-t')}\mathrm{Tr}\Big[G^>_1(t,t')TG^<_2(t',t)T^\dagger - G^<_1(t,t')TG^>_2(t',t)T^\dagger\Big]. \tag{2.69}$$

where $V \equiv V_1 - V_2$. Now upon assuming that the Green's functions are only functions of the time difference $t-t'$ we can Fourier transform wrt. only one time-variable, which after some work results in:

$$I = \int\frac{d\omega}{2\pi}\mathrm{Tr}\Big[G^>_1(\omega)TG^<_2(\omega+eV)T^\dagger - G^<_1(\omega)TG^>_2(\omega+eV)T^\dagger\Big], \tag{2.70}$$

which upon inserting the relations between lesser and greater Green's functions and the spectral function (here $n_F(\omega)$ is the Fermi function):

$$iG^>(\nu,\omega) = A(\nu,\omega)(1-n_F(\omega));\qquad -iG^<(\nu,\omega) = A(\nu,\omega)n_F(\omega) \tag{2.71}$$

leads us to the formula:

$$I = \int_{-\infty}^{\infty}\frac{d\omega}{2\pi}\mathrm{Tr}\Big[A_1(\omega)TA_2(\omega+eV)T^\dagger\Big](n_F(\omega+eV)-n_F(\omega)). \tag{2.72}$$

Now in this thesis we will be working the basis $\mu = (\mathbf{k}_1,\sigma_1)$, $\nu = (\mathbf{k}_2,\sigma_2)$. Writing out the trace over $\mathbf{k}_1$ and $\mathbf{k}_2$ explicitly yields the formula for the particle-current:

$$I = \int_{-\infty}^{\infty}\frac{d\omega}{2\pi}|T|^2\sum_{\mathbf{k}_1,\mathbf{k}_2}\mathrm{Tr}_\sigma[A_1(\mathbf{k_1},\omega)A_2(\mathbf{k_2},\omega+eV)](n_F(\omega+eV)-n_F(\omega)), \tag{2.73}$$

where the Tr_σ is defined to only run over the spin-degrees of freedom of the particles.

2.5 Introduction to Majorana Physics

The following draws from ref. [2]. Here we will go through the basics of two important theoretical papers, which explain the fundamentals of Majorana bound states in nanowires.

2.5.1 Kitaev

Kitaev's paper (ref. [15]) from 2001 is an important landmark on the road towards realizing Majorana fermions in condensed matter systems and is continuously referenced as the underlying model that is sought after. We will therefore explain the basic features of the paper and try to emphasize its important implications.

Kitaev presents a 1D-chain model with L sites, and nearest-neighbor hopping terms. The sites can be occupied or un-occupied by fermions. Furthermore the chain is superconducting by being proximitized by a large bulk superconductor with a p-wave superconducting pairing. Here *p-wave* follows since the model is spinless and the pairing is therefore of the triplet-kind. If we denote the second-quantized fermion operators as $a, a^\dagger$ this gives us the following Hamiltonian for the chain in real space:

$$H = \sum_j \left(-w\left(a_j^\dagger a_{j+1} + a_{j+1}^\dagger a_j\right) - \mu\left(a_j^\dagger a_j - \frac{1}{2}\right) + \Delta a_j a_{j+1} + \Delta^* a_{j+1}^\dagger a_j^\dagger \right), \tag{2.74}$$

where w is the nearest-neighbor pairing strength, μ is the chemical potential, and $\Delta = |\Delta| e^{i\theta}$ is the induced superconducting pairing. Now we define some new fermionic operators, which we will call Majorana operators (and for simplicity set $\theta = 0$ in what follows):

$$c_{2j-1} = a_j + a_j^\dagger; \qquad c_{2j} = -ia_j + ia_j^\dagger, \; j = 1, \ldots, L. \tag{2.75}$$

Evidently these operators are hermitian. We see that this new definition basically splits up each fermion site into two pieces, thus doubling the number of 'sites' in the model. Now we can rewrite the Hamiltonian in terms of this new basis, which yields:

$$H_1 = \frac{i}{2} \sum_j (-\mu c_{2j-1} c_{2j} + (w + |\Delta|) c_{2j} c_{2j+1} + (-w + |\Delta|) c_{2j-1} c_{2j+2}) \tag{2.76}$$

Let us look at two limiting cases:

$|\Delta| = w = 0, \mu < 0$**:** Here the Hamiltonian reduces to:

$$H_1 = -\mu \sum_{j=1}^{L} (a_j^\dagger a_j - 1/2) = \frac{i}{2}(-\mu) \sum_{j=1}^{L} c_{2j-1} c_{2j}. \tag{2.77}$$

The important thing to note is that here the Hamiltonian can be written in terms of a product of Majorana operators from the same fermionic site. The ground state is the unoccopied state.

$|\Delta| = w > 0$**,** $\mu = 0$**:** In this case the Hamiltonian reduces to:

$$H_1 = iw \sum_{j=1}^{L-1} c_{2j} c_{2j+1}, \tag{2.78}$$

which we see couples Majorana operators from *different* fermionic sites. Also the c_1 and c_{2L}-operators remain unpaired, i.e. they do not enter the Hamiltonian. This means that any ground state of the system, $|\psi_0\rangle$, will be degenerate in that adding the fermionic state we get from combining c_1 and c_{2L} will cost zero energy.
The interesting thing to note is that if the state with the two unpaired Majorana operators is realized,

this means that we have two "unpaired" Majoranas in each end of the chain. And it is exactly the lack of pairing to neighboring Majoranas that makes these two Majoranas immune to local perturbations in the environment. More specifically, since we can construct a fermionic state out of combining c_1 and c_{2L}, if this fermion has to be perturbed in some way the perturbation has to affect both Majorana operators. And since these are spatially separated, local perturbations cannot affect this joint fermionic state.

Now how do we realize the two phases of the system, i.e. with the fermionic state from combining c_1 and c_{2L} occupied or not? In ref. [15], Kitaev argues that the two phases extend to connected domains in the parameter space where the spectrum is gapped. To move from one type of Majorana paring to the other, the gap in the spectrum has to close and reopen.
This explains in an informal way why we talk about *topologically protected* phases. We know that topology is the study of objects that remain *invariant* under some kind of transformation - like the well known example of a cup that can be continously deformed into a torus, which renders the two objects topologically equivalent. In the same manner we can say that any transformation (meaning changing of system parameters) that does not close the energy gap will then keep the system in the same phase, i.e. our system is "topologically trivial" in the regimes without delocalized Majoranas at the ends, and "topologically non-trivial" in the phase with delocalized Majoranas at the ends. An effective tool to actually determine which topological phase the system is in for given parameters is establishing a so-called *topological invariant*; see ref. [16] for further explanation.

This explains the basic idea of why Majoranas are expected to be useful for quantum computing. The immunity to local perturbations is essential, since small, local perturbations (for example thermal perturbations) is a recurring obstacle in quantum physics that is hard to circumvent. However, an important ingredient in the paper was the p-wave superconductivity. (It is p-wave since there is no spin-dependency in the model.) The problem is that actually obtaining and manipulating a p-wave superconductor is not experimentally realistic. Conversely, conventional s-wave superconductors are abound. A footnote on page 4 in ref. [15] is interesting in this regard: "*It appears that only a triplet (p-wave) superconductivity in the 3-dimensional sub-strate can effectively induce the desired pairing between electrons with the same spin direction — at least, this is true in the absence of spin-orbit interaction*". It turned out some years later that actually spin-orbit interaction would be important to overcome this problem.

2.5.2 Oreg et. al.

Around 2009-2010 some different papers [17, 18] came up with a similar idea; an, at least in theory, experimentally viable idea to realize an effective p-wave superconductor. Here we will explain the basics of the paper ref. [18] because of its simplicity[1].

In the article [18] we are presented with BdG Hamiltonian (see section 2.3) for a continuous 1D wire (longitudinal in the y-direction) with spatially varying electrochemical potential, Rashba spin-orbit interaction, a Zeeman term and conventional s-wave superconductivity induced via the proximity effect given by:

$$\int \bar{\Psi}^\dagger(y)\mathcal{H}\bar{\Psi}(y)dy. \tag{2.79}$$

$$\mathcal{H} = \left[\frac{p^2}{2m} - \mu(y)\right]\tau_z + up\sigma_z\tau_z + B(y)\sigma_x + \Delta(y)\tau_x,$$

with the notation convention that:

[1] The following draws from sections of a hand-in made in the course CMT2 at the University of Copenhagen in 2016. The report was made by authors Mads Jørgensen and Bjarke Nicolaisen, and permission to reprint parts of this hand-in here has been given by both authors.

$$\tau_i \equiv \hat{\sigma}_i \otimes \mathbb{1}; \qquad \sigma_i \equiv \mathbb{1} \otimes \hat{\sigma}_i; \qquad \sigma_i \tau_j \equiv \hat{\sigma}_j \otimes \hat{\sigma}_i, \tag{2.80}$$

with $\hat{\sigma}$ being the i'th pauli matrix. Here u is the spin-orbit coupling strength, Δ is the superconducting order parameter, and B is the magnetic field.

It is interesting to study the energy spectrum for constant parameters, which is:

$$E_{\pm}^2 = B^2 + \Delta^2 + \xi_p^2 + (up)^2 \pm 2\sqrt{B^2\Delta^2 + B^2\xi_p^2 + (up)^2\xi_p^2}, \tag{2.81}$$

where we defined $\xi_p \equiv [\frac{p^2}{2m} - \mu(y)]$. By inspecting the spectrum in different parameter regimes, we can see some interesting behaviour. We include figure 2.5.1 from the article, which shows the energy spectrum for single particles for different parameter values.

The point of figure 2.5.1 is to show that when varying either parameter μ, B and Δ, we can close and open the energy gap at $p = 0$. The idea is to drive a part of the wire topologically non-trivial; if it is surrounded by topologically trivial regions with a gap closing at the interface, we can achieve Majorana bound states in the ends of the topological wire segments. The biggest problem lies in tuning the wire into the topologically non-trivial phase. In this concrete system the topology of a region is determined by whether $B - \sqrt{\Delta^2 + \mu^2}$ is positive or negative, which they show directly in the paper. But the major point of the paper is this: By having a wire with Rashba SOI, a Zeeman term and proximitizing this wire by an *s-wave* superconductor the result is that we can in principle tune the wire in and out of the topologically non-trivial phase by spatially varying μ, B or Δ.

This result explains the underlying motivation for what system we study in this thesis. We will conduct analysis on a 2DEG proximitized by a conventional superconductor, with a Zeeman term from a magnetic field and Rashba SOI. Even though the systems under consideration in this thesis do not immediately contain Majoranas, and we do not focus on Majoranas in our analysis, the underlying motivation for studying these systems with exactly these parameters is that hopefully the work will prove useful in the hunt for Majorana bound states.

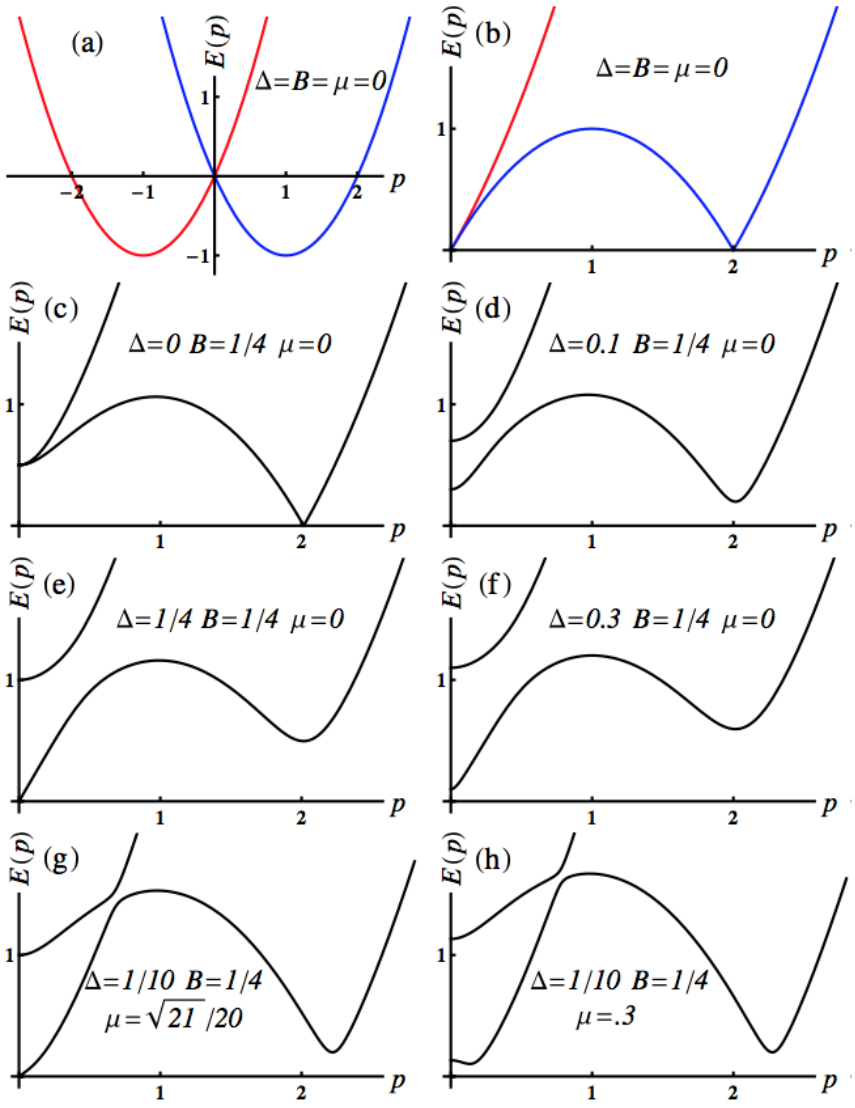

Figure 2.5.1: Figure from [18]. (a) The energy spectrum for different parameter values. The color 'red' corresponds to spin-up, 'blue' to spin-down in the z-direction. (b) shows the excitation spectrum (excitation because the energy is relative to the chemical potential, which is here equal to zero) with the same parameter values. The hole-branch is now included. (c) Here we change $B = 0 \to B = 1/4$, which means that we open up a gap in the excitation spectrum at $p = 0$. Note that the spin-colors have now been switched off, to indicate that the energy branches no longer have a well-defined spin in the z-direction since we now have a SOI-term with σ_z and magnetic field with σ_x. Still electron and hole branches are well-defined though. (d) Now $\Delta = 0.1$, which opens up another gap just like for the magnetic field; however, this one is now between electron and hole branches. Therefore there are new branch gaps at $p = 0$ and also for $p = 2$ where before the hole and electron gaps touched. (e) Now $\Delta = B$ and we clearly see the new splitting induced by the larger Δ making the excitation branches split even further; now at $p = 0$ we have one branch at energy 1, and one for $E = 0 = \mu$. Therefore we can say that the energy gap has been closed. (f) Now $\Delta = 0.3 > 1/4 = B$, which makes the gap at $p = 0$ reappear. (g) Here we decrease Δ again to $\Delta = 0.1$, but let $\mu = \sqrt{21/20}$. We see as in (e) that the gap at $p = 0$ closes. (h) Increasing μ reopens the $p = 0$ gap once again.

2.6 Experimental Considerations

We will throughout the report compare some of our results with some experimental results obtained in the Center for Quantum Devices at the University of Copenhagen. Here we present basic explanations of the relevant experimental designs.

2.6.1 2DEG design at QDev

In ref. [19] there is a nice description of the 2DEG-growth and characterization in QDev. Here we highlight some of the points that are relevant for the understanding of this thesis.

The basic idea of a 2DEG is to "freeze out" one dimension of propagation by confining the electrons in this dimension to a narrow quantum well, while allowing them to propagate freely in the two planar dimensions. A problem that has been persistent in junctions involving 2DEGs is that it has been hard to get a clean interface between the two regions. However with the device seen in figure 2.6.1 they managed to build a system which is devoid of this problem and has a close to perfect transition between the layers.

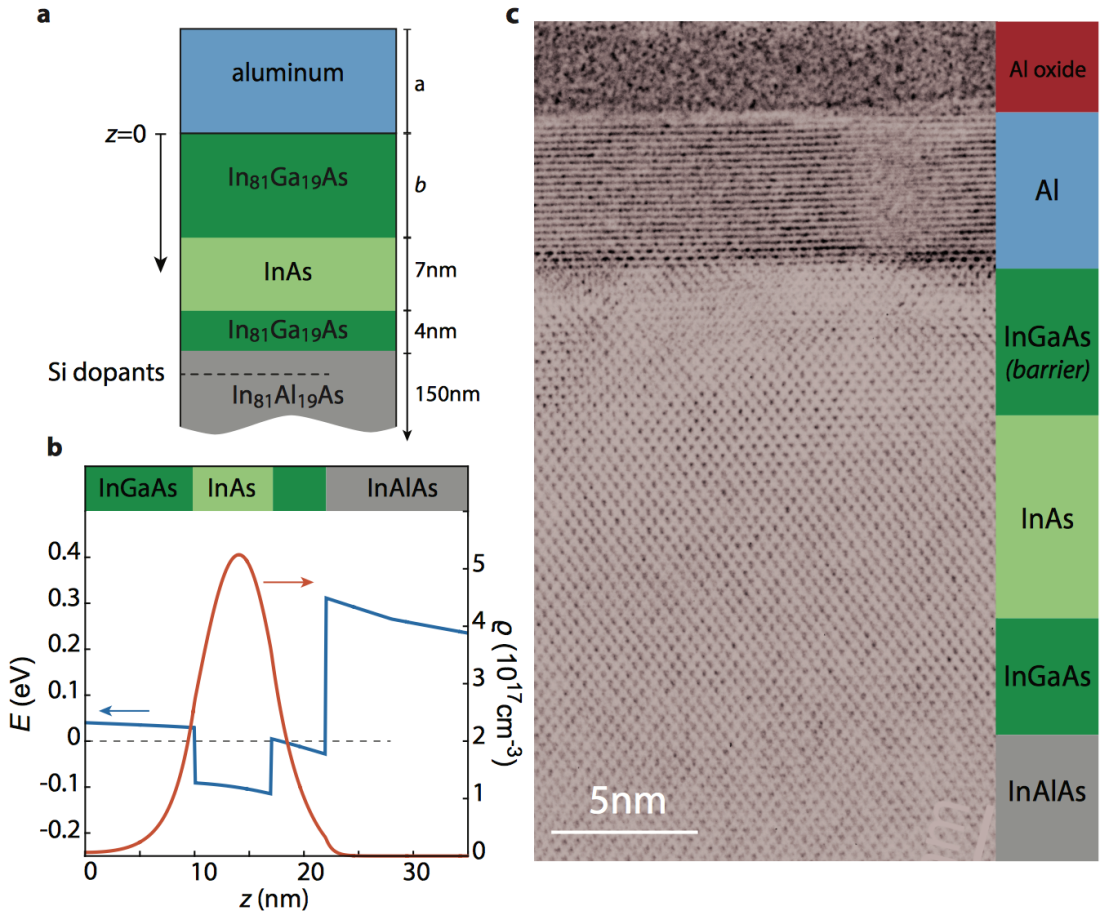

Figure 2.6.1: Figure from [19]. **a** Sketch of the total wafer where the growth direction is vertical. **b** Self-consistent Poisson equation calculation which shows both the potential (blue) and the wavefunction probability density (red) as a function of length in the growth direction. **c** An actual picture of a device using Transmission Electron Microscopy (TEM).

As can be seen from figure 2.6.1 **b)** they have succesfully established a quantum well in the 2DEG InAs material. In this thesis we will model this system simply by a 2DEG region of one material with

a hard-wall barrier on one side, and a delta-function barrier to a superconductor, which we model as being semi-infinite.

2.6.2 Quantum Point Contact

It is now a well-known result [20]-[21] that the conductance through a sufficiently narrow constriction in a 2DEG is quantized - see figure 2.6.2 **b** for some theoretical conductance plots, where indeed the conductance is quantized for some parameter values. The mechanism to control the conductance can be explained schematically as such: Imagine you have a 2DEG. Then put a dielectric on top. On top of this you deposit two pieces of electrodes as in figure 2.6.2 **a**. Now you put on a voltage difference over the electrodes. Since the underlying 2DEG is connected to ground, the conduction electrons from the electrodes would like to propagate there, but due to the dielectric they cannot. Thus under the electrodes we will establish something like an effective capacitor with an electric field penetrating down through the sample in the growth direction. Since the 2DEG is a semiconductor with only a few conduction electrons available it is possible to deplete the regions below the electrodes of conduction electrons. Now there only remain a few conduction electrons in the narrow region between the two electrode-tips. By further enhancing the electrode voltage and thus the electric field, the edge electric field effects of the capacitor will deplete this region too, so that finally we reach the quantized conduction regime and can essentially turn off the conductance altogether.

Experimentally this means that the QPC electrode-gate voltage control allows for tuning into the so-called *tunneling regime*, which means a regime where the conductance is almost zero. To model the systems involving QPCs in this thesis we will therefore ab initio invoke the tunneling approximation.

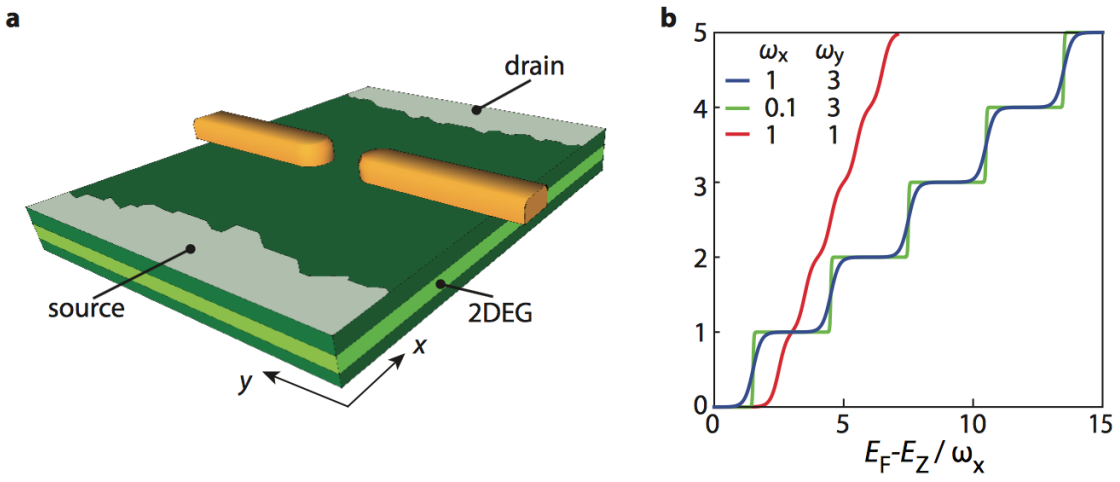

Figure 2.6.2: Figure from [19]. **a** A schematic of the QPC design on top of the 2DEG wafer. **b** Theoretical conductance curves assuming low bias, low temperature, and quadratic potential $V(x,y,z) = -\frac{1}{2}m\omega_x^2x^2 + \frac{1}{2}m\omega_y^2y^2 + V(z)$.

Chapter 3

Wave-function approach to a S-2DEG-junction

Our aim in this section is to perform analysis on the system showed in figure 3.0.1. We want to get a solution for the subgap (i.e. energy $|E| < \Delta$) energy solutions to understand the general behaviour of the system. From the energy solutions we want in particular to extract information about the induced gap in the 2DEG and the effective g-factor of the sub-gap excitations in the system, and investigate its relation to the wavefunction probability density.

In the following we follow closely the treatment of a similar system (though without Zeeman energy) in ref. [22]. Consider a junction with a superconductor for $z < 0$, and a 2DEG in the region $0 < z < d$. We assume infinite planar directions in the xy-plane where the Hamiltonian separates into $H = H_z + H_{xy}$. The eigenstates of H_{xy} are plane waves such that the interesting problem lies in solving for the eigenstates of H_z. We will leave as many free parameters as possible for flexibility of the model. We assume different effective masses in the superconductor (m_s) and 2DEG semiconductor (m_n); we assume a potential energy difference V_0 of the conduction band bottoms of the two regions; we assume a delta-function potential barrier $U_a\delta(z)$ to model the Schottky barrier of the interface. Furthermore we also apply a constant magnetic field with only a z-component B, such that we get a Zeeman-contribution to the Hamiltonian. We leave the effective g-factors in the two regions, g_s and g_n, as parameters as well.

Since we have a non-trivial Hamiltonian in both particle-hole- and spin-space we would normally work in the full 4×4-BdG-basis described in section 2.3. However, since the only nontrivial spin-term is the magnetic field, we can actually work only with a 2×1 Nambu-spinor, containing one electron

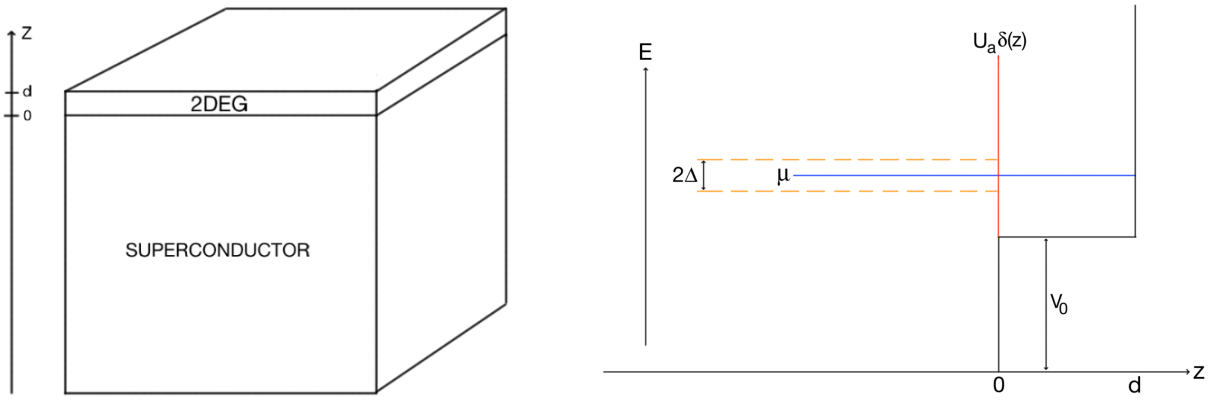

Figure 3.0.1: *On the left*: A shematic of our system. A finite 2DEG proximitized to a semi-infinite superconductor. *On the right:* A schematic of the potential felt by a single-particle excitation in the system as a function of distance.

part with spin-up or -down, and one hole part with the opposite spin:

$$\bar{\Psi}(\mathbf{r}) = \begin{pmatrix} \Psi_{\uparrow}(\mathbf{r}) \\ \Psi^{\dagger}_{\downarrow}(\mathbf{r}) \end{pmatrix}, \tag{3.1}$$

In this way we still keep the structure needed to get a BCS, superconducting gap-term in our Hamiltonian (i.e. a coupling between electrons and holes of opposite spins), and can also include the Zeeman effect by simply choosing B to be positive or negative, depending on which solutions we want to solve for - the electron spin-up and hole spin-down solution, or the one with reversed spins. We will implement this sign by adding a parameter $\sigma = \pm 1$ to the Zeeman energy. All this enables us to write the Hamiltonian in the following way (we set $\hbar \equiv 1$):

$$H = \int d\mathbf{r} \bar{\Psi}^{\dagger}(\mathbf{r}) \mathcal{H} \bar{\Psi}(\mathbf{r}) + \text{const.}, \tag{3.2}$$

where:

$$\begin{aligned} \mathcal{H} = &\left[\left(-\frac{\nabla^2}{2m_s} - \mu + U_a \delta(z) \right) \tau_z + \frac{\mu_B g_s}{2} B\sigma\tau_0 + \Delta\tau_x \right] \theta(-z) \\ &+ \left[\left(-\frac{\nabla^2}{2m_n} - (\mu - V_0) \right) \tau_z + \frac{\mu_B g_n}{2} B\sigma\tau_0 \right] \theta(z)\theta(d-z), \end{aligned} \tag{3.3}$$

written with the same notation as introduced in section 2.3. The BdG equations are:

$$\mathcal{H} \langle \mathbf{r} | \bar{\psi} \rangle = E \langle \mathbf{r} | \bar{\psi} \rangle, \tag{3.4}$$

where the 2×1 eigensolutions to this equation are the excitations of the system. We now seek to solve the eigenequation for eigenenergies. Because the Zeeman term in this Nambu-spinor basis acts as a simple shift of the energies, we will define the following quantities:

$$E_n \equiv E - \frac{\mu_B g_n}{2} B\sigma; \qquad E_s \equiv E - \frac{\mu_B g_s}{2} B\sigma. \tag{3.5}$$

Let us first look at the eigenstates in the 2DEG-region. Here the electron-hole equations are decoupled and we get, defining $\langle \mathbf{r} | \bar{\psi}_n \rangle = \begin{pmatrix} \psi_e(\mathbf{r}) \\ \psi_h(\mathbf{r}) \end{pmatrix}$ as the eigensolution to equation (3.4) in the 2DEG, for the electron-part of the eigensolution:

$$\begin{aligned} \left[-\frac{\nabla^2}{2m_n} - (\mu - V_0) \right] \psi_e(\mathbf{r}) = E_n \psi_e(\mathbf{r}) \Rightarrow \\ \psi_e(\mathbf{r}) = \left[A_+ e^{i\mathbf{k}\cdot\mathbf{r}} - A_- e^{-i\mathbf{k}\cdot\mathbf{r}} \right], \quad \text{where } k = \pm\sqrt{2m_n(E_n + \mu - V_0)}. \end{aligned} \tag{3.6}$$

Now since the solutions in the xy plane are decoupled from the z-direction we introduce $\mathbf{k}_{||} = \begin{pmatrix} k_x \\ k_y \\ 0 \end{pmatrix}$ to account for the plane wave propagation in the xy-plane. Since we are only interested in the z-direction dynamics we will treat the good quantum number $k_{||}$ as a parameter so that the general equation for the electron becomes:

$$\psi_e(\mathbf{r}) = \exp(i\mathbf{k}_{||} \cdot \mathbf{r}) \left[A_+ e^{ik_e z} - A_- e^{-ik_e z} \right], \tag{3.7}$$

where:

$$k_{||}^2 + k_e^2 = 2m_n(E_n + \mu - V_0). \tag{3.8}$$

For the hole-wavefunction $\psi_h(\mathbf{r})$ it is a similar equation, so now we relabel the wavenumber for the hole k_h and achieve:

$$\psi_h(\mathbf{r}) = \exp(i\mathbf{k}_{||}\cdot\mathbf{r})\Big[H_+e^{ik_hz} - H_-e^{-ik_hz}\Big], \tag{3.9}$$

where:

$$k_{||}^2 + k_h^2 = 2m_n(-E_n + \mu - V_0), \tag{3.10}$$

where we see that the energy has changed sign, $E \to -E$, consistent with a hole being the antiparticle of an electron and the Zeeman term has also changed sign, i.e. $E_n \to -E_n$, since our Nambu-spinor in equation (3.1) assumed different spin-directions of the hole and electron.
Now for the superconductor the electron and hole parts couple. Anticipating that our sub-gap states must decay in the superconductor (since sub-gap, single-particle excitations are not allowed in a superconductor), we assume a solution of the form:

$$\langle\mathbf{r}|\,\bar{\psi}_s\rangle = e^{i\mathbf{k}_{||}\cdot\mathbf{r}}e^{(\kappa+ip)z}\begin{pmatrix}u\\v\end{pmatrix}, \quad \kappa,p\in\mathbb{R}; \quad u,v\in\mathbb{C}. \tag{3.11}$$

Note that we also here have $k_{||}$ as the wavenumber in the xy-plane to ensure overall continuity of the wavefunction. Plugging expression (3.11) into the BdG equations (3.4) we obtain:

$$\begin{pmatrix}\left[\frac{-(\kappa+ip)^2+k_{||}^2}{2m_s} - \mu\right]u + \Delta v\\ \Delta u - \left[\frac{-(\kappa+ip)^2+k_{||}^2}{2m_s} - \mu\right]v\end{pmatrix} = E_s\begin{pmatrix}u\\v\end{pmatrix}. \tag{3.12}$$

Now looking for non-trivial solutions to equations (3.12) yields:

$$\det\begin{pmatrix}\frac{-(\kappa+ip)^2+k_{||}^2}{2m_s} - \mu - E_s & \Delta\\ \Delta & -\left[\frac{-(\kappa+ip)^2+k_{||}^2}{2m_s} - \mu\right] - E_s\end{pmatrix} = 0 \Leftrightarrow \tag{3.13}$$

$$\left(\frac{k_{||}^2 - \kappa^2 + p^2}{2m_s} - i\frac{\kappa p}{m_s}\right) - \mu = \pm i\sqrt{\Delta^2 - E_s^2} \tag{3.14}$$

Assuming $|E_s| < \Delta$ we can take the real and imaginary parts of this equation which yields:

$$\frac{1}{2m_s}(k_{||}^2 - \kappa^2 + p^2) = \mu; \tag{3.15}$$

$$-\frac{1}{m_s}\kappa p = \pm\sqrt{\Delta^2 - E_s^2}. \tag{3.16}$$

Now we define:

$$\xi_s \equiv -i\frac{\kappa p}{m_s}, \tag{3.17}$$

whereby equation (3.16) squared assumes the form:

$$E_s^2 = \Delta^2 + \xi_s^2, \tag{3.18}$$

which has the typical appearance for a superconducting spectrum; a superconducting gap Δ and kinetic energy ξ_s.
On a physical background, under the assumption $|E_s| < \Delta$ we demand that the wave function attenuates in the superconducting region $z < 0$ with a characteristic distance κ^{-1}. Thus $\kappa > 0$, whence equation (3.16) leaves us two choices for b for the other parameters given.

Now we want to determine the eigenstates corresponding to the above eigenvalues. Since we can

only determine the coefficients u, v up to a normalization, we choose $u^2 + v^2 = 1$. The BdG equations (3.12) under the condition (3.15) becomes:

$$\begin{pmatrix} \xi_s u + \Delta v \\ \Delta u - \xi_s v \end{pmatrix} = E_s \begin{pmatrix} u \\ v \end{pmatrix} \Rightarrow \tag{3.19}$$

$$u = \frac{\Delta}{E_s - \xi_s} v \Rightarrow \tag{3.20}$$

$$u^2 = \left(1 + \frac{(E_s - \xi_s)^2}{\Delta^2}\right)^{-1} = \left(1 + \frac{(E_s - \xi_s)^2}{E_s^2 - \xi_s^2}\right)^{-1} = \left(1 + \frac{E_s - \xi_s}{E_s + \xi_s}\right)^{-1} = \frac{1}{2}\left(1 + \frac{\xi_s}{E_s}\right). \tag{3.21}$$

This of course means that $v^2 = \frac{1}{2}\left(1 - \frac{\xi_s}{E_s}\right)$. The two choices of sign for p explained earlier gives us two different solutions; if $p \to -p$ then also $\xi_s \to -\xi_s$, which in turn means that $u \leftrightarrow v$. In result we have:

$$\left\langle \mathbf{r} \middle| \bar{\psi}_s \right\rangle = e^{i\mathbf{k}_{||}\cdot\mathbf{r}} \left[B_+ e^{(\kappa + ip)z} \begin{pmatrix} u \\ v \end{pmatrix} - B_- e^{(\kappa - ip)z} \begin{pmatrix} v \\ u \end{pmatrix} \right]. \tag{3.22}$$

3.1 Matching Boundary Conditions

Now we want to proceed by using the boundary conditions. Firstly we have continuity of the wave function at the superconductor-2DEG boundary:

$$\langle \mathbf{r}|\bar{\psi}\rangle\big|_{z=0^+} = \langle \mathbf{r}|\bar{\psi}\rangle\big|_{z=0^-} \Leftrightarrow \tag{3.23}$$

$$\langle \mathbf{r}|\bar{\psi}_n\rangle\big|_{z=0} = \langle \mathbf{r}|\bar{\psi}_s\rangle\big|_{z=0} \Leftrightarrow \tag{3.24}$$

$$\begin{pmatrix} A_+ - A_- \\ H_+ - H_- \end{pmatrix} = \begin{pmatrix} B_+u - B_-v \\ B_+v - B_-u \end{pmatrix}. \tag{3.25}$$

Next we have the boundary condition for the derivative of the wave function. Here we get from Schrödinger's equation:

$$-\frac{1}{2m(z)}\partial_z^2\langle \mathbf{r}|\bar{\psi}\rangle = (E - V(z))\langle \mathbf{r}|\bar{\psi}\rangle \Rightarrow \tag{3.26}$$

$$\lim_{\epsilon\to 0}\left(\int_{-\epsilon}^{0}\frac{1}{2m_s}\partial_z^2\langle \mathbf{r}|\bar{\psi}\rangle dz + \int_0^{\epsilon}\frac{1}{2m_n}\partial_z^2\langle \mathbf{r}|\bar{\psi}\rangle dz\right) = \lim_{\epsilon\to 0}\left(\int_{-\epsilon}^{\epsilon}(V(z)-E)\langle \mathbf{r}|\bar{\psi}\rangle dz\right) = U_a\langle \mathbf{r}|\bar{\psi}\rangle\big|_{z=0} \Rightarrow \tag{3.27}$$

$$\frac{1}{2m_n}\partial_z\langle \mathbf{r}|\bar{\psi}_n\rangle\big|_{z=0} - \frac{1}{2m_s}\partial_z\langle \mathbf{r}|\bar{\psi}_s\rangle\big|_{z=0} = U_a\langle \mathbf{r}|\bar{\psi}\rangle\big|_{z=0} \Leftrightarrow \tag{3.28}$$

$$\begin{pmatrix} A_+(\frac{ik_e}{2m_n} - U_a) + A_-(\frac{ik_e}{2m_n} + U_a) - B_+u\frac{(ip+\kappa)}{2m_s} + B_-v\frac{(\kappa-ip)}{2m_s} \\ H_+(\frac{ik_h}{2m_n} - U_a) + H_-(\frac{ik_h}{2m_n} + U_a) - B_+v\frac{(ip+\kappa)}{2m_s} + B_-u\frac{(\kappa-ip)}{2m_s} \end{pmatrix} = 0. \tag{3.29}$$

The third boundary condition is dictated by the finite size of the 2DEG, where we demand that at the boundary the wavefuntion is zero:

$$\langle \mathbf{r}|\bar{\psi}_n\rangle\big|_{z=0} = d \Rightarrow \tag{3.30}$$

$$\begin{pmatrix} A_+e^{ik_ed} - A_-e^{-ik_ed} \\ H_+e^{ik_hd} - H_-e^{-ik_hd} \end{pmatrix} = 0. \tag{3.31}$$

Combining these three boundary conditions yields:

$$\begin{pmatrix} u & -v & -1 & 1 & 0 & 0 \\ v & -u & 0 & 0 & -1 & 1 \\ -\frac{u(\kappa+ip)}{2m_s} & \frac{v(\kappa-ip)}{2m_s} & \frac{i\hbar^2k_e}{2m_n} - U_a & \frac{ik_e}{2m_n} + U_a & 0 & 0 \\ -v\frac{(ip+\kappa)}{2m_s} & u\frac{(\kappa-ip)}{2m_s} & 0 & 0 & \frac{ik_h}{2m_n} - U_a & \frac{ik_h}{2m_n} + U_a \\ 0 & 0 & e^{ik_ed} & -e^{-ik_ed} & 0 & 0 \\ 0 & 0 & 0 & 0 & e^{ik_hd} & -e^{-ik_hd} \end{pmatrix}\begin{pmatrix} B_+ \\ B_- \\ A_+ \\ A_- \\ H_+ \\ H_- \end{pmatrix} = 0. \tag{3.32}$$

Looking for non-trivial solutions to this equation by setting the determinant of the above $6\times 6-$matrix equal to 0 and using equation (3.21), we get an equation for the excitation energies in the system:

$$0 = ip\frac{E_s}{\xi_s}(k_h\cos dk_h\sin dk_e - k_e\sin dk_h\cos dk_e) + \frac{m_s}{m_n}k_hk_e\cos dk_h\cos dk_e + \tag{3.33}$$

$$\sin dk_h\sin dk_e\left(\frac{m_n}{m_s}\left(p^2 + [\kappa + 2U_am_s]^2\right)\right) + \sin dk_h\cos dk_e(k_e[\kappa + 2U_am_s]) + \cos dk_h\sin dk_e(k_e[\kappa + 2U_am_s]).$$

This is the equation for the spectrum in this model.

3.2 Almost Infinite Square Well-Approximation

While we can solve equation (3.33) numerically to obtain the excitation spectrum for a given set of parameters, we would like to get an expression that is easier to understand analytically, for example to see which parameters the induced gap in the 2DEG depends on. Therefore we follow a similar procedure as used in ref. [22]: we define the following:

$$s \equiv \frac{p_z m_n}{k_0 m_s}; \quad w \equiv \frac{2U_a m_n}{k_0} + \frac{m_n \kappa}{m_s k_0}; \quad k_e \equiv k_0 + \delta k_0; \quad k_h \equiv k_0 + \bar{\delta} k_0 \quad \alpha_k \equiv d\delta k_0; \quad \bar{\alpha}_k \equiv d\bar{\delta} k_0, \tag{3.34}$$

where $k_0 \equiv \pi/d$, the wavenumber of the ground state of an infinite square well of width d.
We now assume that only the lowest subband in the 2DEG is occupied, and that to a good approximation the wavenumber in the 2DEG matches that of the ground state in the infinite square well; under this approximation, the following holds:

$$\frac{\delta k_0}{k_0}, \frac{\bar{\delta} k_0}{k_0} << 1 \;\Leftrightarrow\; \alpha_k, \bar{\alpha}_k << 1. \tag{3.35}$$

We will call this approximation the "Almost Infinite Square Well"-approximation (AISW). Now expanding the sines and cosines in equation (3.33) to first order in $\alpha_k, \bar{\alpha}_k$ we get:

$$is\frac{E_s}{\xi_s}(\alpha_k - \bar{\alpha}_k) + 1 + \alpha_k \bar{\alpha}_k \left(s^2 + w^2\right) + w(\alpha_k + \bar{\alpha}_k) = 0. \tag{3.36}$$

Now we need to rewrite the $\alpha_k, \bar{\alpha}_k$ in terms of the variables we want to end up with in an equation. Let us first define the following:

$$\xi_n \equiv \frac{k_{||}^2 - k_{F0}^2}{2m_n}; \quad \frac{k_{F0}^2}{2m_n} = \mu - V_0 - \frac{k_0^2}{2m_n}, \tag{3.37}$$

where k_{F0} is the fermi-wavenumber in the absence of any coupling to the superconductor, and ξ_n is the kinetic energy relative to the Fermi energy with infinite barrier between the two materials.

If we invoke the definitions from equations (3.34) and (3.37), and use that in our BDG equations (3.4), we can arrive at the following relations:

$$E_n = \xi_n + \frac{k_0 \delta k_0}{m_n} = -\left(\xi_n + \frac{k_0 \delta \bar{k}_0}{m_n}\right). \tag{3.38}$$

From these relations we can arrive at:

$$\alpha_k \equiv d\delta k_0 = \frac{d m_n}{k_0}(E_n - \xi_n) = \frac{d^2 m_n}{\pi}(E_n - \xi_n) = \frac{E_n - \xi_n}{\epsilon_0}. \tag{3.39}$$

Similar calulations lead to:

$$\bar{\alpha_k} = -\frac{E_n + \xi_n}{\epsilon_0}; \quad \alpha_k \bar{\alpha_k} = \frac{\xi_n^2 - E_n^2}{\epsilon_0^2}; \quad \alpha_k^2 + \bar{\alpha_k}^2 = \frac{2(\xi_n^2 + E_n^2)}{\epsilon_0^2}. \tag{3.40}$$

Invoking these rewritings into equation (3.36) leads to:

$$0 = 1 + \frac{\xi_n^2 - E_n^2}{\epsilon_0^2}(w^2 + s^2) - 2w\frac{\xi_n}{\epsilon_0} - \frac{2sE_nE_s}{\epsilon_0(\Delta^2 - E_s^2)^{1/2}} \Leftrightarrow \tag{3.41}$$

$$E_n^2 + \frac{2s\epsilon_0 E_n E_s}{(\Delta^2 - E_s^2)^{1/2}(w^2 + s^2)} = \xi_s^2 + \frac{\epsilon_0^2}{w^2 + s^2} - \frac{2w\epsilon_0 \xi_n}{w^2 + s^2}. \tag{3.42}$$

Now defining:

$$\epsilon_{g0} \equiv \frac{s\epsilon_0}{w^2 + s^2}, \tag{3.43}$$

and rearranging a bit, equation (3.42) becomes:

$$\left[E_n^2 + \frac{2\epsilon_{g0}E_nE_s}{(\Delta^2 - E_s^2)^{1/2}}\right] = \left(\xi_n - \frac{w}{s}\epsilon_{g0}\right)^2 + \epsilon_{g0}^2. \tag{3.44}$$

This is the final form of the equation for the spectrum in this approximation. Let us investigate some limits of equation (3.44) for a moment. We see that for $\epsilon_{g0} \to 0$ the terms that contain E_s vanish; this effectively can be understood as if the superconductor plays no role in the equation anymore. Thus we might conjecture that ϵ_{g0} has something to do with the coupling between the superconducting and the 2DEG regions. Also we see on the RHS of equation (3.44) that the kinetic energy in the 2DEG in the absence of coupling, ξ_n, is renormalized into an effective kinetic energy, ξ:

$$\xi \equiv \xi_n - \frac{w}{s}\epsilon_{g0}. \tag{3.45}$$

We also see in equation (3.44) that both the magnetic field in the superconductor and the semiconductor figurate, so that the slope of the energy as a magnetic field may be some combination of the two g-factors, which can in principle be found by solving the above equation for E; this is not doable analytically, but numerically it is easy. Some analysis on this is the subject of the next section.

From equation (3.44) we can try to find the induced superconducting gap in the 2DEG, similarly to what is done in ref. [22]. The induced gap is defined by:

$$\Delta_{ind} \equiv \min_{k_{||}} E(k_{||}). \tag{3.46}$$

If we make the assumption:

$$\frac{\epsilon_{g0}}{\Delta} << 1, \tag{3.47}$$

we can ignore the second term in the LHS parenthesis in equation (3.44), leading to:

$$E_n = \pm\left[(\xi_n - \frac{w}{s}\epsilon_{g0})^2 + \epsilon_{g0}^2\right]^{1/2}. \tag{3.48}$$

This has exactly the form we expect for a particle in a superconductor; a kinetic term which varies quadratically as a function of $k_{||}$ and then a constant energy contribution - a gap that the particle has as a minimum possible energy. Thus we can simply read off the induced gap in the approximation (3.47) as:

$$\Delta_{ind} = \epsilon_{g0} = \frac{\epsilon_0 s}{s^2 + w^2}. \tag{3.49}$$

If we want a more exact form of the induced gap, we need of course only solve equation (3.44) for the minimum energy as a function of $k_{||}$ for given parameters.

We will compare equation (3.44) to the energy spectrum you get in a tunneling model in section 4.

3.3 Effective g-factor in the AISW-Approximation

We have seen from equation (3.44) that both the magnetic field in the superconductor and the semiconductor mix in the equation for the sub-gap spectrum. One question that we will try to answer is whether the effective g-factor tells us something about the microscopics of our system. In the next section we will do some analysis on the relation between the effective g-factor and the wavefunction probability density. We will also investigate the effective g-factor analytically in the small-B-field limit.

3.3.1 Relation to the Wavefunction Probability Density

The Hamiltonian we have can be written as:

$$\mathcal{H} = \mathcal{H}_0 + \mathcal{H}'; \qquad \mathcal{H}' = g(z)B\sigma; \qquad g(z) = g_s\Theta(-z) + g_n\Theta(z)\Theta(d-z), \tag{3.50}$$

where $\sigma = \pm 1$. Say we treat the magnetic field as a perturbation. Then using the well-known result from 1st order perturbation (see e.g. ref. [23]), we get the change in the energy to be:

$$\Delta E = \langle\bar{\psi}_0|\mathcal{H}'|\bar{\psi}_0\rangle = \int \mathrm{d}\mathbf{r}|\langle\mathbf{r}|\,\bar{\psi}_0\rangle|^2 Bg(z)\sigma = \left(g_sB\int_{-\infty}^{0}\mathrm{d}z|\bar{\psi}_0(z)|^2 + g_nB\int_0^d \mathrm{d}z|\bar{\psi}_0(z)|^2\right)\left[\int \mathrm{d}\mathbf{r}_{||}|\bar{\psi}_0(\mathbf{r}_{||})|^2\right] \tag{3.51}$$

$$= \left(g_s\frac{\int_{-\infty}^{0}\mathrm{d}z|\bar{\psi}_0(z)|^2}{\int_{-\infty}^{d}\mathrm{d}z|\bar{\psi}_0(z)|^2} + g_n\frac{\int_0^d\mathrm{d}z|\bar{\psi}_0(z)|^2}{\int_{-\infty}^{d}\mathrm{d}z|\bar{\psi}_0(z)|^2}\right)B \equiv g^*B. \tag{3.52}$$

So we see that in 1st order perturbation, the effective g-factor is a mix of g_n and g_s, weighted by where the quasiparticle lives. The question is then: How far does this result extend when the magnetic field becomes a more dominating factor in the calculations?

The Feynman-Hellmann Theorem [23] is very useful here. It states simply that for a Hamiltonian which is a function of some parameter λ and has eigenfunctions $\psi_n(\lambda)$ with non-degenerate eigenvalues $E_n(\lambda)$ the eigenenergies satisfy the following relation:

$$\frac{\partial E_n}{\partial\lambda} = \langle\psi_n|\frac{\partial H}{\partial\lambda}|\psi_n\rangle \tag{3.53}$$

In our case with the Hamiltonian from equation (3.50) we see that this becomes:

$$\frac{\partial E_n}{\partial B} = \langle\bar{\psi}_n|\frac{\partial H}{\partial B}|\bar{\psi}_n\rangle = \int d\mathbf{r}|\bar{\psi}_n(\mathbf{r})|^2 g(z). \tag{3.54}$$

So we see that the instantaneous slope of an eigenenergy of our system must similarly to the 1st order perturbation result be a linear sum of g_n weighted by the weight of the wavefunction probability density in the normal region, and g_s weighted by the weight in the superconducting region. So on a general basis, the slope of the energy must be related to where the wavefunction lives.

Now what is experimentally interesting is not so much the information about how the wavefunction probability density changes as a function of magnetic field, but rather where the quasiparticle is located at zero field since this says something about the design of the 2DEG (i.e. to which extent the system confines the wavefunction as intended etc.). Therefore it is interesting to look at the formula for the effective g-factor at small B-fields.

3.3.2 Effective g-factor for Small B-fields

It is of interest to derive how the effective g-factor varies as a function of the model parameters. The basic question is whether there is some knowledge about the system to be had by extracting the effective g-factor in an experiment, and if so, what knowledge? The experimentally relevant limit is for small B-fields, but without other approximations on the parameters. Let us now start from the expression for the energy, equation (3.44):

$$E_n^2 + 2\epsilon_{g0}\frac{E_n E_s}{\sqrt{\Delta^2 - E_s^2}} = \xi^2 + \epsilon_{g0}^2 \tag{3.55}$$

We assume that we have solved for the sub-gap state energies at zero B-field, E_0:

$$E_0^2\left(1 + \frac{2\epsilon_{g0}}{\sqrt{\Delta^2 - E_0^2}}\right) = \xi^2 + \epsilon_{g0}^2 \tag{3.56}$$

The positive-energy solution to this equation is plotted in figure 3.3.1 (the negative energy that follows from particle-hole symmetry is ignored here). Here we see that the minimal energy solution is always found for zero renormalized kinetic energy, $\xi = 0$ (see equation (3.45)). Note that only the square of ξ figurates in equation (3.55), so negative ξ is redundant. This means that we can find the induced gap, Δ_{ind} (see equation (3.46)) as the solution to the equation (3.56) with $\xi = 0$, for zero B-field. Also, interestingly the curve is not monotonous as a function of ϵ_{g0} for $\xi \neq 0$.

We are now interested in how the energy E_0 changes for small magnetic fields. Let us therefore define the following:

$$E = E_0 - g^* B, \tag{3.57}$$

where we neglect higher order terms in the magnetic field. g^* defines the effective g-factor. Then inserting this value in the energy equation (3.55) yields:

$$(E_0 - (g^* + g_n\sigma)B)^2 + \frac{2\epsilon_{g0}(E_0 - (g^* + g_s\sigma)B)(E_0 - (g^* + g_n\sigma)B)}{\sqrt{\Delta^2 - (E_0 - (g^* + g_s\sigma)B)^2}} = \xi^2 + \epsilon_{g0}^2. \tag{3.58}$$

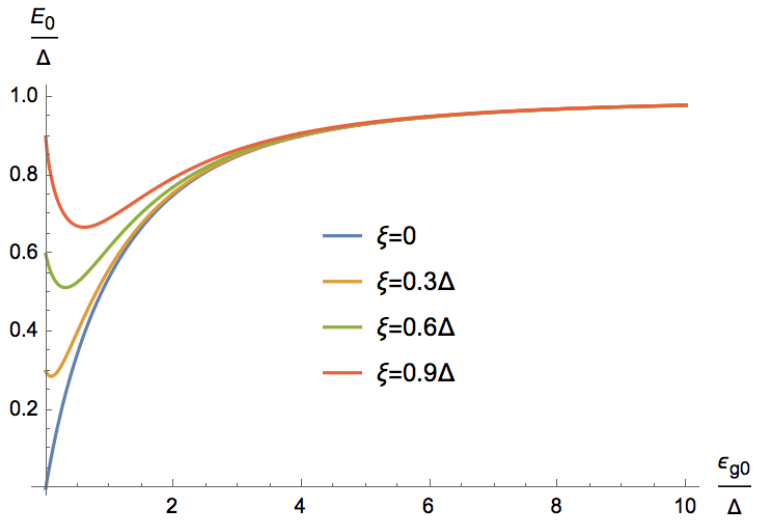

Figure 3.3.1: Here we see how the positive energy changes as a function of the variable ϵ_{g0} for a choice of kinetic energies $\xi < \Delta$. The curve for $\xi = 0$ is equal to the curve for the induced gap as explained in the text.

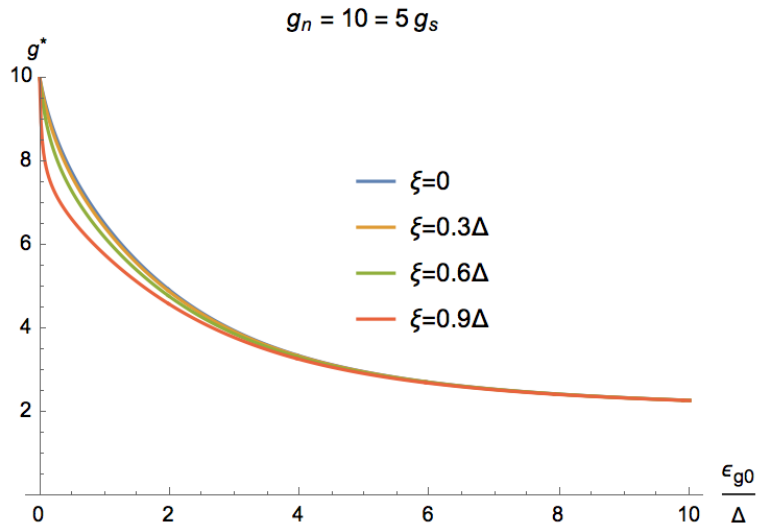

Figure 3.3.2: Here we see how the positive effective g-factor solution varies as a function of ϵ_{g0}, the tunnel coupling strength parameter for a choice of kinetic energies $\xi < \Delta$.

Now we expand on both sides of equation (3.58) to only first order in the magnetic field:

$$E_0^2 - 2(g^* + g_n\sigma)E_0 B + \frac{2\epsilon_{g0}}{\sqrt{\Delta^2 - E_0}} E_0(-(g^* + g_s\sigma) - (g^* + g_n\sigma))B \ldots \tag{3.59}$$

$$\ldots + \frac{2E_0^2\epsilon_{g0}}{\sqrt{\Delta^2 - E_0^2}} + \frac{2E_0^3\epsilon_{g0}}{(\Delta^2 - E_0^2)^{3/2}}(-(g^* + g_s\sigma)B) = \xi^2 + \epsilon_{g0}^2. \tag{3.60}$$

Now differentiating with respect to B we obtain:

$$-2(g^*+g_n\sigma)\omega_0 + \frac{2\epsilon_{g0}}{\sqrt{\Delta^2 - E_0}} E_0(-(g^* + g_s\sigma) - (g^* + g_n\sigma)) + \frac{2E_0^3\epsilon_{g0}}{(\Delta^2 - E_0^2)^{3/2}}(-(g^*+g_s\sigma)) = 0 \Rightarrow \tag{3.61}$$

$$g^*\left[-2 - 4\frac{\epsilon_{g0}}{\sqrt{\Delta^2 - E_0^2}} - 2\frac{E_0^2\epsilon_{g0}}{(\Delta^2 - E_0^2)^{3/2}}\right] = g_n\sigma\left[2 + 2\frac{\epsilon_{g0}}{\sqrt{\Delta^2 - E_0^2}}\right] + g_s\sigma\left[2\frac{\epsilon_{g0}}{\sqrt{\Delta^2 - E_0^2}} + \frac{2\epsilon_{g0}E_0^2}{(\Delta^2 - E_0^2)^{3/2}}\right] \Rightarrow \tag{3.62}$$

$$g^* = \pm\frac{g_n\left[1 + \frac{\epsilon_{g0}}{\sqrt{\Delta^2 - E_0^2}}\right] + g_s\left[\frac{\epsilon_{g0}}{\sqrt{\Delta^2 - E_0^2}} + \frac{\epsilon_{g0}E_0^2}{(\Delta^2 - E_0^2)^{3/2}}\right]}{1 + 2\frac{\epsilon_{g0}}{\sqrt{\Delta^2 - E_0^2}} + \frac{E_0^2\epsilon_{g0}}{(\Delta^2 - E_0^2)^{3/2}}}, \tag{3.63}$$

where the $\pm$ originates from the $\sigma = \pm 1$. We have plotted the positive effective g-factor solution for some choices of kinetic energy in figure 3.3.2. Note that we choose $\xi < \Delta$ so that we only look at sub-gap energy states (see figure 3.3.1). Since (3.55) only depends on the square of ξ we do not investigate negative ξ.

We see from figure 3.3.2 that $g^* \to g_n$ for $\epsilon_{g0} \to 0$. Since $\epsilon_{g0} \to 0$ means there is no induced gap in the 2DEG and thus no proximity effect to the superconductor we can see this limit as an "isolated 2DEG"-limit, where it makes sense that $g^* \to g_n$. Conversely, we see from figure 3.3.2 that when ϵ_{g0} increases the finite semiconductor begins to become negligible due to the infinite superconductor; thus $g^* \to g_s$, i.e. the wavefunction lives mostly in the superconductor. Also we found that the induced gap in the 2DEG depends critically on ϵ_{g0}, according to figure 3.3.1 with $\xi = 0$.

3.4 Numerical analysis

In this section we will calculate the effective g-factor and compare it with where the wavefunction lives, both via solving analytic equations numerically - see section 8.2 for details about the procedure. To do this we of course have to specify the model parameters. We choose these not to match experiment, but to exemplify the theory up until this point. We choose the bulk aluminium superconducting gap (see e.g. [24] p. 268):

$$U_a = 0; \quad \frac{m_n}{m_s} = 0.1; \quad \mu = 6\text{eV}; \quad \Delta = 0.340\text{meV} \quad d = 20\text{nm}; \quad \mu - V_0 = 27.05\Delta. \tag{3.64}$$

To check that we are really in the AISW-approximation regime we calculate for these parameters for $k_{||} = 0$:

$$\frac{k_e}{k_0} = 1.005; \quad \frac{k_h}{k_0} = 0.976. \tag{3.65}$$

So we see that we are indeed in the AISW-approximation regime. We want now to calculate the factor ϵ_{g0} for our parameters:

$$\frac{\epsilon_{g0}}{\Delta} = \frac{s}{s^2 + w^2}\frac{\epsilon_0}{\Delta} = 2.19. \tag{3.66}$$

From the discussion of figure 3.3.1 we know that we can find the induced gap, Δ_{ind} by solving the energy equation for the above value of ϵ_{g0} with $\xi = 0$:

$$\Delta_{\text{ind}}^2 \left(1 + \frac{2\epsilon_{g0}}{\sqrt{\Delta^2 - \Delta_{\text{ind}}^2}}\right) = \epsilon_{g0}^2 \Rightarrow \tag{3.67}$$

$$\Delta_{\text{ind}} = 0.78\Delta, \tag{3.68}$$

as can also be confirmed by looking at figure 3.4.1, where we solved equation (3.33). Also due to this figure we can tell that for $k_{||} = 0$ we are very close to the minimum energy value, $\xi = 0$.

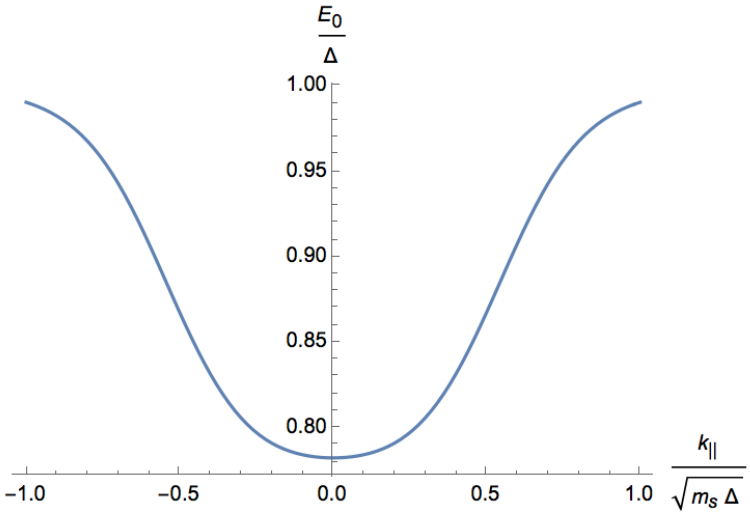

Figure 3.4.1: Here we see how the positive energy solution to equation (3.33) (the negative hole energy solution is ignored here) changes as a function of the variable $k_{||}$. It is clear that an induced gap of approximately 0.78Δ is induced for this set of parameters.

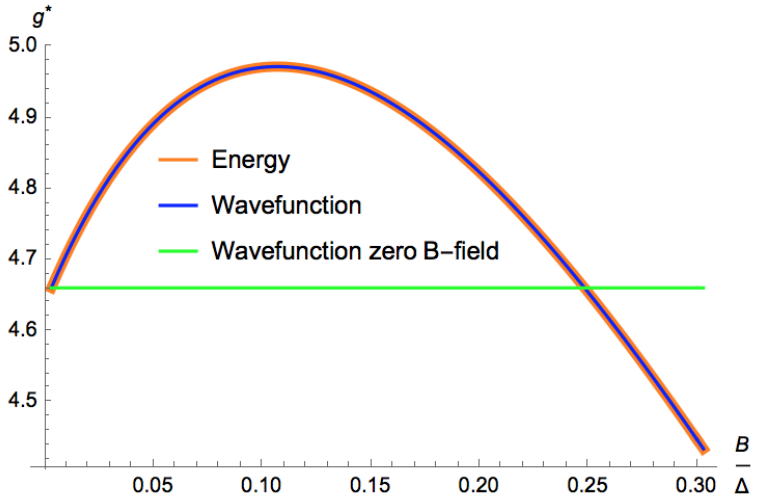

Figure 3.4.2: Here we see how the effective g-factor (the negative hole energy solution is ignored here) changes as a function of the variable ϵ_{g0}. The 'Energy'-curve is found via solving equation (3.33) numerically. The 'Wavefunction'-curves are found numerically via solving for the wavefunction as explained in Appendix B.

Now we want to compare finding the effective g-factor by calculating the wavefunction numerically and comparing with explicitly finding the slope of the energy with respect to magnetic field. This is done in figure 3.4.2.

First of all the curve 'Energy' and 'Wavefunction' lie perfectly on top of each other, indicating that the Feynman-Hellmann Theorem is indeed applicable in this system. Secondly we see that indeed the correct $\frac{\partial E}{\partial B}$ changes as a function of the magnetic field, confirming that the 1st order perturbation result is indeed perturbative in B. However, the discrepancy for these parameters is actually not very significant, even when g^*B becomes of order Δ.

It is important to stress though that these findings are specific to the parameters chosen here, and that the parameters would have to be changed for another sysem and the analysis redone to see exactly for how large magnetic fields one could still use the slope of the energy wrt. magnetic field as an indication of where the wavefunction lives.

Finally we include some plots of the wavefunction probability density for zero magnetic field in

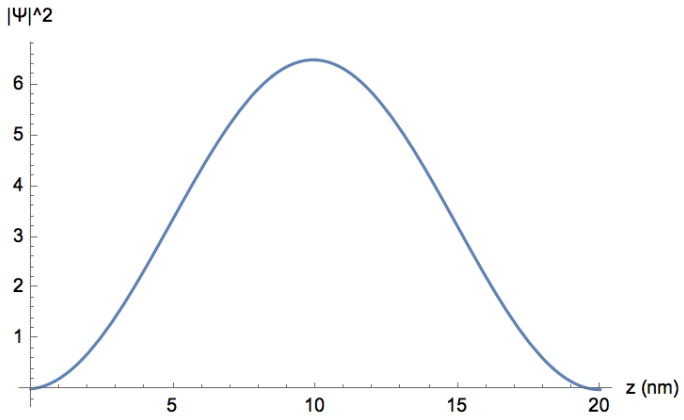

Figure 3.4.3: Here we see how the wavefunction probability density for zero B-field varies as a function of distance, z, inside the 2DEG. The superconductor-2DEG interface is located at $z = 0$.

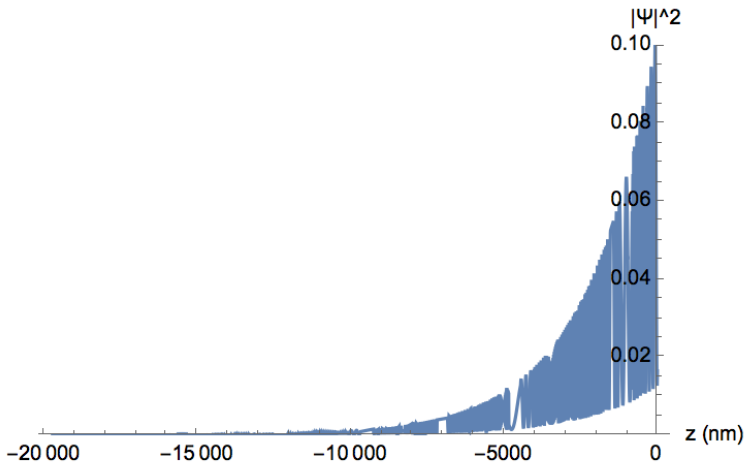

Figure 3.4.4: Here we see how the wavefunction probability density for zero B-field varies as a function of distance, z, inside the superconductor. The superconductor-2DEG interface is located at $z = 0$. Clearly the probability density per length is much lower than in the 2DEG, figure 3.4.3, but the decay length is sufficiently big to ensure a substantial weight when integrated over the semi-infinite superconductor.

figures 3.4.3, 3.4.4. The shape confirms the notion that we have something like an approximate ground state of the infinite square well in the 2DEG, with a minimal tail inside the superconductor, where the wave-function attenuates exponentially. However, since the decay length in the superconductor is so large for our system, the tail will actually result in a substantial weight when integrated up over all of the superconductor's space. This also highlights one of the problems of this model when trying to compare with the experiments at the Center of Quantum Devices; there they have a nanometer thin layer of Aluminium. Since the wave-function dies out so slowly in the superconductor, this means that the half-infinite superconductor used in this model is likely not a good approximation. It would not be too difficult to include a finite-size superconductor as well, but the analysis would have to be redone.

Chapter 4

Green's Function Approach to an N-S Junction

In order to tackle the problem with both spin-orbit, zeeman field and superconductivity, we will use a greens-function approach. We will be working in the imaginary-time regime in real space (see e.g. ref. [13] chpt. 10), i.e. work with Matsubara Green's-functions such as:

$$\mathcal{G}(\mathbf{r}\tau\sigma, \mathbf{r}'\tau'\sigma') \equiv -\Big\langle T_\tau\Big(\Psi_\sigma(\mathbf{r},\tau)\Psi^\dagger_{\sigma'}(\mathbf{r}',\tau')\Big)\Big\rangle. \tag{4.1}$$

It will prove useful to solve the equations of motion in a matrix structure, using the following definition:

$$\underline{\underline{\mathcal{G}}}(\mathbf{r}\tau, \mathbf{r}'\tau') = -\left\langle T_\tau\left(\begin{pmatrix}\Psi_\uparrow(\mathbf{r},\tau)\\ \Psi_\downarrow(\mathbf{r},\tau)\\ \Psi^\dagger_\downarrow(\mathbf{r},\tau)\\ \Psi^\dagger_\uparrow(\mathbf{r},\tau)\end{pmatrix}\otimes\begin{pmatrix}\Psi^\dagger_\uparrow(\mathbf{r}',\tau') & \Psi^\dagger_\downarrow(\mathbf{r}',\tau') & \Psi_\downarrow(\mathbf{r}',\tau') & \Psi_\uparrow(\mathbf{r}',\tau')\end{pmatrix}\right)\right\rangle \equiv -\Big\langle T_\tau(\bar\Psi\otimes\bar\Psi^\dagger)\Big\rangle \tag{4.2}$$

A couple of useful relations are:

$$\{\bar\Psi(\mathbf{r}), \bar\Psi^\dagger(\mathbf{r}')\} \equiv \bar\Psi(\mathbf{r})\otimes\bar\Psi^\dagger(\mathbf{r}') + \bar\Psi^\dagger(\mathbf{r}')\otimes\bar\Psi(\mathbf{r}) = \delta(\mathbf{r}-\mathbf{r}')\mathbb{1}_{4\times4}, \tag{4.3}$$

and:

$$\{\bar\Psi(\mathbf{r}), \bar\Psi(\mathbf{r}')\} = \delta(\mathbf{r}-\mathbf{r}')\begin{pmatrix}0&0&0&-1\\0&0&1&0\\0&1&0&0\\-1&0&0&0\end{pmatrix} \equiv \underline{\underline{\chi}}\delta(\mathbf{r}-\mathbf{r}'). \tag{4.4}$$

which can be verified explicitly. Interestingly, we recognize $\underline{\underline{\chi}}$ as the same matrix that figurates in the particle-hole symmetry operator, equation (2.48). This suggests that the approach we are using in setting up the model captures the particle-hole symmetry of the problem (see section 2.3.1), which we will see explicitly later on.

Let us now proceed to solve the problem. First we must write up our tunneling Hamiltonian in the Bogoliubov-de-Gennes formalism (see section 2.3):

$$H = H_n + H_s + H_t = \frac{1}{2}\int d\mathbf{r}\left[\bar\Psi^\dagger_\alpha(\mathbf{r})\mathcal{H}^n_{\alpha\alpha'}\bar\Psi_{\alpha'}(\mathbf{r}) + \bar\Phi^\dagger_{\alpha'}(\mathbf{r})\mathcal{H}^s_{\alpha\alpha'}\bar\Phi_{\alpha'}(\mathbf{r}) + \left(\int d\mathbf{r}'\bar\Psi^\dagger_\alpha(\mathbf{r})\tilde T_{\alpha\alpha'}\bar\Phi_{\alpha'}(\mathbf{r}') + h.c.\right)\right] \tag{4.5}$$

where $\alpha, \alpha' \in \{1,2,3,4\}$. Also note that the Ψ's are confined in real space to the 2DEG region, whereas the Φ's are confined to live in the superconductor. The parts that make up the 1st quantized Hamiltonian are, for an in-plane magnetic field:

$$\mathcal{H}_n = \left(\frac{k_x^2+k_y^2+k_z^2}{2m_n} - \mu_n\right)\tau_z + B_n\sigma_x + \alpha(k_y\sigma_x - k_x\sigma_y)\tau_z; \qquad \mathcal{H}_s = \left(\frac{p_x^2+p_y^2+p_z^2}{2m_s} - \mu_s\right)\tau_z + B_s\sigma_x + \Delta\tau_x; \tag{4.6}$$

Note that the magnetic field could also be chosen to be $B\sigma_z$, in order to model a magnetic field out of the 2DEG plane. For the tunneling term we choose the simplest approach, which is to say that the tunneling is local in space, only takes place in the interface between the two materials and does not involve any spin- or particle-hole-coupling terms:

$$\tilde{T}(\mathbf{r},\mathbf{r}') = \delta(\mathbf{r}_{||} - \mathbf{r}'_{||})\delta(z)\delta(z')t_0\mathbb{1} = \delta(\mathbf{r}-\mathbf{r}')\delta(z)t_0\mathbb{1} \tag{4.7}$$

Thus we can also write the tunneling term in the Hamiltonian in the same way as the other terms:

$$H_T = \frac{1}{2}\int \mathrm{d}\mathbf{r}\int \mathrm{d}\mathbf{r}'\bar{\Psi}^\dagger_\alpha(\mathbf{r})\tilde{T}_{\alpha\alpha'}\bar{\Phi}_{\alpha'}(\mathbf{r}') + h.c. = \frac{1}{2}\int \mathrm{d}\mathbf{r}\bar{\Psi}^\dagger_\alpha(\mathbf{r})T_{\alpha\alpha'}\bar{\Phi}_{\alpha'}(\mathbf{r}) + h.c., \tag{4.8}$$

where:

$$T \equiv \delta(z)t_0\mathbb{1}. \tag{4.9}$$

Now we write up the equation of motion:

$$-\partial_\tau G(\mathbf{r}\tau,\mathbf{r}'\tau') = +\partial_\tau\Big\langle T_\tau\Psi(\mathbf{r},\tau)\otimes\Psi^\dagger(\mathbf{r}',\tau')\Big\rangle = \tag{4.10}$$

$$\partial_\tau\Big\langle\theta(\tau-\tau')\Psi(\mathbf{r},\tau)\otimes\Psi^\dagger(\mathbf{r}',\tau') - \theta(\tau'-\tau)\Psi^\dagger(\mathbf{r}',\tau')\otimes\Psi(\mathbf{r},\tau)\Big\rangle =$$

$$\mathbb{1}\delta(\mathbf{r}-\mathbf{r}')\delta(\tau-\tau') + \Big\langle T_\tau[H,\Psi(\mathbf{r})](\tau)\otimes\Psi^\dagger(\mathbf{r}',\tau')\Big\rangle.$$

So we will need to find the equal-time commutator between the Hamiltonian and the quantum field operator $\Psi(\mathbf{r})$. Digging right in, by looking at an arbitrary component of the $\bar{\Psi}(\mathbf{r})$-vector yields (with Einstein summation-convention of repeated indices):

$$[H,\bar{\Psi}_\beta(\mathbf{r})] = \frac{1}{2}\int d\mathbf{r}'\Big[\bar{\Psi}^\dagger_\alpha(\mathbf{r}')\mathcal{H}^n_{\alpha\alpha'}\bar{\Psi}_{\alpha'}(\mathbf{r}') + \bar{\Phi}^\dagger_{\alpha'}(\mathbf{r}')\mathcal{H}^s_{\alpha\alpha'}\bar{\Phi}_{\alpha'}(\mathbf{r}') + \Big(\bar{\Psi}^\dagger_\alpha(\mathbf{r}')T_{\alpha\alpha'}\bar{\Phi}_{\alpha'}(\mathbf{r}') + h.c.\Big),\bar{\Psi}_\beta(\mathbf{r})\Big] = \tag{4.11}$$

$$\frac{1}{2}\int d\mathbf{r}'\Big(\mathcal{H}^n_{\alpha,\alpha'}\Big[\bar{\Psi}^\dagger_\alpha(\mathbf{r}')\bar{\Psi}_{\alpha'}(\mathbf{r}'),\bar{\Psi}_\beta(\mathbf{r})\Big] + T_{\alpha,\alpha'}\Big[\bar{\Psi}^\dagger_\alpha(\mathbf{r}')\bar{\Phi}_{\alpha'}(\mathbf{r}'),\bar{\Psi}_\beta(\mathbf{r})\Big] + T^*_{\alpha',\alpha}\Big[\bar{\Phi}^\dagger_{\alpha'}(\mathbf{r}')\bar{\Psi}_\alpha(\mathbf{r}'),\bar{\Psi}_\beta(\mathbf{r})\Big]\Big) = \tag{4.12}$$

$$\frac{1}{2}\int d\mathbf{r}'\Bigg(\mathcal{H}^n_{\alpha,\alpha'}\Big(\bar{\Psi}^\dagger_\alpha(\mathbf{r}')\{\bar{\Psi}_{\alpha'}(\mathbf{r}'),\bar{\Psi}_\beta(\mathbf{r})\} - \{\bar{\Psi}^\dagger_\alpha(\mathbf{r}'),\bar{\Psi}_\beta(\mathbf{r})\}\Big)\ldots \tag{4.13}$$

$$\ldots - T_{\alpha,\alpha'}\{\bar{\Psi}^\dagger_\alpha(\mathbf{r}'),\bar{\Psi}_\beta(\mathbf{r})\}\bar{\Phi}_{\alpha'}(\mathbf{r}') + T^*_{\alpha',\alpha}\bar{\Phi}^\dagger_{\alpha'}(\mathbf{r}')\{\bar{\Psi}_\alpha(\mathbf{r}'),\bar{\Psi}_\beta(\mathbf{r})\}\Bigg) =$$

$$\frac{1}{2}\Big(\mathcal{H}^n_{\alpha,\alpha'}\Big[\chi_{\alpha'\beta}\bar{\Psi}^\dagger_\alpha(\mathbf{r}) - \mathbb{1}_{\alpha\beta}\bar{\Psi}_{\alpha'}(\mathbf{r})\Big] - \mathbb{1}_{\alpha\beta}\bar{\Phi}_{\alpha'}(\mathbf{r})T_{\alpha\alpha'} + \chi_{\alpha\beta}\bar{\Phi}^\dagger_{\alpha'}(\mathbf{r})T^*_{\alpha'\alpha}\Big). \tag{4.14}$$

From this we can extract the underlying matrix structure. This results in the following:

$$-\partial_\tau\underline{\underline{\mathcal{G}}}(\mathbf{r}\tau,\mathbf{r}'\tau') = \mathbb{1}\delta(\mathbf{r}-\mathbf{r}')\delta(\tau-\tau') + \Big\langle T_\tau[H,\Psi(\mathbf{r})](\tau)\otimes\Psi^\dagger(\mathbf{r}',\tau')\Big\rangle = \tag{4.15}$$

$$\delta(\tau-\tau')\delta(\mathbf{r}-\mathbf{r}')\mathbb{1}+\frac{1}{2}\Bigg(\Big\langle T_\tau\Big(\Big(\bar{\Psi}^\dagger(\mathbf{r},\tau)\mathcal{H}_n\chi\Big)^T\otimes\bar{\Psi}^\dagger(\mathbf{r}',\tau')\Big)\Big\rangle-\Big\langle T_\tau\Big(\mathcal{H}^n\bar{\Psi}(\mathbf{r},\tau)\otimes\bar{\Psi}^\dagger(\mathbf{r}',\tau')\Big)\Big\rangle\ldots$$

$$\ldots-\Big\langle T_\tau\Big(T\bar{\Phi}(\mathbf{r},\tau)\otimes\bar{\Psi}^\dagger(\mathbf{r}',\tau')\Big)\Big\rangle+\Big\langle T_\tau\Big(\Big(\bar{\Phi}^\dagger(\mathbf{r},\tau)T\chi\Big)^T\otimes\bar{\Psi}^\dagger(\mathbf{r}',\tau')\Big)\Big\rangle\Bigg).$$

Here we have four different types of Green's function-matrices:

$$\Big\langle T_\tau\Big(\bar{\Psi}(\mathbf{r},\tau)\otimes\bar{\Psi}^\dagger(\mathbf{r}',\tau')\Big)\Big\rangle;\quad\Big\langle T_\tau\Big(\Big(\bar{\Psi}^\dagger(\mathbf{r},\tau)\Big)^T\otimes\bar{\Psi}^\dagger(\mathbf{r}',\tau')\Big)\Big\rangle;\tag{4.16}$$

$$\Big\langle T_\tau\Big(\bar{\Phi}(\mathbf{r},\tau)\otimes\bar{\Psi}^\dagger(\mathbf{r}',\tau')\Big)\Big\rangle;\quad\Big\langle T_\tau\Big(\Big(\bar{\Phi}^\dagger(\mathbf{r},\tau)\Big)^T\otimes\bar{\Psi}^\dagger(\mathbf{r}',\tau')\Big)\Big\rangle.$$

So normally we would have to repeat the equation of motion-technique on each of these kinds of Green's matrices in order to close the set of equations. However, this is where our the artificial doubling of the spectrum in choosing a 4×4 Nambu spinor comes in play (see section 2.3). Now we can use the particle-hole symmetry to limit our computations. Using the following identities:

$$\mathcal{H}^\dagger=\mathcal{H}\Leftrightarrow\mathcal{H}^T=\mathcal{H}^*;\quad\chi^T=\chi;\quad\chi\chi=1;\quad\big(\chi\bar{\Psi}\big)^T=\bar{\Psi}^\dagger;\quad\big(\chi\bar{\Phi}\big)^T=\bar{\Phi}^\dagger.\tag{4.17}$$

we can perform rewritings similar to the following:

$$\Big(\bar{\Psi}^\dagger(\mathbf{r},\tau)\mathcal{H}_n\chi\Big)^T=\chi^T\mathcal{H}_n^T\bar{\Psi}^{\dagger T}(\mathbf{r},\tau)=\chi\mathcal{H}_n^*\bar{\Psi}^{\dagger T}(\mathbf{r},\tau)=\chi\mathcal{H}_n^*\chi\bar{\Psi}.\tag{4.18}$$

From this we can finally arrive at a nice equation of motion for $\underline{\underline{\mathcal{G}}}(\mathbf{r}\tau,\mathbf{r}'\tau')$, i.e. equation (4.15) becomes:

$$-\partial_\tau\underline{\underline{\mathcal{G}}}(\mathbf{r}\tau,\mathbf{r}'\tau')=\delta(\tau-\tau')\delta(\mathbf{r}-\mathbf{r}')\mathbb{1}+\frac{1}{2}\Bigg(\chi\mathcal{H}_n^*\chi\Big\langle T_\tau\Big(\bar{\Psi}^\dagger(\mathbf{r},\tau)\otimes\bar{\Psi}^\dagger(\mathbf{r}',\tau')\Big)\Big\rangle-\mathcal{H}^n\Big\langle T_\tau\Big(\bar{\Psi}(\mathbf{r},\tau)\otimes\bar{\Psi}^\dagger(\mathbf{r}',\tau')\Big)\Big\rangle\ldots\tag{4.19}$$

$$\ldots-T\Big\langle T_\tau\Big(\bar{\Phi}(\mathbf{r},\tau)\otimes\bar{\Psi}^\dagger(\mathbf{r}',\tau')\Big)\Big\rangle+\chi T^*\chi\Big\langle T_\tau\Big(\bar{\Phi}(\mathbf{r},\tau)\otimes\bar{\Psi}^\dagger(\mathbf{r}',\tau')\Big)\Big\rangle\Bigg)\Rightarrow$$

$$-\partial_\tau\underline{\underline{\mathcal{G}}}(\mathbf{r}\tau,\mathbf{r}'\tau')=\delta(\tau-\tau')\delta(\mathbf{r}-\mathbf{r}')\mathbb{1}+\frac{1}{2}\Big((-\chi\mathcal{H}_n^*\chi+\mathcal{H}^n)\underline{\underline{\mathcal{G}}}(\mathbf{r}\tau,\mathbf{r}'\tau')+(-\chi T^*\chi+T)\underline{\underline{\mathcal{F}}}(\mathbf{r}\tau,\mathbf{r}'\tau')\Big).\tag{4.20}$$

Here we have introduced the definition:

$$\underline{\underline{\mathcal{F}}}\equiv-\Big\langle T_\tau\bar{\Phi}\otimes\bar{\Psi}^\dagger\Big\rangle.\tag{4.21}$$

Note that we have now reduced our problem to one only involving two unknowns, $\underline{\underline{\mathcal{G}}}$ and $\underline{\underline{\mathcal{F}}}$. Now to close the equations we need to find the equation of motion for $\underline{\underline{\mathcal{F}}}$. Performing the same procedure as above we obtain:

$$-\partial_\tau\underline{\underline{\mathcal{F}}}(\mathbf{r}\tau,\mathbf{r}'\tau')=(\mathcal{H}_s-\chi\mathcal{H}_s^*\chi)\underline{\underline{\mathcal{F}}}(\mathbf{r}\tau,\mathbf{r}'\tau')+(T^*-\chi T\chi)\underline{\underline{\mathcal{G}}}(\mathbf{r}\tau,\mathbf{r}'\tau').\tag{4.22}$$

Now we make a Fourier-transformation of the imaginary time, using that all Matsubara Green's functions' time-dependence only depends on the time difference, i.e. (for $\tau>\tau'$):

$$\mathcal{G}(\tau,\tau')=\mathcal{G}(\tau-\tau').\tag{4.23}$$

This leads to the equations:

$$i\omega_n\underline{\underline{\mathcal{G}}}(\mathbf{r},\mathbf{r}',i\omega_n)=\delta(\mathbf{r}-\mathbf{r}')\mathbb{1}+\frac{1}{2}\Big((\mathcal{H}^n-\chi\mathcal{H}_n^*\chi)\underline{\underline{\mathcal{G}}}(\mathbf{r},\mathbf{r}',i\omega_n)+(T-\chi T^*\chi)\underline{\underline{\mathcal{F}}}(\mathbf{r},\mathbf{r}',i\omega_n)\Big);\tag{4.24}$$

$$i\omega_n \underline{\underline{\mathcal{F}}}(\mathbf{r},\mathbf{r}',i\omega_n) = \frac{1}{2}\Big((\mathcal{H}_s - \chi\mathcal{H}_s^*\chi)\underline{\underline{\mathcal{F}}}(\mathbf{r},\mathbf{r}',i\omega_n) + (T^* - \chi T\chi)\underline{\underline{\mathcal{G}}}(\mathbf{r},\mathbf{r}',i\omega_n)\Big). \tag{4.25}$$

Combining equations (4.24) and (4.25) we can solve for the Green's function:

$$\underline{\underline{\mathcal{F}}} = \left(i\omega_n + \frac{1}{2}(\chi\mathcal{H}_s^*\chi - \mathcal{H}_s)\right)^{-1}(T^* - \chi T\chi)\underline{\underline{\mathcal{G}}} \Rightarrow \tag{4.26}$$

$$\underline{\underline{\mathcal{G}}} = \left(i\omega_n + \frac{1}{2}(\chi\mathcal{H}_n^*\chi - \mathcal{H}_n)\right)^{-1}\left(\delta(\mathbf{r}-\mathbf{r}')\mathbb{1} + \frac{1}{2}(T - \chi T^*\chi)\left(i\omega_n + \frac{1}{2}(\chi\mathcal{H}_s^*\chi - \mathcal{H}_s)\right)^{-1}\frac{1}{2}(T^* - \chi T\chi)\underline{\underline{\mathcal{G}}}\right). \tag{4.27}$$

We see from this result a clear Dyson-equation structure. This means that we can simply read off the self-energy contribution:

$$\Sigma = \frac{1}{2}(T - \chi T^*\chi)\left(i\omega_n + \frac{1}{2}(\chi\mathcal{H}_s^*\chi - \mathcal{H}_s)\right)^{-1}\frac{1}{2}(T^* - \chi T\chi) \tag{4.28}$$

Now we can simplify this using the following relations:

$$\chi\mathcal{H}_n^*\chi = -\mathcal{H}_n; \quad \chi\mathcal{H}_s^*\chi = -\mathcal{H}_s; \quad \chi T^*\chi = -T; \tag{4.29}$$

These identities follow directly from the particle-hole symmetry in our system (see section 2.3.1):

$$P\mathcal{H}P^\dagger = -\mathcal{H} \Leftrightarrow \chi\mathcal{H}^*\chi = -\mathcal{H}. \tag{4.30}$$

This results in:

$$\Sigma(\mathbf{r},\mathbf{r}',i\omega_n) = T(i\omega_n - \mathcal{H}_s)^{-1}T^* = T\underline{\underline{\mathcal{G}_{0s}}}(\mathbf{r},\mathbf{r}',i\omega_n)T^* \tag{4.31}$$

Using the expression for the tunneling terms, equation (4.7), yields:

$$\Sigma(\mathbf{r},\mathbf{r}',i\omega_n) = \delta(z)\delta(z')|t_0|^2\underline{\underline{\mathcal{G}_{0s}}}(\mathbf{r},\mathbf{r}',i\omega_n). \tag{4.32}$$

From here on we follow the procedure outlined in ref. [25]. We rewrite this in the momentum-space representation:

$$\underline{\underline{\mathcal{G}_{0s}}}(\mathbf{r},\mathbf{r}',i\omega_n) = -\Big\langle T_\tau \bar{\Psi}(\mathbf{r}) \otimes \bar{\Psi}^\dagger(\mathbf{r}')(i\omega_n)\Big\rangle \tag{4.33}$$

$$= -\left\langle T_\tau \frac{1}{V}\sum_{\mathbf{k},\mathbf{k}'} e^{i(\mathbf{k}\cdot\mathbf{r}-\mathbf{k}'\cdot\mathbf{r}')}\bar{c}_{\mathbf{k}} \otimes \bar{c}^\dagger_{\mathbf{k}'}(i\omega_n)\right\rangle = \frac{1}{V}\sum_{\mathbf{k},\mathbf{k}'} e^{i(\mathbf{k}\cdot\mathbf{r}-\mathbf{k}'\cdot\mathbf{r}')}\underline{\underline{\mathcal{G}_{0s}}}(\mathbf{k},\mathbf{k}',i\omega_n). \tag{4.34}$$

Now assuming that the superconducting Green's function is translationally invariant we get:

$$\underline{\underline{\mathcal{G}_{0s}}}(\mathbf{r},\mathbf{r}',i\omega_n) = \frac{1}{V}\sum_{\mathbf{k},\mathbf{k}'} e^{i\mathbf{k}\cdot(\mathbf{r}-\mathbf{r}')}e^{i(\mathbf{k}-\mathbf{k}')\cdot\mathbf{r}'}\underline{\underline{\mathcal{G}_{0s}}}(\mathbf{k},\mathbf{k}',i\omega_n) \equiv \underline{\underline{\mathcal{G}_{s0}}}(\mathbf{r}-\mathbf{r}',i\omega_n) \tag{4.35}$$

Since the RHS of the above equation only depends on the relative position, so must the middle part, which means that:

$$\underline{\underline{\mathcal{G}_{0s}}}(\mathbf{k},\mathbf{k}',i\omega_n) = \delta_{\mathbf{k},\mathbf{k}'}\underline{\underline{\mathcal{G}_{0s}}}(\mathbf{k},i\omega_n) \Rightarrow \tag{4.36}$$

$$\underline{\underline{\mathcal{G}_{0s}}}(\mathbf{r},\mathbf{r}',i\omega_n) = \int \frac{\mathrm{d}\mathbf{k}}{(2\pi)^3}e^{i\mathbf{k}\cdot(\mathbf{r}-\mathbf{r}')}\underline{\underline{\mathcal{G}_{0s}}}(\mathbf{k},i\omega_n). \tag{4.37}$$

This means that the self-energy equation (4.32) becomes

$$\Sigma(\mathbf{r},\mathbf{r}',i\omega_n)=\delta(z)\delta(z')|t_0|^2\int\frac{\mathrm{d}\mathbf{k}}{(2\pi)^3}e^{i\mathbf{k}\cdot(\mathbf{r}-\mathbf{r}')}\underline{\underline{\mathcal{G}_{0s}}}(\mathbf{k},i\omega_n), \tag{4.38}$$

Now we want to Fourier transform the self-energy into a momentum-space representation:

$$\Sigma=\int\frac{\mathrm{d}\mathbf{k}}{(2\pi)^3}\underline{\underline{\mathcal{G}_{0s}}}(\mathbf{k},i\omega_n)\int\mathrm{d}(\mathbf{r}_{||}-\mathbf{r}'_{||})e^{i(\mathbf{k}-\mathbf{p})(\mathbf{r}_{||}-\mathbf{r}'_{||})}\int\mathrm{d}z\int\mathrm{d}z'e^{-i(p_z-k_z)z}e^{-i(p'_z+k_z)z'}\delta(z)\delta(z')|t_0|^2 \tag{4.39}$$

$$=|t_0|^2\int\frac{\mathrm{d}\mathbf{k}}{(2\pi)^3}\underline{\underline{\mathcal{G}_{0s}}}(k,i\omega_n)\int\mathrm{d}(\mathbf{r}_{||}-\mathbf{r}'_{||})e^{i(\mathbf{k}-\mathbf{p})(\mathbf{r}_{||}-\mathbf{r}'_{||})}=|t_0|^2\int\frac{\mathrm{d}\mathbf{k}}{(2\pi)^3}\underline{\underline{\mathcal{G}_{0s}}}(\mathbf{k},i\omega_n)(2\pi)^2\delta(\mathbf{p}_{||}-\mathbf{k}_{||})\Rightarrow \tag{4.40}$$

$$\Sigma(\mathbf{p}_{||},i\omega_n)=|t_0|^2\int\frac{\mathrm{d}p_z}{2\pi}\underline{\underline{\mathcal{G}_{0s}}}(\mathbf{p},i\omega_n). \tag{4.41}$$

From here we will transform to energy space, and make the usual approximations to get a momentum-independent self-energy expression. First we write a trivial statement:

$$\Sigma(\mathbf{p}_{||},i\omega_n)=|t_0|^2\int\frac{\mathrm{d}p_z}{2\pi}\underline{\underline{\mathcal{G}_{0s}}}(\mathbf{p},i\omega_n)=|t_0|^2\int_{-\lambda_1}^{\lambda_2}\mathrm{d}\epsilon\int\frac{\mathrm{d}p_z}{2\pi}\delta(\epsilon-\xi_{\mathbf{p}})\underline{\underline{\mathcal{G}_{0s}}}(\epsilon,i\omega_n), \tag{4.42}$$

where λ_1,λ_2 mark the bottom and top of the conduction band, i.e. $\lambda_2-\lambda_1$ is the bandwidth. We also know that we can change between an integral over momentum to one over energy by using the density of states ν, so that we for example have:

$$\int\frac{\mathrm{d}p_z}{2\pi}\underline{\underline{G}}(\mathbf{p},\omega)=\int\mathrm{d}\epsilon\underline{\underline{G}}(\epsilon,\omega)\nu(\epsilon,\mathbf{p}_{||}). \tag{4.43}$$

Thus we can identify the density of states from the two above equations:

$$\nu(\epsilon,\mathbf{p}_{||})=\int\frac{\mathrm{d}p_z}{2\pi}\delta(\epsilon-\xi_{\mathbf{p}}). \tag{4.44}$$

Now we assume that the density of states varies slowly enough with energy that we may take it outside the integral and write:

$$\Sigma(\mathbf{p}_{||},i\omega_n)\approx\Sigma(i\omega_n)=|t_0|^2|\nu(0)|\int\mathrm{d}\xi^s_{\mathbf{p}}\underline{\underline{\mathcal{G}}}(\xi^s_{\mathbf{p}},i\omega_n)=|t_0|^2|\nu(0)|\int_{-\lambda_1}^{\lambda_2}\mathrm{d}\xi^s_{\mathbf{p}}\big(i\omega_n-(\xi^s_{\mathbf{p}}\tau_z+B_s\sigma_x+\Delta\tau_x)\big)^{-1}, \tag{4.45}$$

where the $\xi^s_{\mathbf{p}}$ is the superconducting kinetic energy term from equation (4.6). At this point we perform the analytic continuation of the Matsubara Green's function, which gives us the retarded self-energy as a function of the regular frequency and an infinitesimal imaginary part $i\eta$:

$$\Sigma^R(\omega)=\Sigma(i\omega_n\to\omega+i\eta)=|t_0|^2|\nu(0)|\int_{-\lambda_1}^{\lambda_2}\mathrm{d}\xi^s_{\mathbf{p}}\big(\omega+i\eta-(\xi^s_{\mathbf{p}}\tau_z+B_s\sigma_x+\Delta\tau_x)\big)^{-1} \tag{4.46}$$

Now we can solve for this inverse structure. To solve this we will be looking at the kind of design where the magnetic field goes is in the z-direction, which gives us a magnetic field-contribution of $B\sigma_z$ instead. This means that G_{0s} is diagonal in spin-space, which allows us an easy inversion of it.
Since the inverse of a diagonal matrix is simply the inverse of its entries, we can treat such an inverse as a number in our calculations. And since we can decompose our 4×4 matrix into 4 blocks of 2×2 matrices that are each diagonal, we can treat each of those diagonal blocks as a number, and invert our matrix as a 2×2 matrix in τ space, which yields:

$$\big(\omega + i\eta - (\xi^s_{\mathbf{p}}\tau_z + B_s\sigma_z + \Delta\tau_x)\big)^{-1} = \frac{\omega + \xi^s_{\mathbf{p}}\tau_z - B_s\sigma_z + \Delta\tau_x}{(\omega + i\eta - B_s\sigma_z)^2 - \xi^2_{\mathbf{p}} - \Delta^2} \tag{4.47}$$

The σ_z in the denominater here is to be understood as a number that changes sign in spin-space just as if it was in the numerator.

Let us now consider the integral in equation (4.46):

$$\Sigma^R(\omega) = \Sigma(\omega + i\eta) = |t_0|^2|\nu(0)| \int_{-\lambda_1}^{\lambda_2} \mathrm{d}\xi^s_{\mathbf{p}} \frac{\omega + \xi^s_{\mathbf{p}}\tau_z - B_s\sigma_z + \Delta\tau_x}{(\omega + i\eta - B_s\sigma_z)^2 - (\xi^s_{\mathbf{p}})^2 - \Delta^2} \tag{4.48}$$

Expanding the parenthesis in the denominator yields:

$$(\omega + i\eta - B_s\sigma_z)^2 \approx (\omega_s)^2 + i\mathrm{Sign}(\omega_s)\eta., \tag{4.49}$$

where we defined:

$$\omega_s \equiv \omega - B_s\sigma_z. \tag{4.50}$$

Now we use the fact that:

$$\frac{1}{x + i\eta} \longrightarrow_{\eta\to 0^+} \mathcal{P}\frac{1}{x} - i\pi\delta(x), \tag{4.51}$$

where $\mathcal{P}f(x)$ denotes the Cauchy principle part of $f(x)$. Then the self-energy becomes:

$$\Sigma^R(\omega) = |t_0|^2|\nu(0)| \int_{-\lambda_1}^{\lambda_2} \mathrm{d}\xi^s_{\mathbf{p}} \frac{\omega_s + \xi^s_{\mathbf{p}}\tau_z + \Delta\tau_x}{\omega_s^2 + i\mathrm{Sign}(\omega_s)\eta - (\xi^s_{\mathbf{p}})^2 - \Delta^2} = \tag{4.52}$$

$$|t_0|^2|\nu(0)| \int_{-\lambda_1}^{\lambda_2} \mathrm{d}\xi^s_{\mathbf{p}} \left[\mathcal{P}\frac{1}{\omega_s^2 - (\xi^s_{\mathbf{p}})^2 - \Delta^2} - \mathrm{Sign}(\omega_s) i\pi\delta\{(\xi^s_{\mathbf{p}})^2 - (\omega_s^2 - \Delta^2)\}\right](\omega_s + \xi^s_{\mathbf{p}}\tau_z + \Delta\tau_x). \tag{4.53}$$

Let us look at the delta-function part first. We can use the well-known decomposition of the delta-function of a function:

$$\delta(f(x)) = \sum_i \frac{\delta(x - a_i)}{|\frac{\partial f}{\partial x}(a_i)|}, \tag{4.54}$$

where the a_i are the roots of the function $f(x)$. Using this for the variable $\xi_{\mathbf{p}}$ we get that:

$$\delta(\xi^2_{\mathbf{p}} - (\omega_s^2 - \Delta^2)) = \frac{\delta(\xi^s_{\mathbf{p}} - \sqrt{\omega_s^2 - \Delta^2}) + \delta(\xi_{\mathbf{p}} + \sqrt{\omega_s^2 - \Delta^2})}{2|\xi^s_{\mathbf{p}}|}. \tag{4.55}$$

Here we see that there is 'phase transition' at $|\omega_s| = \Delta$: for $|\omega_s| < \Delta$ the delta functions will not contribute to the self-energy because then $\sqrt{\omega_s^2 - \Delta^2} \notin \mathbb{R}$, which means that the integral over real values of $\xi^s_{\mathbf{p}}$ can never attain this value. Let us therefore look at these two regions seperately:

4.0.1 $|\omega_s| < \Delta$:

Here the self-energy is the following:

$$\Sigma^R(\omega) = -|t_0|^2|\nu(0)|\mathcal{P} \int_{-\lambda_1}^{\lambda_2} \mathrm{d}\xi^s_{\mathbf{p}} \frac{\omega_s + \xi^s_{\mathbf{p}}\tau_z + \Delta\tau_x}{(\xi^s_{\mathbf{p}})^2 + \Delta^2 - \omega_s^2}. \tag{4.56}$$

Using the identities ($a^2 > 0$):

$$\int dx \frac{1}{x^2+a^2} = \frac{1}{a}\arctan\Big(\frac{x}{a}\Big); \qquad \int dx \frac{x}{x^2+a^2} = \frac{1}{2}\log(a^2+x^2), \tag{4.57}$$

and defining:

$$\gamma \equiv \pi |t_0|^2 |\nu(0)|, \tag{4.58}$$

we get:

$$\Sigma^R(\omega) = -\frac{1}{2}\log\left(\frac{\lambda_2^2+\Delta^2-\omega_s^2}{\lambda_1^2+\Delta^2-\omega_s^2}\right)\tau_z - \frac{\gamma}{\pi}\frac{\omega_s+\Delta\tau_x}{\sqrt{\Delta^2-\omega_s^2}}\left[\arctan\left(\frac{\lambda_2}{\sqrt{\Delta^2-\omega_s^2}}\right) - \arctan\left(-\frac{\lambda_1}{\sqrt{\Delta^2-\omega_s^2}}\right)\right]. \tag{4.59}$$

Now under the assumption that $\lambda_1, \lambda_2 >> |\sqrt{\Delta^2-\omega_s^2}|$, the self-energy simplifies considerably, resulting in:

$$\Sigma^R(\omega) = -\gamma\left(\frac{1}{\pi}\log\frac{\lambda_2}{\lambda_1}\tau_z + \frac{\omega_s+\tau_x\Delta}{\sqrt{\Delta^2-\omega_s^2}}\right). \tag{4.60}$$

Since $\lambda_2 - \lambda_1$ is the bandwidth of e.g. an aluminium band it should be of order electron volts, which is around 3 or 4 orders of magnitude larger than Δ, so $\lambda_1, \lambda_2 >> |\sqrt{\Delta^2-\omega_\sigma^2}|$ is a safe approximation.

4.0.2 $|\omega_s| > \Delta$:

In this parameter-regime the delta-function from equation (4.55) will indeed contribute to the self-energy. Again under the assumption that $\lambda_1, \lambda_2 >> |\sqrt{\Delta^2-\omega_s^2}|$ both delta-functions will contribute under integration yielding a contribution to the self-energy of:

$$-\frac{\gamma}{\pi}\int_{-\lambda_1}^{\lambda_2} \mathrm{d}\xi_{\mathbf{p}}^s \big[\mathrm{Sign}(\omega_s) i\pi\delta\{(\xi_{\mathbf{p}}^s)^2 - (\omega_s^2-\Delta^2)\}\big](\omega_s + \xi_{\mathbf{p}}^s\tau_z + \Delta\tau_x) = \tag{4.61}$$

$$-\gamma\int_{-\lambda_1}^{\lambda_2} \mathrm{d}\xi_{\mathbf{p}}^s \left[\mathrm{Sign}(\omega_s) i\left(\frac{\delta(\xi_{\mathbf{p}}^s - \sqrt{\omega_s^2-\Delta^2}) + \delta(\xi_{\mathbf{p}}^s + \sqrt{\omega_s^2-\Delta^2})}{2|\xi_{\mathbf{p}}^s|}\right)\right](\omega_s + \xi_{\mathbf{p}}^s\tau_z + \Delta\tau_x) = \tag{4.62}$$

$$-i\gamma\mathrm{Sign}(\omega_s)\frac{1}{\sqrt{|\Delta^2-\omega_s^2|}}(\omega_s + \Delta\tau_x). \tag{4.63}$$

Now the contribution not stemming from the delta-function can be calculated using the identities ($a^2 > 0$):

$$\int dx \frac{1}{x^2-a^2} = \frac{1}{2a}\log\left(\frac{x-a}{x+a}\right); \qquad \int dx \frac{x}{x^2-a^2} = \frac{1}{2}\log\big(x^2-a^2\big). \tag{4.64}$$

Thus we get a contribution:

$$-\frac{\gamma}{\pi}\mathcal{P}\int_{-\lambda_1}^{\lambda_2} \mathrm{d}\xi_{\mathbf{p}}^s \left[\frac{\omega_s + \xi_{\mathbf{p}}^s\tau_z + \Delta\tau_x}{(\xi_{\mathbf{p}}^s)^2 + \Delta^2 - \omega_s^2}\right] \tag{4.65}$$

$$= -\frac{\gamma}{\pi}\left[\frac{1}{2\sqrt{\omega_\sigma^2-\Delta^2}}\log\left(\frac{\lambda_2 - \sqrt{\omega_\sigma^2-\Delta^2}}{\lambda_2 + \sqrt{\omega_\sigma^2-\Delta^2}}\frac{\lambda_1 + \sqrt{\omega_\sigma^2-\Delta^2}}{\lambda_1 - \sqrt{\omega_\sigma^2-\Delta^2}}\right) + \frac{1}{2}\log\left(\frac{\lambda_2^2 - (\omega_\sigma^2-\Delta^2)}{\lambda_1^2 - (\omega_\sigma^2-\Delta^2)}\right)\tau_z\right] \tag{4.66}$$

$$\approx -\frac{\gamma}{\pi}\left[0 + \log\left(\frac{\lambda_2}{\lambda_1}\right)\tau_z\right], \tag{4.67}$$

where again we invoked the assumption $\lambda_1, \lambda_2 >> |\sqrt{\Delta^2 - \omega_\sigma^2}|$. Thus the total self-energy in this parameter-regime becomes:

$$\Sigma^R(\omega) = -\gamma\left(\frac{1}{\pi}\log\left(\frac{\lambda_2}{\lambda_1}\right)\tau_z + i\text{Sign}(\omega_s)\frac{\omega_s + \Delta\tau_x}{\sqrt{|\Delta^2 - \omega_s^2|}}\right). \tag{4.68}$$

Comparing equations (4.60) and (4.68) we see that the only difference between the two regimes $|\omega| < \Delta$ and $|\omega| > \Delta$ is the factor $i\text{Sign}(\omega_\sigma)$ that is multiplied onto the second term in the self-energy in the latter regime.

Let us stop for a second and reflect on what we have done. We set up a tunneling model. We then assumed the simplest tunneling coupling possible, i.e. one without spin-flip processes. By using the equation of motion-approach we then obtained a Dyson equation which allowed an easy identification of the self-energy which contains all the non-trivial information of the system. Then we integrated out the superconductor's degree of freedom by performing an integral over all k_z-values, thereby getting a local self-energy. Then naturally there were two different regimes, $\omega_s > \Delta$ and $\omega_s < \Delta$, which we treated independently. In the end we ended up with an analytic solution to the self-energy that corresponds to what has been obtained before in literature, see e.g. ref. [25].

Now that we have established the Green's function we can proceed to for example solving for bound states energies or looking at the density of states and conductance measurements.

Chapter 5

Wave-function and Tunneling Model Correspondence

Using the result from section 4 we can then find the poles of the retarded Green's function in k space by writing:

$$\underline{\underline{G^R}}(\mathbf{k},\omega) = \left(\underline{\underline{G^R_{n0}}}^{-1}(\mathbf{k},\omega) - \Sigma^R(\omega)\right)^{-1}, \tag{5.1}$$

And from solving for the poles of the Green's function, i.e. solving the equation:

$$\det(\underline{\underline{G^R}})^{-1}(\mathbf{k},\omega) = 0, \tag{5.2}$$

we get the energy solutions in our system.

At this point we will take a step back and compare the expression for the energy that we get in the Green's function approach with the one we got for the system in the AISW approximation, section 3.2. What we would like is some kind of correspondence between the tunneling rate, t_0, see equation (4.9), from the Green's function model and the parameters from the wave-function model. The motivation to do so is that the tunneling rate does not have a clear microscopic interpretation; a connection between the two would then give us a better understanding of what constitutes the tunneling rate.

The expression from the wave-function model in the AISW approximation we know from equation (3.44):

$$E_n^2 + \frac{2\epsilon_{g0}E_nE_s}{(\Delta^2 - E_s^2)^{1/2}} = \left(\xi_n - \frac{w}{s}\epsilon_{g0}\right)^2 + \epsilon_{g0}^2, \tag{5.3}$$

where we remember:

$$E_{n,s} \equiv E - \frac{g_{n,s}\mu_B}{2}B\sigma. \tag{5.4}$$

To find the corresponding form of the bound state energies from the Green's function model without SOI we will define the following parameters for a clearer derivation:

$$\tilde{\xi}_n \equiv \xi_n - \frac{\gamma \log\frac{\lambda_2}{\lambda_1}}{\pi}; \qquad \omega_{n,s} \equiv \omega - B_{n,s}\sigma, \tag{5.5}$$

where ξ_n is the kinetic energy in the 2DEG from equation (4.6). Note that without SOI we can just like in the AISW approximation treat the spin as a parameter because spin is a good quantum number, i.e. $\sigma_z \to \sigma = \pm 1$. Then solving for the bound states energies, with $|\omega_s| < |\Delta|$, using the relevant self-energy expression from equation (4.60) yields:

$$\det(\underline{\underline{G^R}})^{-1}(\mathbf{k},\omega) = 0 \Leftrightarrow \det\left[\omega_n - \tilde{\xi}_n\tau_z + \gamma\frac{\omega_s + \tau_x\Delta}{\sqrt{\Delta^2-\omega_s^2}}\right] = 0 \Leftrightarrow \tag{5.6}$$

$$0 = \left(\omega_n + \gamma\frac{\omega_s}{\sqrt{\Delta^2-\omega_s^2}}\right)^2 - \tilde{\xi}_n^2 - \frac{\gamma^2\Delta^2}{\Delta^2-\omega_s^2} \Leftrightarrow \tag{5.7}$$

$$\omega_n^2 + \frac{2\gamma\omega_n\omega_s}{\sqrt{\Delta^2-\omega_s^2}} = \tilde{\xi}_n^2 + \gamma^2. \tag{5.8}$$

When comparing equations (5.3) and (5.8) we see a complete correspondence (interpreting ω as the energy) given the following equalities:

$$\frac{\gamma}{\pi}\log\frac{\lambda_2}{\lambda_1} = \frac{w}{s}\epsilon_{g0}; \qquad \gamma = \epsilon_{g0}. \tag{5.9}$$

The first equality is a relation between the renormalizations of the chemical potential in the two different models.
The second equality is quite interesting - it gives us a direct correspondence between the tunneling coefficient, which lives inside γ, and the microscopic quantities of the wave-function model, which stem from ϵ_{g0}. To remind ourselves, we had:

$$\epsilon_{g0} = \frac{s}{s^2+w^2}\epsilon_0, \tag{5.10}$$

where:

$$s \equiv \frac{m_n}{m_s}\frac{p}{k_0}; \qquad w \equiv \frac{2U_a m_n}{k_0} + \frac{m_n}{m_s}\frac{\kappa}{k_0}; \qquad \epsilon_0 \equiv \frac{\pi}{m_n d^2}, \tag{5.11}$$

where m_n, m_s are the masses in the 2DEG, S region respectively, p is to a good approximation the fermi wavenumber in the superconductor, $k_0 \equiv \frac{\pi}{d}$ is the ground state standing wave-wavenumber of the 2DEG of width d, U_a is the delta-function barrier amplitude between the two materials, and κ is the inverse decay-length in the superconductor.

The scope of this result is that mathematically the tunneling model can be described by the AISW approximation in a wave-function model with a possibly different renormalization of the chemical potentials in the two models, and under the relation $\gamma = \epsilon_{g0}$. That the AISW in this manner corresponds mathematically to a tunneling model is not immediately clear when setting up the models. Importantly this result gives us a way to connect the tunneling rate $|t_0|$ to microscopic parameters, which is usually not easy. This result also expands the scope of the tunneling model, since now in principle we can take a wave-function model and test if the AISW approximation is a good approximation to the system; if so, then we might as well model the system by a tunneling model, which is sometimes easier. Concretely all the analysis we did in sections 3.3.2-3.4 can now be directly seen to also apply in the tunneling model case, remembering the shift in chemical potential.

Another thing to note is that this approach might also be extended to a system including SOI. In principle the approach would be the same as described above, but one would have to do the analysis to see if there exists a similar, general correspondence between the two models.

This concludes our analysis on the wave-function model. We will now turn to analysis on tunneling spectroscopy of proximitized 2DEGs.

Chapter 6

Tunneling Spectroscopy of Proximitized 2DEGs

In this section we will use the analysis from section 4 to analyze the tunneling spectroscopy in junctions involving a proximitized 2DEG. In particular we will study a (pS)-QPC-(pS)-junction, and on the way get information about a (pS)-QPC-N junction. Here (pS) denotes a 2DEG that via the proximity effect has inherited a superconducting gap from the superconductor, see e.g. equation (4.60). QPC denotes a Quantum Point Contact (see section 2.6.2), N denotes a normal conductor. As described in section 2.4 the QPC acts to effectively drive the system into the tunneling regime. We are going to investigate the conductance in the linear response regime, at zero temperature. In order to find the conductance in the (pS)-QPC-(pS) setup we will determine the density of states (DOS), which is directly connected to conductance in the (pS)-QPC-N setup.

As has been explained in section 2.6, the Center for Quantum Devices at the University of Copenhagen has made conductance measurements on devices of the type (pS)-QPC-(pS) and (pS)-QPC-N, ultimately in the search for Majorana fermions. To get Majoranas in the design, the idea would be to experimentally define a 1D-channel in the 2DEG to simulate the physics known from nanowires. This is not contained in the analysis we have done so far. However, since the understanding of the proximitized 2DEG is still in its early stages, in a hope to understand the physics of the proximitized 2DEG, conductance measurements on setups *without* a 1D-channel are also interesting. An attempt to model these experiments can be done by referencing our analysis with the Green's functions. Here we use the self-energy to effectively integrate out the semi-infinite superconductor on top of the 2DEG and be left with a (pS)-(pS) system where the two regions are tunnel-coupled. The proximitized Green's function is really a bulk Green's function, so by using this approach we neglect edge effects. Then to find the current and conductance we compute the spectral function and use the linear-response result for the current (see section 2.4).

We acknowledge Michael Hell from the CMT group at the Niels Bohr Institute for his collaboration with the work in this chapter.

6.1 Experimental Results from the Center for Quantum Devices

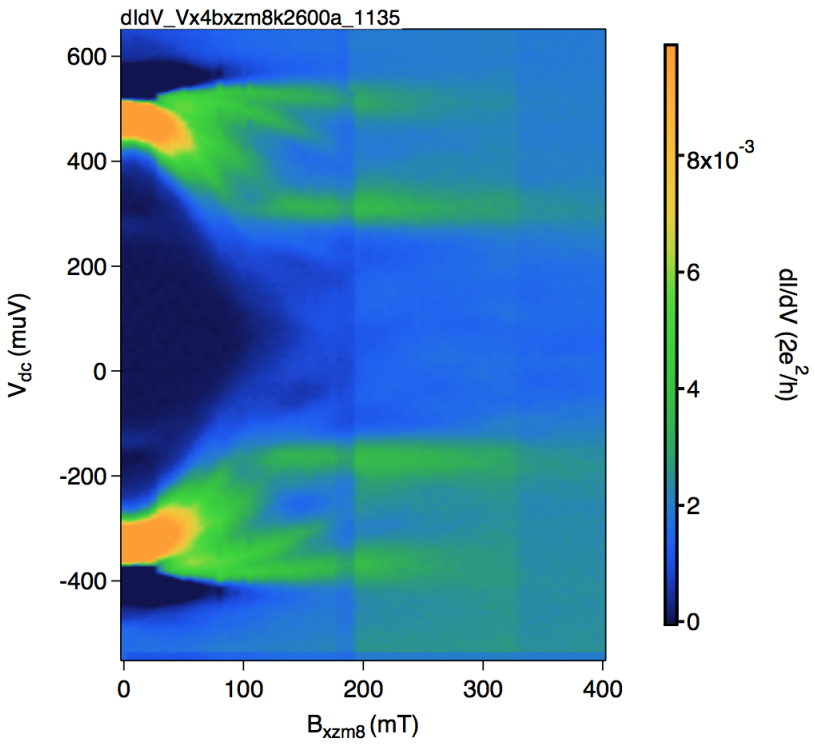

Figure 6.1.1: An experimental 2D conductance plot of a (pS)-QPC-(pS) junction, courtesy of the Center for Quantum Devices at the University of Copenhagen. The x-axis is in-plane magnetic field, the y-axis is source-drain bias. Note that the y-axis is misplaced: $V_{dc} = 0$ should be in the symmetry point on the y-axis. Also note that the experimentalists have employed a colour-cutoff, so that all negative conductance has been set equal to 0 conductance. By applying a gate voltage over the QPC as described in section 2.6.2 the system has been driven into the tunneling regime.

The results shown in figure 6.1.1 are fairly recent and show a tunneling spectroscopy conductance measurement on a (pS)-QPC-(pS) device. The setup is similar to that presented in section 2.6.1, with Aluminium as the superconductor proximitizing the 2DEG. In the rest of this chapter we present analysis that tries to model the experimental setup used to obtain figure 6.1.1. From similar experiments in other designs the Center for Quantum Devices infer the following parameters:

$$\frac{m_n}{m_s} = 0.023; \qquad \Delta \equiv \Delta_{\mathrm{Al}} = 235\mu\mathrm{eV}; \qquad \alpha \sim 0.5\mathrm{eV\AA}. \tag{6.1}$$

Note that the SOI strength is actually not well-known. This is part of the motivation to look into the conductance of this device - if there is some way to deduce the SOI strength from conductance measurements this would be useful. The choice of the renormalized chemical potential, $\tilde{\mu}$ (see section 5) is not normally known in experiment. We do, however, expect the chemical potential to be substantially larger than Δ_{Al}.

Also the value of the tunnel-coupling parameter γ is debatable. If we use the result from chpt. 5 and estimate γ via the wave-function model of chpt. 3, using the experimental parameters, we get $\gamma \approx 50\Delta_{\mathrm{Al}}$. We will argue later (section 6.5.1) why this is an unrealistic size. Therefore we will try some different values of both $\tilde{\mu}$ and γ and see how this affects our results.

6.2 Numerical Conductance Analysis

Here follows an explanation of how we obtain all numerical results to follow. In an attempt to obtain simpler expressions we will not include the magnetic field in the superconductor in all numerical work that follows, unless stated otherwise. This approximation is relevant when the effective g-factor in the 2DEG is much larger than that in the superconductor.

We want to look only at the electron current in this thesis. This means that we only consider the electron-sector in our BdG-matrices (see equation (2.45)), i.e. all matrices that appear from now on are only 2×2-matrices. To find the conductance we can use the formula derived in equation (2.73):

$$I = \int_{-\infty}^{\infty} \frac{d\omega}{2\pi} |t_0|^2 \mathrm{Tr}_\sigma \left[\sum_{\mathbf{k}_1, \mathbf{k}_2} \underline{\underline{A_1}}(\mathbf{k}_1, \omega) \underline{\underline{A_2}}(\mathbf{k}_2, \omega + eV) \right] [n_F(\omega + eV) - n_F(\omega)], \tag{6.2}$$

To treat this numerically we will do the following: First of all we will write the sums over k as integrals:

$$I = \int_{-\infty}^{\infty} \frac{d\omega}{2\pi} |t_0|^2 \mathrm{Tr}_\sigma \left[\frac{L_x L_y}{(2\pi)^2} \int\int dk_{1x} dk_{1y} \underline{\underline{A_1}}(\mathbf{k}_1, \omega) \right] \ldots \tag{6.3}$$

$$\ldots \left[\frac{L_x L_y}{(2\pi)^2} \int\int dk_{2x} dk_{2y} \underline{\underline{A_2}}(\mathbf{k}_2, \omega + eV) \right] [n_F(\omega + eV) - n_F(\omega)]$$

Now our next approximation in treating this system is to assume that we are at zero temperature. This means that the fermi-functions become step-functions, and the current formula reduces to:

$$I \longrightarrow \int_{-eV}^{0} \frac{d\omega}{2\pi} |t_0|^2 \mathrm{Tr}_\sigma \left[\frac{L_x L_y}{(2\pi)^2} \int\int dk_{1x} dk_{1y} \underline{\underline{A_1}}(\mathbf{k}_1, \omega) \right] \left[\frac{L_x L_y}{(2\pi)^2} \int\int dk_{2x} dk_{2y} \underline{\underline{A_2}}(\mathbf{k}_2, \omega + eV) \right]. \tag{6.4}$$

Note that here we had to introduce the volume $L_x L_y$, which we do not really know how to estimate for our system. Therefore all our conductance results will be given with an arbitrary scaling factor.

In our model we have identical superconductors on both sides of the junction: therefore $\underline{\underline{A_1}} = \underline{\underline{A_2}}$. This enables us to do the above numerical integration altogether in a smart way. We discretize the ω-integral, so that we only need to evaluate a finite number of ω-points. Then for each ω-value we calculate the integral over k using the a built-in numerical integration function in Mathematica, "NIntegrate". We calculate this integral over k for values of ω in the range $\omega \in [-eV, eV]$ and collect them in a vector with matrix-entries, $\underline{\underline{d_{e\sigma}}}(\omega)$:

$$\underline{\underline{d_{e\sigma}}}(\omega) \equiv \frac{1}{(2\pi)^3} \int\int \mathrm{d}k_x \mathrm{d}k_y \underline{\underline{A}}(\mathbf{k}, \omega) \equiv \begin{pmatrix} d_{e\uparrow\uparrow}(\omega) & d_{e\uparrow\downarrow}(\omega) \\ d_{e\downarrow\uparrow}(\omega) & d_{e\downarrow\downarrow}(\omega) \end{pmatrix}. \tag{6.5}$$

From this we can easily find the electron density of states (DOS) as a function of energy, $d_e(\omega)$:

$$d_e(\omega) = \mathrm{Tr}_\sigma \underline{\underline{d_{e\sigma}}}(\omega). \tag{6.6}$$

We will call $\underline{\underline{d_{e\sigma}}}(\omega)$ the DOS-matrix. Knowing the DOS-matrix we can calculate the convolution (i.e. the product of the DOS with itself) in equation (6.4) for an $\omega \in [-eV, 0]$ in the following way:

$$\left[\int\int dk_{1x} dk_{1y} \underline{\underline{A}}(\mathbf{k}_1, \omega) \right] \left[\int\int dk_{2x} dk_{2y} \underline{\underline{A}}(\mathbf{k}_2, \omega + eV) \right] = (2\pi)^6 \underline{\underline{d_{e\sigma}}}(\omega) \cdot \underline{\underline{d_{e\sigma}}}(\omega + eV) \Rightarrow \tag{6.7}$$

$$I \propto \int_{-eV}^{0} \mathrm{d}\omega \mathrm{Tr}_\sigma \left[\underline{\underline{d_{e\sigma}}}(\omega) \cdot \underline{\underline{d_{e\sigma}}}(\omega + eV) \right]. \tag{6.8}$$

So by calculating $\underline{\underline{d_{e\sigma}}}(\omega)$ (with as many ω-points as is needed for convergence of the integral in equation (6.8)), we have all the information we need to find the electron density of state and the conductance in the system.

There are some things to consider regarding the numerical integration. First of all, for $|\omega_s| < \Delta$ we have to do someting about the $i\eta$ that appears in the Green's function, see e.g. equation (4.60). We implement this numerically by choosing a finite value for η. We have to choose it so that it is sufficiently small to act as an infinitesimal in the calculations, and sufficiently large that it does not vanish in the numerical integration done by the "NIntegrate"-function in Mathematica. We therefore chose to test two different values: $\eta = 1\mu$eV and $\eta = 5\mu$eV. Both of these produced similar results, which lead us to conclude that the choice of η has the right size for these calculations.

Furthermore, to do the numerical calculation we chose to only integrate over a finite range of k-values. Since the other energy scales in this problem are of order 100μeV-1meV we integrated over a region in k-space such that the maximum kinetic energy was of order 0.5eV, which is much larger than the excitation energies expected in the system. Then all the dynamics should be safely captured by the model.

Lastly, in working with a predefined integration routine like "NIntegrate" in Mathematica, it is wise to have some check of whether the results make sense. The results were compared to results obtained by other means by Michael Hell in the CMT group at the Niels Bohr Institute without SOI, for $\gamma = 180\mu$eV, $\eta = 1\mu$eV, and found to be in good correspondence. Also, "NIntegrate" is built to display the estimated error if the numerical integration does not converge quickly enough. The errors were usually of the order of 1% or less of the result of the integration, which is satisfactory for our needs with the following analysis. An exception to this was e.g. for energies inside the induced gap-energy region where we know the electron DOS should be equal to zero, but where the numerical integration yielded a small value for the integration, with an error of approximately the size of the integration result. However this is not a problem since the integration result is relatively small compared to the values of the DOS in energy domains outside the induced gap.

6.3 (pS)-QPC-N System

In setting out to get results for the (pS)-QPC-(pS) system in the above explained way we find the DOS-matrix (equation (6.5)) on the way to establishing the current and from that the differential conductance. However, the DOS is actually very interesting because it is related to the conductance of a (pS)-QPC-N system.

Let us say we have a (pS)-QPC-N system in 2 dimensions. This means that the DOS-matrix in the normal region, $\underline{\underline{d^n_{e\sigma}}}(\omega)$, will be constant as a function of energy, unlike the superconducting $\underline{\underline{d^s_{e\sigma}}}(\omega)$; therefore we can write for the current:

$$I \propto \int_{-eV}^{0} \mathrm{Tr}_\sigma \left[\underline{\underline{d^n_{e\sigma}}}(\omega)\underline{\underline{d^s_{e\sigma}}}(\omega + eV)\right] d\omega \tag{6.9}$$

$$= \int_{0}^{eV} \mathrm{Tr}_\sigma \left[\underline{\underline{d^n_{e\sigma}}}(0)\underline{\underline{d^s_{e\sigma}}}(\omega)\right] d\omega, \tag{6.10}$$

Since only the superconducting DOS depends on the energy, we get:

$$\frac{dI}{dV} \propto \mathrm{Tr}_\sigma \left[\underline{\underline{d^s_{e\sigma}}}(eV)\underline{\underline{d^n_{e\sigma}}}(0)\right] \tag{6.11}$$

This is an important result; it says that in the linear response-regime the conductance in a (pS)-QPC-N experiment can be found for any value of the bias by multiplying the DOS-matrix of the superconductor at the bias voltage-energy with some constant matrix for the system without superconductivity,

and then taking the trace over spins. So by solving for the DOS-matrix for a proximitized 2DEG we also harvest information about a (pS)-QPC-N setup.

If we further assume that the normal region has trivial spin-structure, then equation (6.11) reduces to:

$$\frac{dI}{dV} \propto \mathrm{Tr}_\sigma \left[\underline{\underline{d^s_{e\sigma}}}(eV) \right] = d_e(eV). \tag{6.12}$$

This says that the density of states in a proximitized 2DEG is proportional to the conductance of a (pS)-QPC-N system, with N being a simple normal conductor. This gives us an extra incentive to study plots of the DOS for the proximitized 2DEG. We will not compare our density of states-measurements with experiment in this thesis though.

6.4 Analysis Without SOI

6.4.1 Analytical Calculation of the DOS in a Proximitized 2DEG Without SOI

When working in the regime without SOI there is no coupling between different spins, i.e. spin-up and spin-down in the magnetic field-direction are good quantum numbers, and we can therefore look only at one spin projection at a time. Mathematically this will be represented by a factor $\sigma = \pm 1$, as many times earlier in this thesis, where the sign depends on whether we look at the spin-up- or spin-down-projection.

Here we will work with the following abbreviations:

$$\omega_s \equiv \omega - B_s\sigma; \qquad \omega_n \equiv \omega - B_n\sigma. \tag{6.13}$$

As was derived in section 4, the self-energy changes dramatically between the two regimes $|\omega_s| < \Delta$ and $|\omega_s| > \Delta$. Therefore we will have to treat the two independently when finding the local DOS. Here we will only derive analytically the DOS for $|\omega_s| < \Delta$ and refer the reader to some numerically obtained plots in e.g. figure 6.4.4 for a view of the whole energy spectrum.

$|\omega_s| < \Delta$**:**

In this regime we have the following retarded Green's function:

$$\underline{\underline{G^R}}(\mathbf{k},\omega) = \underline{\underline{\mathcal{G}}}(\mathbf{k},\omega+i\eta) = \left[\omega_n + i\eta - \tilde{\xi}_n\tau_z + \gamma\frac{\omega_s + i\eta + \tau_x\Delta}{\sqrt{\Delta^2 - (\omega_s+i\eta)^2}}\right]^{-1}. \tag{6.14}$$

Now we neglect the $i\eta$'s that do not contribute to any poles in our regime of ω_s:

$$\underline{\underline{G^R}}(\mathbf{k},\omega) = \left[\omega_n + i\eta - \tilde{\xi}_n\tau_z + \gamma\frac{\omega_s + i\eta + \tau_x\Delta}{\sqrt{\Delta^2 - \omega_s^2}}\right]^{-1}. \tag{6.15}$$

Let us now rewrite the Green's function in terms of some "quasi-particle weight" Z:

$$\underline{\underline{\mathcal{G}}}(\mathbf{k},\omega+i\eta) = \frac{1}{\omega_n + i\eta - \tilde{\xi}_n\tau_z + \gamma\frac{\omega_s+i\eta+\Delta\tau_x}{\sqrt{\Delta^2-\omega_s^2}}} \tag{6.16}$$

$$= \frac{1}{\left(1+\frac{\gamma}{\sqrt{\Delta^2-\omega_s^2}}\right)(\omega+i\eta) - B(\omega)\sigma - \tilde{\xi}_n\tau_z + \frac{\gamma\Delta\tau_x}{\sqrt{\Delta^2-\omega_s^2}}} \tag{6.17}$$

$$= Z(\omega)\frac{1}{\omega + i\eta + Z(\omega)\Big(-B(\omega)\sigma - \tilde{\xi}_n\tau_z + \delta(\omega)\tau_x\Big)}, \tag{6.18}$$

where we defined:

$$Z(\omega) \equiv \frac{1}{\left(1+\frac{\gamma}{\sqrt{\Delta^2-\omega_s^2}}\right)}; \qquad \delta(\omega) \equiv \frac{\gamma\Delta}{\sqrt{\Delta^2-\omega_s^2}} \qquad B(\omega) \equiv B_n + \frac{\gamma B_s}{\sqrt{\Delta^2-\omega_s^2}} \tag{6.19}$$

From here the calculation of the DOS is completely similar to what we did when finding the BCS quasiparticle density of states (section 2.2.2). Defining:

$$\omega_\sigma \equiv \omega - Z(\omega)B(\omega)\sigma; \qquad E_k \equiv +|\sqrt{\tilde{\xi}_n^2 + \Delta(\omega)^2}\,|. \tag{6.20}$$

We then rewrite the Green's function to obtain:

$$\underline{\underline{\mathcal{G}}}(\mathbf{k},\omega+i\eta) = Z(\omega)\frac{1}{\omega+i\eta+Z(\omega)\Big(-B(\omega)\sigma-\tilde{\xi}_n\tau_z+\delta(\omega)\tau_x\Big)} \tag{6.21}$$

$$= Z(\omega)\frac{\omega+i\eta+Z(\omega)(-B(\omega)\sigma+\tilde{\xi}_n\tau_z-\delta(\omega)\tau_x)}{(\omega+i\eta-Z(\omega)\sigma B(\omega))^2-Z(\omega)^2(\tilde{\xi}_n^2+\delta^2(\omega))} \tag{6.22}$$

$$= Z(\omega)\frac{\omega_\sigma+i\eta+Z(\omega)(\tilde{\xi}_n\tau_z-\delta(\omega)\tau_x)}{\Big((\omega_\sigma+i\eta)-Z(\omega)\sqrt{\tilde{\xi}_n^2+\delta(\omega)^2}\Big)\Big((\omega_\sigma+i\eta)+Z(\omega)\sqrt{\tilde{\xi}_n^2+\delta(\omega)^2}\Big)} \tag{6.23}$$

$$= Z(\omega)\left(\frac{1}{(\omega_\sigma+i\eta)-Z(\omega)E_k}-\frac{1}{(\omega_\sigma+i\eta)+Z(\omega)E_k}\right)\frac{\omega_\sigma+Z(\omega)(\tilde{\xi}_n\tau_z-\delta(\omega)\tau_x)}{2Z(\omega)E_k} \tag{6.24}$$

$$= \left(\frac{1}{(\omega_\sigma+i\eta)-Z(\omega)E_k}-\frac{1}{(\omega_\sigma+i\eta)+Z(\omega)E_k}\right)\frac{\omega_\sigma+Z(\omega)(\tilde{\xi}_n\tau_z-\delta(\omega)\tau_x)}{2E_k}. \tag{6.25}$$

To find the electron density of states, $d_e(\omega)$, we write (remembering that all matrices are 2×2-matrices in spin-space):

$$d_e(\omega) = \frac{1}{2\pi V}\sum_{\mathbf{k},\sigma}\underline{\underline{A}}(\mathbf{k},\omega)_{\sigma\sigma} = -\frac{1}{\pi V}\sum_{\mathbf{k},\sigma}\mathrm{Im}\underline{\underline{G^R}}(\mathbf{k},\omega)_{\sigma\sigma} = -\frac{1}{\pi V}\sum_{\mathbf{k},\sigma}\mathrm{Im}\underline{\underline{\mathcal{G}}}(\mathbf{k},\omega+i\eta)_{\sigma\sigma} = \tag{6.26}$$

$$\frac{1}{V}\sum_{\mathbf{k},\sigma}(\delta\{\omega_\sigma-Z(\omega)E_k\}-\delta\{\omega_\sigma+Z(\omega)E_k\})\frac{\omega_\sigma+Z(\omega)\tilde{\xi}_n}{2E_k} \tag{6.27}$$

$$= \sum_\sigma\frac{\nu_{2D}}{2}\int_{-\tilde{\mu}}^{\infty}d\tilde{\xi}_n\frac{1}{2}\left[\left(Z(\omega)+\frac{Z(\omega)\tilde{\xi}_n}{E_k}\right)\delta\{\omega_\sigma-Z(\omega)E_k\}+\left(Z(\omega)-\frac{Z(\omega)\tilde{\xi}_n}{E_k}\right)\delta\{\omega_\sigma+Z(\omega)E_k\}\right] \tag{6.28}$$

$$= \sum_\sigma Z(\omega)\frac{\nu_{2D}}{2}\int_{-\tilde{\mu}}^{\infty}d\tilde{\xi}_n\frac{1}{2}\left[\left(1+\frac{\tilde{\xi}_n}{E_k}\right)\delta\{\omega_\sigma-Z(\omega)E_k\}+\left(1-\frac{\tilde{\xi}_n}{E_k}\right)\delta\{\omega_\sigma+Z(\omega)E_k\}\right], \tag{6.29}$$

where we changed variables from a sum over k to an integral over the renormalized kinetic energy $\tilde{\xi}_n$ and also introduced the renormalized chemical potential belonging to $\tilde{\xi}_n$, $\tilde{\mu}$, and the free electron, spin-traced density of states in 2 dimensions, ν_{2D}:

$$\tilde{\mu} = \mu+\frac{\gamma}{\pi}\log\left(\frac{\lambda_2}{\lambda_1}\right); \qquad \nu_{2D} = \frac{m_n}{\pi}. \tag{6.30}$$

Let us for the following *only consider* $\omega_\sigma > 0$:

$$d_e(\omega_\sigma>0) = \frac{Z(\omega)\nu_{2D}}{4}\sum_\sigma\int_{-\tilde{\mu}}^{\infty}d\tilde{\xi}_n\left(1+\frac{\tilde{\xi}_n}{E_k}\right)\delta\{\omega_\sigma-Z(\omega)E_k\} \tag{6.31}$$

$$= \frac{Z(\omega)\nu_{2D}}{4}\sum_\sigma\int_{-\tilde{\mu}}^{\infty}d\tilde{\xi}\left(1+\frac{\tilde{\xi}_n}{E_k}\right)\Big[\delta(\tilde{\xi}_n-\sqrt{\omega_\sigma^2/Z(\omega)^2-\delta(\omega)^2})\ldots \tag{6.32}$$

$$\ldots+\delta(\tilde{\xi}_n+\sqrt{\omega_\sigma^2/Z(\omega)^2-\delta(\omega)^2})\Big]\frac{|\omega_\sigma/Z(\omega)|}{|\sqrt{\omega_\sigma^2-Z(\omega)^2\delta(\omega)^2}|}.$$

This means that the density of states becomes:

$$\frac{d_e(\omega_\sigma > 0)}{\nu_{2D}} = \tag{6.33}$$

$$\begin{cases} \sum_\sigma \frac{1}{4}\left(1 + \frac{\sqrt{\omega_\sigma^2 - Z(\omega)^2\delta(\omega)^2}}{|\omega_\sigma|}\right)\frac{|\omega_\sigma|}{|\sqrt{\omega_\sigma^2 - Z(\omega)^2\delta(\omega)^2}|}\theta(\omega_\sigma - Z(\omega)\delta(\omega)), & \text{for } \tilde{\mu} < \sqrt{\omega_\sigma^2/Z(\omega)^2 - \delta(\omega)^2} \\ \sum_\sigma \frac{|\omega_\sigma|}{2|\sqrt{\omega_\sigma^2 - Z(\omega)^2\delta(\omega)^2}|}\theta(\omega_\sigma - Z(\omega)\delta(\omega)), & \text{for } \tilde{\mu} > \sqrt{\omega_\sigma^2/Z(\omega)^2 - \delta(\omega)^2} \end{cases} \tag{6.34}$$

$$= \frac{1}{2}\sum_\sigma \left(1 - \frac{1}{2}\left[1 - \frac{\sqrt{\omega_\sigma^2 - Z(\omega)^2\delta(\omega)^2}}{|\omega_\sigma|}\right]\theta(\sqrt{\omega_\sigma^2/Z(\omega)^2 - \delta(\omega)^2} - \tilde{\mu})\right)\ldots \tag{6.35}$$

$$\ldots \times \frac{|\omega_\sigma|}{|\sqrt{\omega_\sigma^2 - Z(\omega)^2\delta(\omega)^2}|}\theta(\omega_\sigma - Z(\omega)\delta(\omega)).$$

From this result we see that we expect three features in the DOS: The first is a peak at the energy which solves the equation $\omega_\sigma = Z(\omega)\delta(\omega)$. Since this is the lowest-energy non-zero value of the DOS this energy is the induced gap, or Δ_{ind}. Also we expect a peak at the divergence point $\omega_s \to \Delta$, since here $\frac{1}{\sqrt{\omega_\sigma^2 - Z(\omega)^2\delta(\omega)^2}}$ diverges for zero B-field, which means that the DOS diverges. But we also see a third 'dip' in the DOS, namely that at the energy, ω_{dip}, that solves the equation $\tilde{\mu} = \sqrt{\omega_\sigma^2/Z(\omega)^2 - \delta(\omega)^2}$ the DOS should be discontinuously changed by an amount dictated by equation (6.35). Since the DOS is proportional to the differential conductance in a (pS)-QPC-N experiment, one should in principle be able to identify the chemical potential from this experiment by examining the energy at which the dip in the density of states lies.

We can do the same kind of analysis for $\omega_\sigma < 0$. This results in a density of states given by:

$$\frac{d_e(\omega)}{\nu_{2D}} = \frac{1}{2}\sum_\sigma \left(1 - \frac{1}{2}\left[1 - \text{Sign}(\omega_\sigma)\frac{\sqrt{\omega_\sigma^2 - Z(\omega)^2\delta(\omega)^2}}{|\omega_\sigma|}\right]\theta(\sqrt{\omega_\sigma^2/Z(\omega)^2 - \delta(\omega)^2} - \tilde{\mu})\right)\ldots \tag{6.36}$$

$$\ldots \times \frac{|\omega_\sigma|}{|\sqrt{\omega_\sigma^2 - Z(\omega)^2\delta(\omega)^2}|}\theta(|\omega_\sigma| - Z(\omega)\delta(\omega)).$$

Here it is clear to see that the DOS is symmetric in ω_σ as long as $|\sqrt{\omega_\sigma^2/Z^2 - \Delta^2}| < \tilde{\mu}$; from then on there is a discontinous change in the DOS, with different magnitude depending on the sign of ω_σ. A comparison of the analytical solution to a numerical solution for three different values of $\tilde{\mu}$ is shown in figures 6.4.1, 6.4.2, and 6.4.3. The numerical solution was obtained by the same methods as explained in section 6.2. The reason why the numerical solution seems more smooth around the discontinuities is that in obtaining the numerical solution we had to introduce a finite value for the $\eta = 0^+$.

Note that we have two peaks in the DOS here - one at the induced gap and one at $\omega \to \Delta$, as explained earlier. The asymmetry in the density of states is clear for $\tilde{\mu} = 200\mu$eV in figure 6.4.2; but for a too small $\tilde{\mu}$ it never occurs, as in figure 6.4.1. And for a $\tilde{\mu}$ too large the "dip" where the asymmetry occurs is pushed so far into the peak at $\omega = \Delta$ that it becomes nearly invisible. Therefore for large $\tilde{\mu}$ this effect seems to not be a good way to determine the chemical potential.

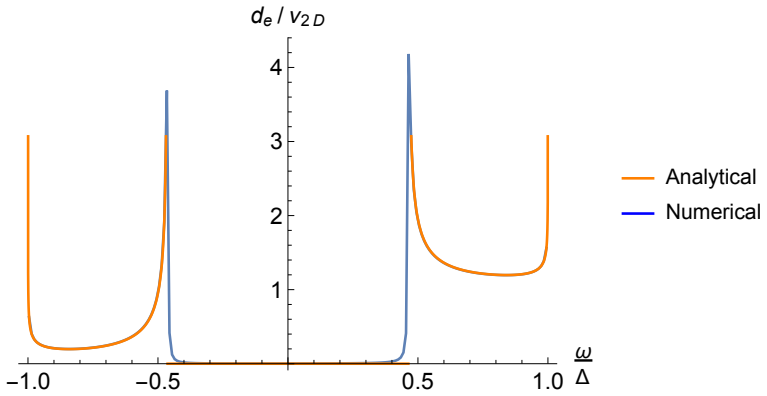

Figure 6.4.1: $\tilde{\mu} = 0$, $\gamma = 180\mu$eV, $B_n = B_s = 0$. Here we see both an analytical and numerical solution of the proximitized 2DEG density of states for zero magnetic field. The $\tilde{\mu}$-dependent asymmetry from equation (6.36) is not visible because of the low value for $\tilde{\mu}$.

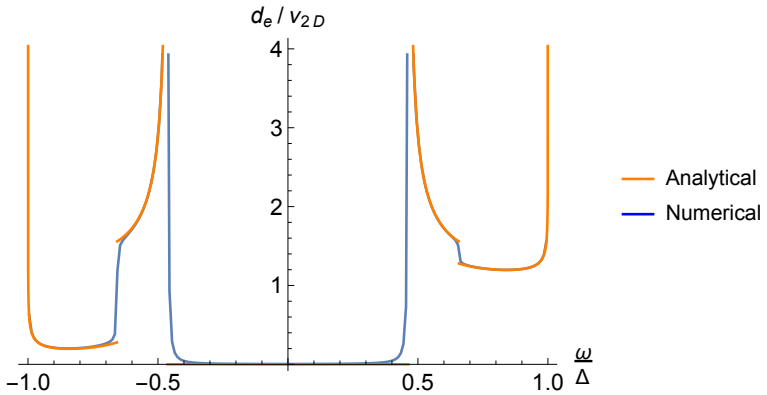

Figure 6.4.2: $\tilde{\mu} = 200$, $\gamma = 180\mu$eV, $B_n = B_s = 0$. Here we see both an analytical and numerical solution of the proximitized 2DEG density of states for zero magnetic field. The $\tilde{\mu}$-dependent asymmetry from equation (6.36) is now visible and sets in at around $\omega = \pm 0.65\Delta$.

Lastly let us discuss when there is a non-zero DOS at zero energy, for any of the spin-projections. The theta-function $\theta(|\omega_\sigma| - Z(\omega)\delta(\omega))$ must have a positive argument for $\omega = 0$ then. We can find the critical parameters where this happens by setting the argument of the theta-function equal to zero for zero ω:

$$\left[|\omega_\sigma| - Z(\omega)\delta(\omega)\right]\big|_{\omega=0} = 0 \Leftrightarrow \tag{6.37}$$

$$|-Z(0)B(\omega)\sigma| = Z(0)\delta(0) \Leftrightarrow \tag{6.38}$$

$$B(\omega) = \gamma. \tag{6.39}$$

So for Zeeman energy $B(\omega)$ larger than γ there will the DOS will be non-zero at $\omega = 0$. This will be important later.

In this section we derived analytically the DOS for a proximitized 2DEG for $\omega_s < \Delta$. We derived that for finite $\tilde{\mu}$ there is an asymmetry in the DOS. In the following section we will find the DOS numerically.

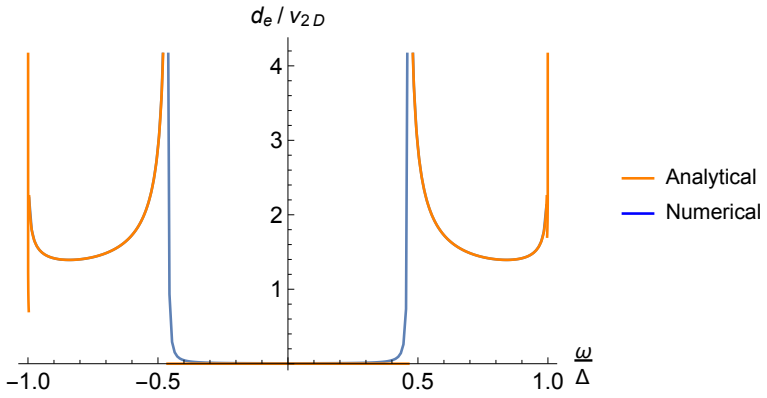

Figure 6.4.3: $\tilde{\mu} = 1000$, $\gamma = 180\mu$eV, $B_n = B_s = 0$. Here we see both an analytical and numerical solution of the proximitized 2DEG density of states for zero magnetic field. The $\tilde{\mu}$-dependent asymmetry from equation (6.36) is not visible because the high value of $\tilde{\mu}$ it has been pushed very close to $\omega = \pm\Delta$ where it is hidden inside the divergence.

6.4.2 Numerical Evaluation of the DOS in a Proximitized 2DEG Without SOI

What we want in this section is to build a foundation upon which our later conductance discussion can be based. This foundation is the electron density of states. We are interested in the diagonal entries of the DOS-matrix, equation (6.5). From now on we denote the Zeeman-energy in the 2DEG as E_{Zeeman} and neglect the magnetic field in the superconductor. We employ the methods described in 6.2.

First we plot the entries for $\gamma = 0.77\Delta$. This is plotted in figures 6.4.4-6.4.6. We see from figure 6.4.4 that for $E_{Zeeman} = 0$ the two spin directions are equivalent. Then in figures 6.4.5-6.4.6 we see how the effect of a magnetic field in the 2DEG is to displace the two spin projections oppositely wrt. energy. It is also interesting to note that the induced gap-peaks in the DOS move as a function of magnetic field whereas the gap at Δ stays the same as a function of magnetic field. Now in figure 6.4.6 we have $E_{Zeeman} > \gamma$ and thus the induced gap has been displaced so much that the density of states is non-zero for $\omega = 0$ (see discussion leading to equation (6.39)). For this large Zeeman-energy we also see a slight dip in the spin-up DOS result close to $\omega = -\Delta$. This is the asymmetry we derived in equation (6.36) due to finite chemical potential. This feature clearly becomes more pronounced with increasing E_{Zeeman}. Interestingly, the asymmetry also becomes much more pronounced for a higher value of γ, which we can see in figures 6.4.7-6.4.8. We have plotted the energy at which the asymmetry happens, ω_{dip}, as a function of magnetic field in figure 6.4.9. Interestingly it changes non-linearly with the magnetic field.

In this section we showed numerical for the DOS for different parameter values. In the next section we will analyze the conductance results on the basis of our understanding of the DOS-matrix.

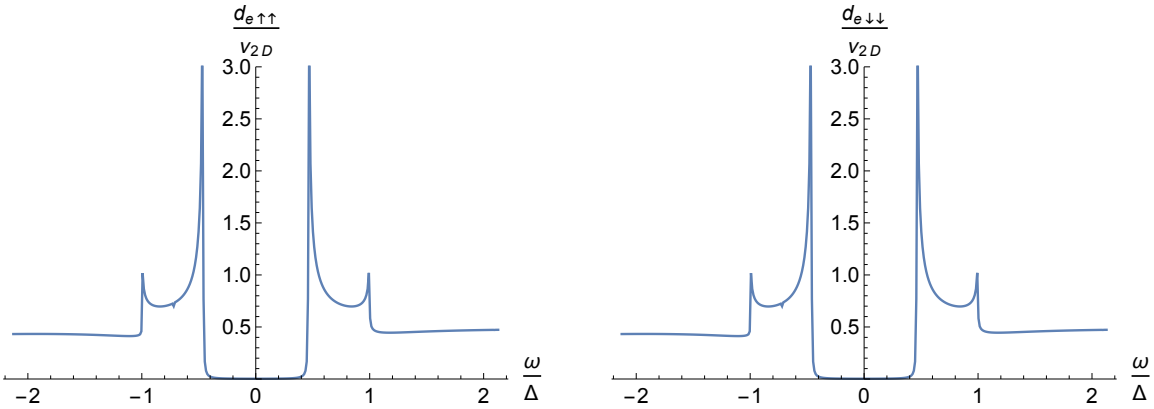

Figure 6.4.4: $E_{Zeeman} = 0$, $\tilde{\mu} = 1000\mu$eV, $\Delta = 235\mu$eV, $\gamma = 0.77\Delta$. The diagonal entries of the DOS-matrix normalized to the 2D free electron density of states, as a function of energy. We see that two spin directions are equivalent without magnetic field.

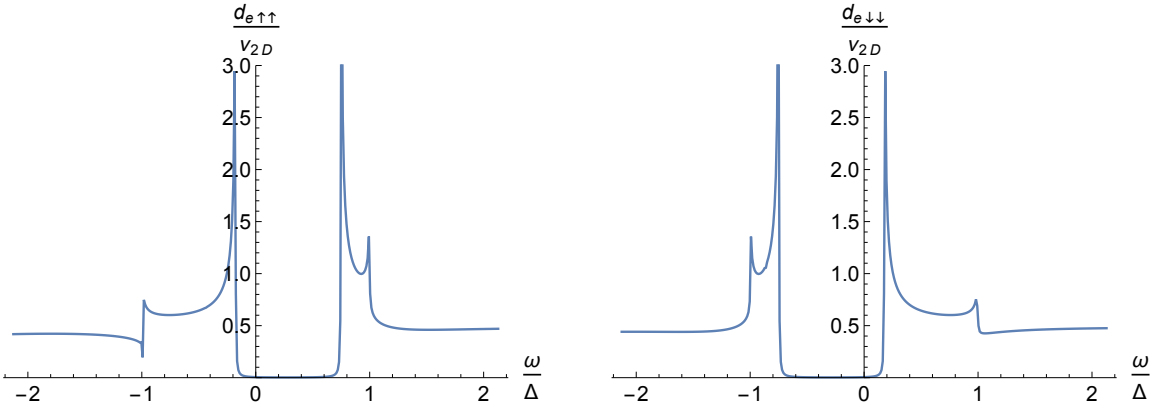

Figure 6.4.5: $E_{Zeeman} = \frac{3}{5}\gamma$, $\tilde{\mu} = 1000\mu$eV, $\Delta = 235\mu$eV, $\gamma = 0.77\Delta$. The diagonal entries of the DOS-matrix normalized to the 2D free electron density of states, as a function of energy. We see that the two spin-directions are displaced oppositely under a non-zero magnetic field.

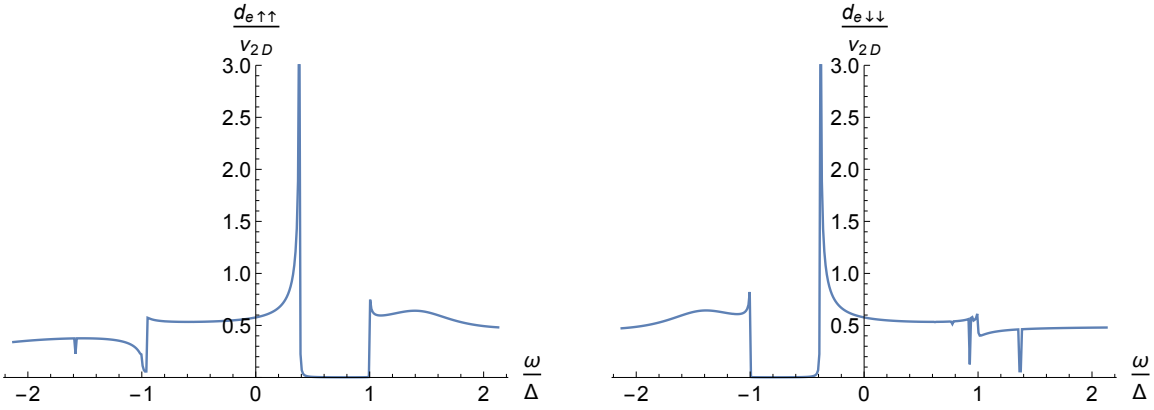

Figure 6.4.6: $E_{Zeeman} = 2\gamma$, $\tilde{\mu} = 1000\mu$eV, $\Delta = 235\mu$eV, $\gamma = 0.77\Delta$. The diagonal entries of the DOS-matrix normalized to the 2D free electron density of states, as a function of energy. Now the Zeeman energy is so large that we have non-zero DOS at $\omega = 0$.

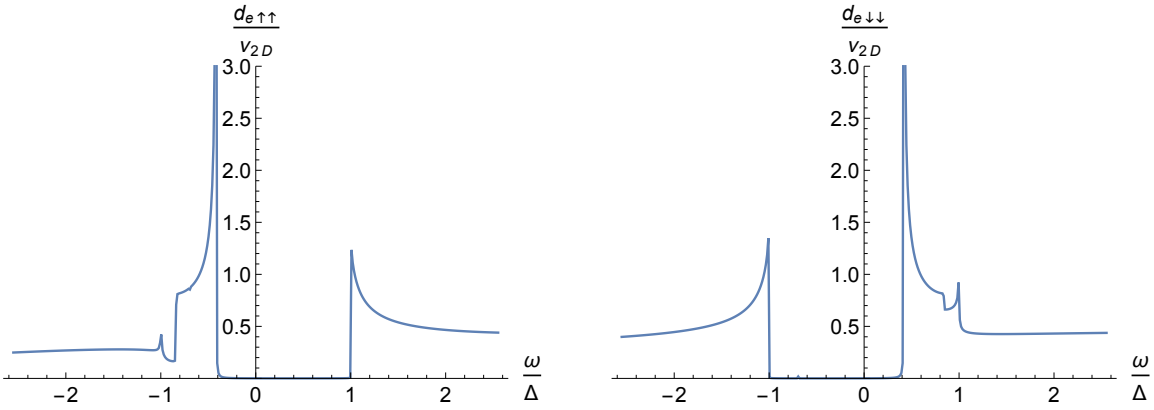

Figure 6.4.7: $\gamma = 3\Delta$, $E_{Zeeman} = \frac{3}{5}\gamma$, $\tilde{\mu} = 1000\mu$eV, $\Delta = 235\mu$eV. The diagonal entries of the DOS-matrix normalized to the 2D free electron density of states, as a function of energy. The dip in the entries close to $\omega = \pm\Delta$ is noticeable.

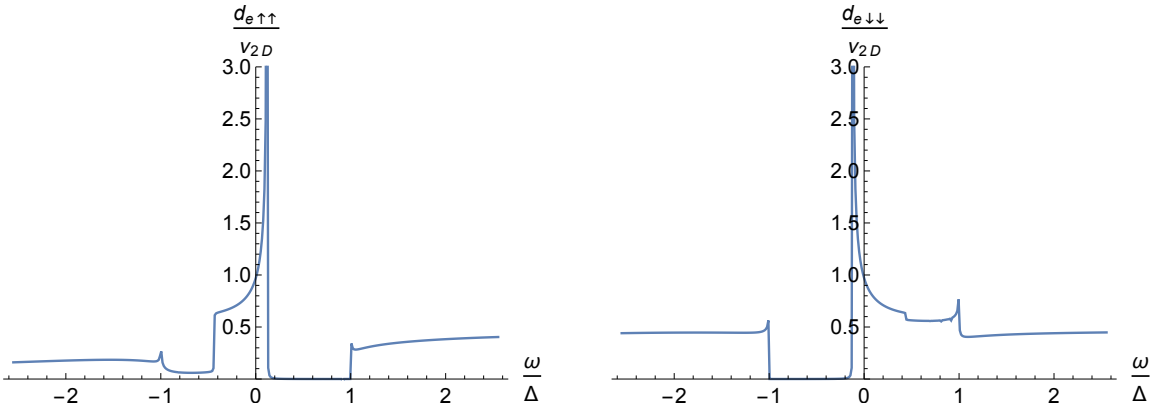

Figure 6.4.8: $\gamma = 3\Delta$, $E_{Zeeman} = \frac{7}{5}\gamma$, $\tilde{\mu} = 1000\mu$eV, $\Delta = 235\mu$eV. The diagonal entries of the DOS-matrix normalized to the 2D free electron density of states, as a function of energy. The two spin directions have now been displaced so much that the density of states is non-zero at $\omega = 0$ and the dip in the entries now occurs closer to $\omega = 0$ compared to figure 6.4.7.

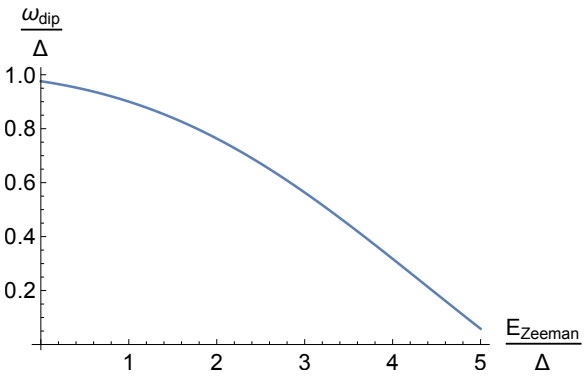

Figure 6.4.9: $\Delta = 235\mu$eV, $\gamma = 3\Delta$, $\tilde{\mu} = 1000\mu$eV. Here we have the energy solution, ω_{dip}, of the equation $0 = \sqrt{\omega_\sigma^2/Z(\omega)^2 - \delta(\omega)^2} - \tilde{\mu}$ plotted as a function of Zeeman energy in the 2DEG. We see that the solution moves non-linearly with the magnetic field.

6.4.3 Conductance Results Without SOI

In the regime without SOI we get conductance results similar to figure 6.4.10. We see some features that happen regardless of which parameters we choose: At zero B-field, moving up on the y-axis from zero source-drain bias, we see three features. It is pretty clear that the last one appears at 2Δ. But there are two other features, which seem to move up and down depending on the parameter γ. Let us try to understand the origin of these features based on the analysis in section 6.4.2.

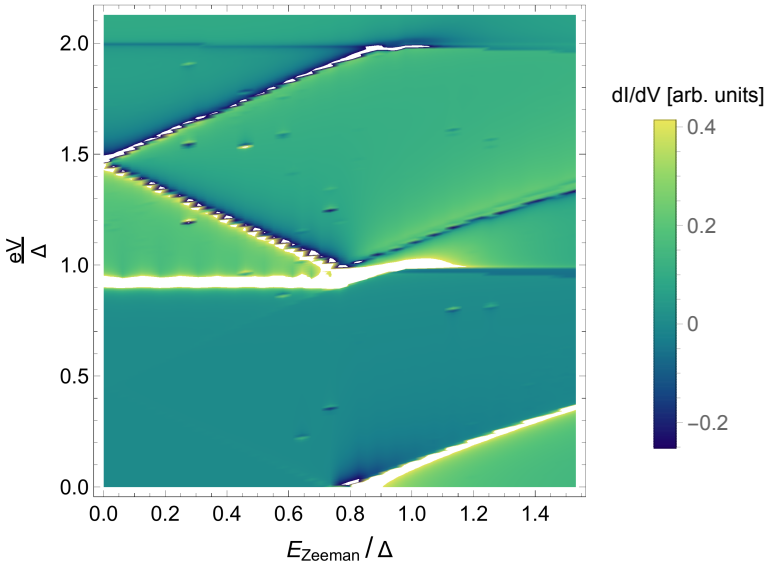

Figure 6.4.10: $\tilde{\mu} = 1000\mu$eV, $\gamma = 180\mu$eV, $\Delta = 235\mu$eV. Here we have a 2D conductance plot in arbitrary units, Zeeman-energy in the 2DEG on the x-axis and source-drain bias energy on the y-axis. Note that we have an upper cut-off in color, so the white parts of the plot are off-scale.

Let us consider the DOS in figure 6.4.4 and the current formula (6.4) at zero B-field. In order to get a noticeable conductance feature we need to find a bias voltage where the current changes a lot. The current from equation (6.4) is a convolution of the DOS-matrix with itself at different energies. Consider now $V \approx 0$. Then the induced gap in the DOS around $\omega = 0$ from figure 6.4.4 means that $d_e(\omega) = 0, \omega \in [0, \Delta_{\text{ind}}]$, and thus for small bias we will get a contribution to the current equal to 0. First at the point where $eV = 2\Delta_{\text{ind}}$ we will have a non-zero contribution. This big change in the current means a big differentical conductance, $G = \frac{dI}{dV}$. From this argument, we expect the first non-zero in a plot of the conductance at zero B-field to be at the point $eV = 2\Delta_{\text{ind}}$.
We know from section 6.4.1 that the DOS has two divergencies at the induced gap Δ_{ind}, and one at

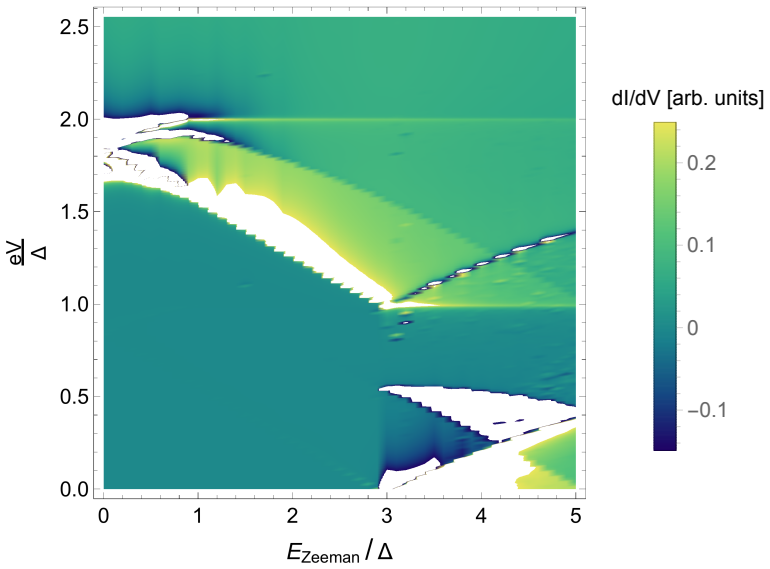

Figure 6.4.11: $\tilde{\mu} = 1000\mu$eV, $\Delta = 235\mu$eV, $\gamma = 3\Delta$. Here we have a 2D conductance plot in arbitrary units, Zeeman-energy in the 2DEG on the x-axis and source-drain bias energy on the y-axis. Note that we have an upper cut-off in color, so the white parts of the plot are off-scale.

the superconducting gap Δ. In between the two divergencies the DOS is non-zero but continuous and rather well-behaved. Therefore we expect a big change in the current at the point $eV = \Delta_{\text{ind}} + \Delta$, where the two divergencies will get convoluted, and thus a noticeable feature in the conductance plot at this same value of the conductance.
In the same manner of arguing, the bias which makes the two divergencies at $\omega = \pm\Delta$ overlap should also produce a noticeable feature in the conductance plot. Thus to conclude, we would expect three features in the conductance plot at zero magnetic field: One at $eV = 2\Delta_{ind}$, one at $eV = \Delta_{\text{ind}} + \Delta$, and one at 2Δ. Notice that these observations give us a clear way to deduce the induced gap from tunneling spectroscopy experiments on devices such as the (pS)-QPC-(pS) one.

When looking at figure 6.4.10 we see features which correspond well to this interpretation. At zero B-field and zero source-drain bias we have no conductance, since here the current is constantly equal to zero. Then at three different bias-strengths, which we interpret as the ones mentioned above, we see strong conductance features. Notice that their relative brightness varies - for example, the third feature up at $eV = 2\Delta$ seems to be a negative conductance line. The lack of a positive conductance feature at $eV = 2\Delta$ can be explained by the divergence at $\omega = \Delta$ having a much lower height than the one at $\omega = \Delta_{\text{ind}}$ in figure 6.4.4, so that they will give rise to different brightnesses in the conductance plots. In the same figure we also see that the DOS falls rapidly after passing the peaks at $\omega \pm \Delta$, which explains the negative conductance feature.

Now let us try to understand what might happen when we apply a Zeeman field in the 2DEG. As explained in section 6.4.1, here spin is a good quantum number, so that the DOS-matrix is diagonal. This means that the trace in equation (6.8) becomes:

$$\text{Tr}_\sigma \left[\underline{\underline{d_{e\sigma}}}(\omega) \underline{\underline{d_{e\sigma}}}(\omega + eV) \right] = d_{e\uparrow\uparrow}(\omega) d_{e\uparrow\uparrow}(\omega + eV) + d_{e\downarrow\downarrow}(\omega) d_{e\downarrow\downarrow}(\omega + eV) \tag{6.40}$$

We conclude that the formula for the current only couples same-spin species of the DOS. This means that the displacement of the spin-species with magnetic field does not matter for the peaks at $eV = 2\Delta_{\text{ind}}$ and we expect a constant feature at $eV = 2\Delta_{\text{ind}}$ as a function of magnetic field, which is also clear from figure 6.4.10.
This same argument does not hold for the second feature at $eV = \Delta_{\text{ind}} + \Delta_{\text{Al}}$. The reason for this is that the induced gap changes as a function of magnetic field, whereas the gap at $\omega = \pm\Delta$ does not.

Therefore the point where we have an overlap of the divergence in the DOS associated with the Δ-gap and the induced gap will scale with magnetic field like the induced gap does. This behavior is clear from figure 6.4.10. The final feature at $2\Delta_{\mathrm{Al}}$ should not change with magnetic field, similar to the feature at $2\Delta_{\mathrm{ind}}$.

When the magnetic field reaches the strength $E_{Zeeman} \sim \gamma$ we see some change in the behavior. We can see from equation (4.60) that for small energies $\omega << \Delta_{\mathrm{Al}}$ the induced gap becomes approximately equal to γ:

$$\Delta_{\mathrm{ind}} \approx \gamma, \quad \omega << \Delta_{Al}. \tag{6.41}$$

When the magnetic field strength becomes larger than the induced gap we will begin to see some features at $eV = 0$ since now the DOS is non-zero for small energies.
Finally there is one more feature in figure 6.4.10, which is important to understand since is repeats in all the results and seems present in figure 6.1.1 too. At the point where the gap closes, a new conductance line seems to appear at a bias energy around $eV = \Delta$. This is due to the "gap closing", i.e. $d_e(\omega = 0) \neq 0$. This means that the divergence at $\omega = -\Delta$ will only appear in the current integral for $eV > \Delta$, not for $eV < \Delta$, which gives a big conductance feature at $eV = \Delta$.

Now we also show results for a different value of γ in figure 6.4.11. The point of this plot is that for this value of γ we get some non-linear conductance feature with increasing Zeeman field, somewhat resembling some of the non-linear features we see in figure 6.1.1. This stems from the finite-chemical-potential induced asymmetry in equation (6.36) and therefore matches with figure 6.4.9. Also we see that the three conductance features at zero magnetic field have somewhat blended together as one big conductance feature at high bias voltage.

Both figure 6.4.10 and 6.4.11 have some shortcomings when trying to compare them to experiment (figure 6.1.1). None of them show the kind of conductance-gap closing as we see happening at about 100mT in figure 6.1.1. And none of them really catch the same kind of non-linear conductance features as in figure 6.1.1. In the next section we will introduce Rashba SOI and see how this affects the conductance results.

6.5 Analysis Including SOI

6.5.1 (pS)-QPC-(pS) Conductance With SOI

When producing results with SOI we put the magnetic field in-plane with the SOI.

Before we produce some results including SOI, let us try to use our knowledge of the system without SOI to interpret the experimental plot in figure 6.1.1. We will only consider positive bias, since the problem is symmetric wrt. bias. We know that we expect to see three features at zero B-field; one at $eV = 2\Delta_{\text{ind}}$, one at $eV = \Delta_{\text{ind}} + \Delta_{\text{Al}}$ and one at $eV = 2\Delta_{\text{Al}}$. When looking at figure 6.1.1 we see a very faint feature at around $eV = 200\mu$eV. Note that the y-axis is not placed properly in the figure 6.1.1, as explained in the figure text it should be symmetric around $Vdc = 0$. Then further up, at around $eV = 400\mu$eV there is a very bright peak indeed, also with some width. How are we to interpret this?

I believe the very faint feature at $eV = 200\mu$eV is simply too vague to be interpreted as $eV = 2\Delta_{\text{ind}}$. In all simulations this peak is very bright because we go from zero current to suddenly convoluting two divergencies in the DOS. The faint feature might be attributable to something called *Andreev reflection* though (see e.g. ref. [26]), which is a 4th order process in the tunneling parameter, which is naturally not captured in our model that only captures features up to second order in the tunneling constant.

Given this interpretation, where are the three distinct features in figure 6.1.1 then? Well, if we conjecture that our parameters are chosen such that $\Delta_{\text{ind}} \approx \Delta$, then we might expect that the three features would blur together as in figure 6.4.11. This could explain the feature in experiment. Now which parameters govern the magnitude of the induced gap? For zero SOI we have shown that the induced gap can be found from solving equation (3.44) for the energy with the constraint $\xi = 0$. From this equation we can see that the only parameters that govern the magnitude of the induced gap in the absence of magnetic field are Δ and γ, given $\epsilon_{g0} = \gamma$ (see chpt. 5). For a given Δ we made a plot of the magnitude of the induced gap as a function of $\epsilon_{g0} = \gamma$ in figure 3.3.1. What is interesting about this graph is that for $\gamma < \Delta$ we have something like $\Delta_{\text{ind}} < 0.5\Delta$. Thus if we are to be consistent with the above interpretation of figure 6.1.1 where we conclude that we have an induced gap close to the value of Δ, we need at least $\gamma > 2\Delta_{\text{Al}}$. Such a value of γ should reproduce something similar to figure 6.1.1.

But actually such a large value for γ introduces a problem with the gap-closing. When including the SOI, we expect the conductance feature for zero B-field at $eV = 2\Delta_{\text{ind}}$ to diminish as a function of magnetic field instead of staying constant as without SOI. We can argue why by building on the intuition from the 1D wire model in ref. [18]. If we just look at the spin-dynamics:

$$\mathcal{H}_{spin} = B\sigma_x + up\sigma_z. \tag{6.42}$$

When looking at the eigenspinors of this Hamiltonian they are:

$$\chi_{\pm} \propto \begin{pmatrix} \frac{up}{B} \pm \sqrt{1 + (\frac{up}{B})^2} \\ 1 \end{pmatrix} \tag{6.43}$$

For $up \to 0$ we get the usual σ_x-eigenspinors in the σ_z basis, while for $B \to 0$ we get the σ_z-eigenvectors. So we see that also including SOI transverse to the Zeeman field mixes the spin of the eigenvectors. Without SOI we saw that the spin-up and spin-down parts of the DOS did not mix, which led to a constant conductance feature at $eV = 2\Delta_{ind}$ for $B_n < \gamma$. However since SOI in this way mixes the spin-up and spin-down parts, we would expect that now there is some coupling between the two,

which would lead to the conductance feature setting in at a lower bias with increasing magnetic field, i.e. a *conductance gap closing*. It is at the point $E_{Zeeman} = \gamma$ that we expect a gap closing and the zero conductance to vanish. As explained earlier we also expect a conductance feature at $eV = \Delta$ to appear at this point. These features are consistent with figure 6.1.1 if we interpret the magnetic field strength $B \approx 100\text{mT}$ to equal the induced gap closing in the DOS.

From these arguments we would look in the $\gamma > \Delta$-regime. However, we also know that the Zeeman energy splitting scales as:

$$E_{Zeeman} = \frac{1}{2} g^* \mu_B B, \tag{6.44}$$

where μ_B is the constant called the Bohr magneton. If we identify the point $B = 100\text{mT}$ as the point where we have gap-closing we can find a correspondence between the effective g-factor and γ:

$$\frac{g^*}{2} \cdot 57.88 \mu\text{eVT}^{-1} \cdot 0.1\text{T} = \gamma \Leftrightarrow \tag{6.45}$$

$$g^* = \frac{\gamma}{2.894} \mu\text{eV}^{-1} \tag{6.46}$$

From this relation we can see that the lower limit for γ, which we established above to be around $\gamma = 2\Delta_{Al} = 470\mu\text{eV}$ would mean we have an effective g-factor equal to or greater than $g^* = 160$. From the experience with proximitized 2DEGs at the Center for Quantum Devices at the University of Copenhagen there is certainly some effective g-factor in the 2DEG, but it is of order 10. $g^* \sim 100$ is a big stretch. And in our model the only way to get a gap-closing is to invoke a magnetic field $E_{Zeeman} > \gamma$. Thus from experience of the range that we expect the effective g-factor to belong to we would most probably need $\gamma < \Delta_{Al}$.

So we have two different arguments, each excluding the other; one predicts $\gamma > \Delta_{\text{Al}}$ and the other $\gamma < \Delta_{\text{Al}}$. At this point we will present the results we get for each regime and see if they bring any clarity to the situation. First we try three different values of γ below Δ_{Al}. These results are presented in figures 6.5.1-6.5.3. Note that we have an upper-color cut-off in all conductance plots. By comparing the figures we see that we have an induced gap that clearly grows as a function of growing γ, as expected. And also the gap closing at $E_{Zeeman} = \gamma$ is clear in all the plots. Also the appearance of the conductance line at $eV = \Delta_{\text{Al}}$ at magnetic fields $E_{Zeeman} > \gamma$ is clearly there in all the plots. The three features that existed without SOI clearly also show themselves here. The resemblance to experiment is poor, though. A major problem in comparing figures 6.5.1-6.5.3 to figure 6.1.1 is that the induced gap is simply not large enough in any of the figures to resemble experiment - as expected. Furthermore, at zero B-field we see the three features quite distinctly in figures 6.5.1-6.5.3, whereas as explained earlier it seems there is only one significant feature in experiment. Also the behaviour of the features with magnetic field seem quite linear in figures 6.5.1-6.5.3, not capturing the non-zero curvature of some of the conductance features that is there in figure 6.1.1.

Now we look to the other regime where $\gamma > \Delta_{\text{Al}}$. The results are shown in figures 6.5.4-6.5.9. All of these results have the common problem described earlier that to get a correspondence with experiment we need a g-factor of $g^* > 160$, which is inconsistent with the experience from experiments with proximitized 2DEGs.

One question that is very relevant to the Center for Quantum Devices at the University of Copenhagen is whether there is a way for them to estimate the Rashba SOI strength from looking at their experiments. Since the SOI is known to change the way features vary with magnetic field it might be that the curvature of the non-linear features in experiment are related to the SOI strength. We therefore plot the conductance for varying SOI strengths in figures 6.5.4-6.5.7. Here we see that for low SOI strength there is something similar to two non-linear conductance features. The top feature seems to be the finite $\tilde{\mu}$-effect from the result without SOI, figure 6.4.11, while the second feature

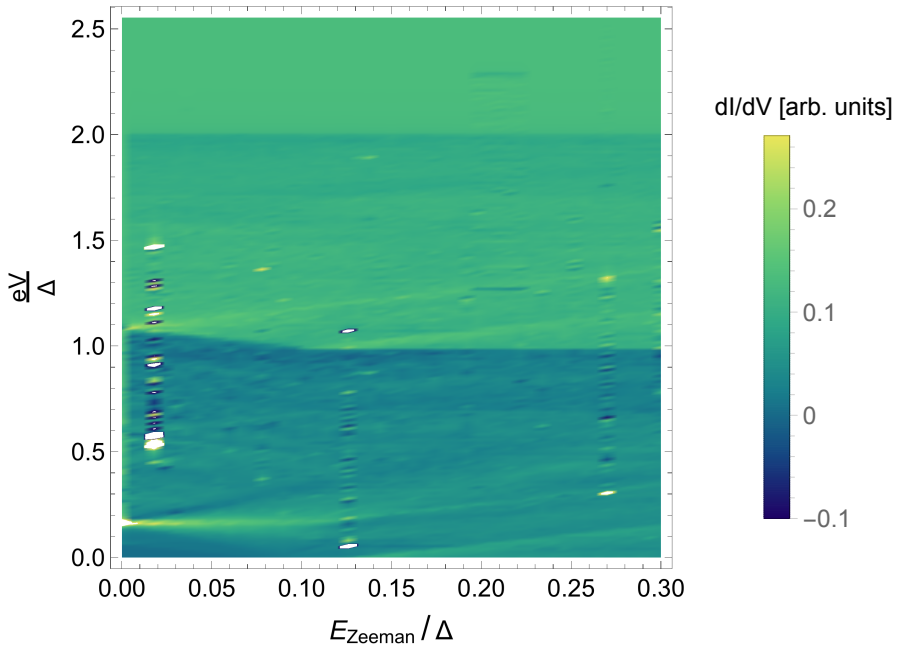

Figure 6.5.1: $\alpha = 0.59\text{eVÅ}$ $\tilde{\mu} = 1000\mu\text{eV}$, $\Delta = 235\mu\text{eV}$, $\gamma = 0.1\Delta$. Here we see a 2D-plot of the differential conductance in arbitrary units, Zeeman energy in the 2DEG on the x-axis and positive source-drain bias voltage energy on the y-axis.

must be due to SOI. However when we increase the SOI strength in the next figures, the two features blend together as one. Thus both parameters $\tilde{\mu}$ and α are relevant when it comes to the non-linear conductance features with magnetic field.

Now to confirm our suspicion that it is the finite $\tilde{\mu}$-effect we derived without SOI that is involved we vary $\tilde{\mu}$. We show this in figures 6.5.8-6.5.9. It is clear that the slope of the conductance feature depends on the size of the renormalized chemical potential. In conclusion it seems that both the chemical potential and the SOI strength affect the curvature of the non-linear conductance features. Finally we include plots of the entries of the DOS-matrix for non-zero SOI in figures 6.5.10-6.5.12, to compare with the conductance measurement in figure 6.5.7. Note that $d_{e\uparrow\uparrow} = d_{e\downarrow\downarrow}$ and $d_{e\uparrow\downarrow} = d_{e\downarrow\uparrow}$, so we do not plot all entries. We see how the diagonal part has a big peak at low Zeeman field, and how this peak diminishes and vanishes for increasing Zeeman field, in correspondence with figure 6.5.7. Note also that the off-diagonal part is not zero here and will affect the current.

In conclusion we can say that including Rashba SOI gave us the kind of conductance-gap closing that we see in experiment, figure 6.1.1. The size of the gap depends on γ, the tunneling coefficient, and we need a value of γ higher than what corresponds to experimental experience to get an induced gap corresponding to experiment. We reproduced in all plots that for Zeeman energies larger than γ we had a conductance feature at Δ and one at 2Δ, which also happens in experiment. For the high values of γ we were also able to show non-linear conductance features, whose curvature depends on both the chemical potential and SOI strength, which resemble experiment, figure 6.1.1.

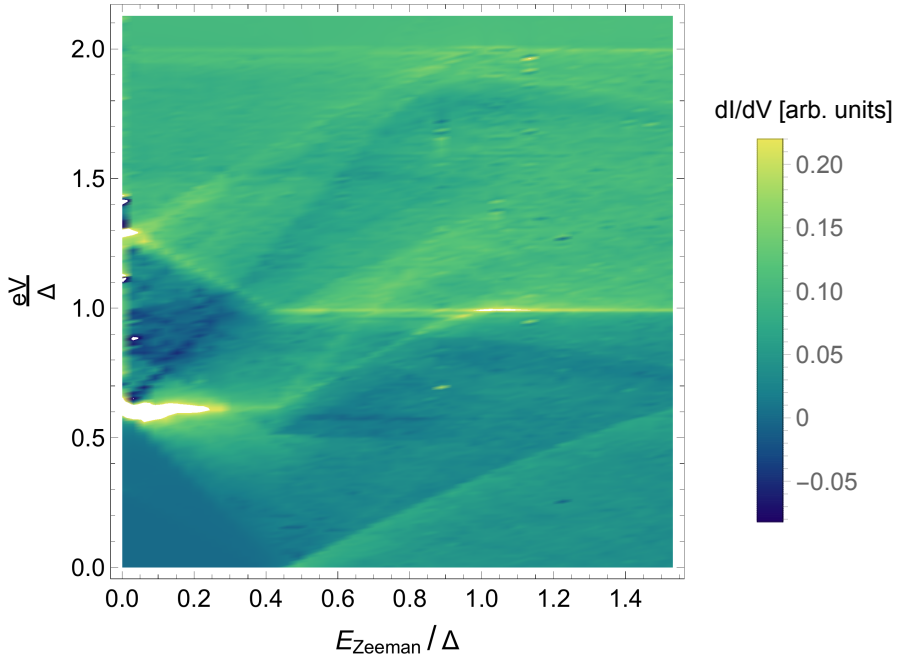

Figure 6.5.2: $\alpha = 0.59\text{eVÅ}$ $\tilde{\mu} = 1000\mu\text{eV}$, $\Delta = 235\mu\text{eV}$, $\gamma = 0.43\Delta$. Here we see a 2D-plot of the differential conductance in arbitrary units, Zeeman energy in the 2DEG on the x-axis and positive source-drain bias energy on the y-axis.

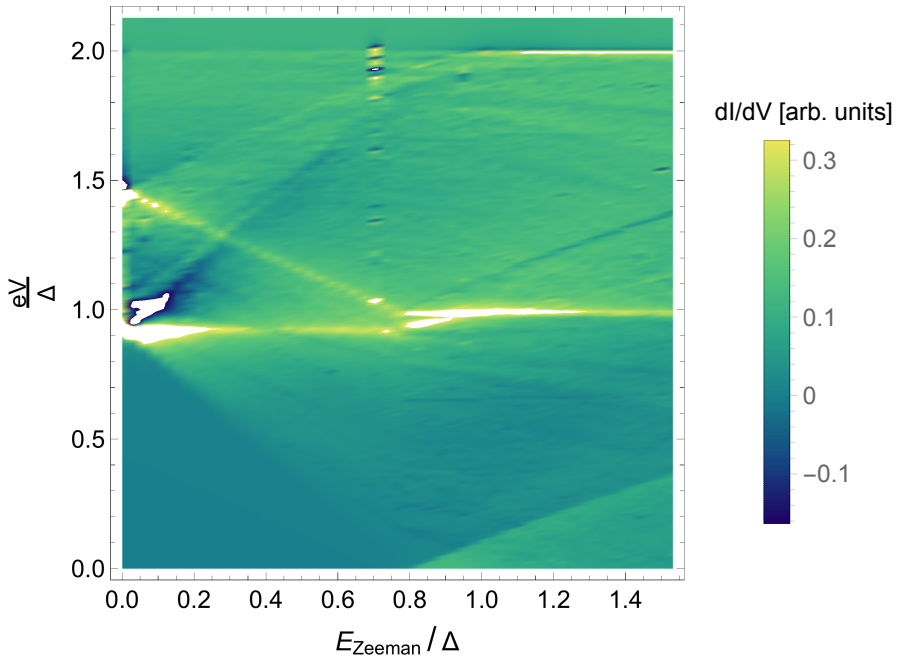

Figure 6.5.3: $\alpha = 0.59\text{eVÅ}$ $\tilde{\mu} = 1000\mu\text{eV}$, $\Delta = 235\mu\text{eV}$, $\gamma = 0.77\Delta$. Here we see a 2D-plot of the differential conductance in arbitrary units, Zeeman energy in the 2DEG on the x-axis and source-drain bias energy on the y-axis.

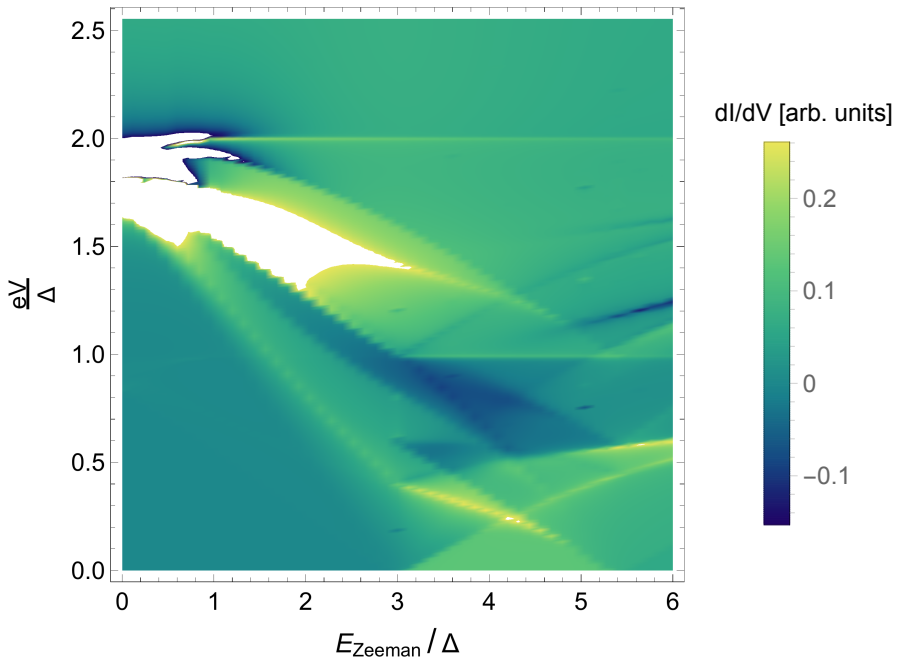

Figure 6.5.4: $\alpha = 0.20\text{eVÅ}$, $\tilde{\mu} = 1000\mu\text{eV}$, $\Delta = 235\mu\text{eV}$, $\gamma = 3\Delta$. Here we have a 2D conductance plot in arbitrary units, Zeeman-energy in the 2DEG on the x-axis and source-drain bias energy on the y-axis.

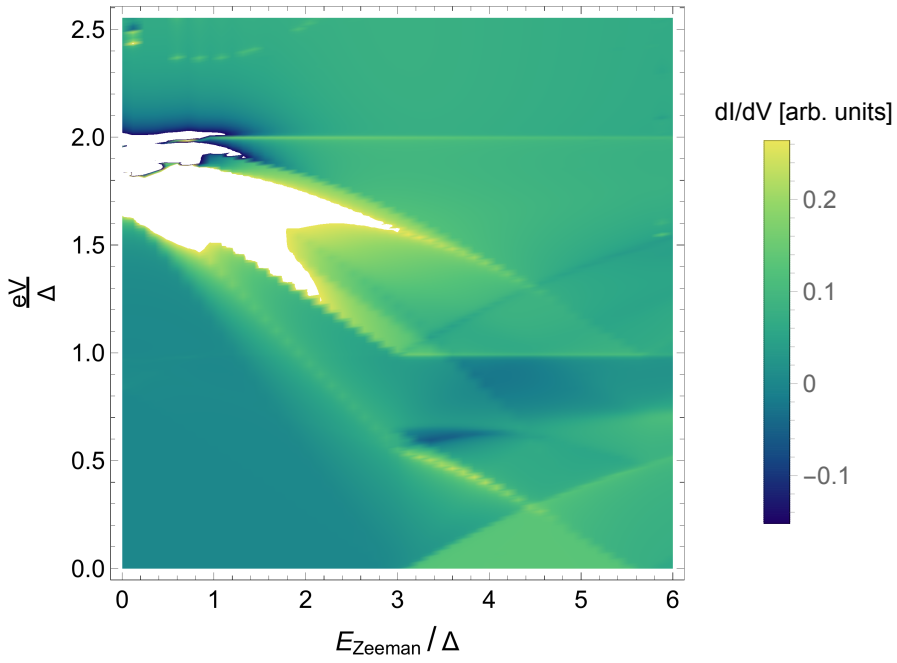

Figure 6.5.5: $\alpha = 0.30\text{eVÅ}$, $\tilde{\mu} = 1000\mu\text{eV}$, $\Delta = 235\mu\text{eV}$, $\gamma = 3\Delta$. Here we have a 2D conductance plot in arbitrary units, Zeeman-energy in the 2DEG on the x-axis and source-drain bias energy on the y-axis.

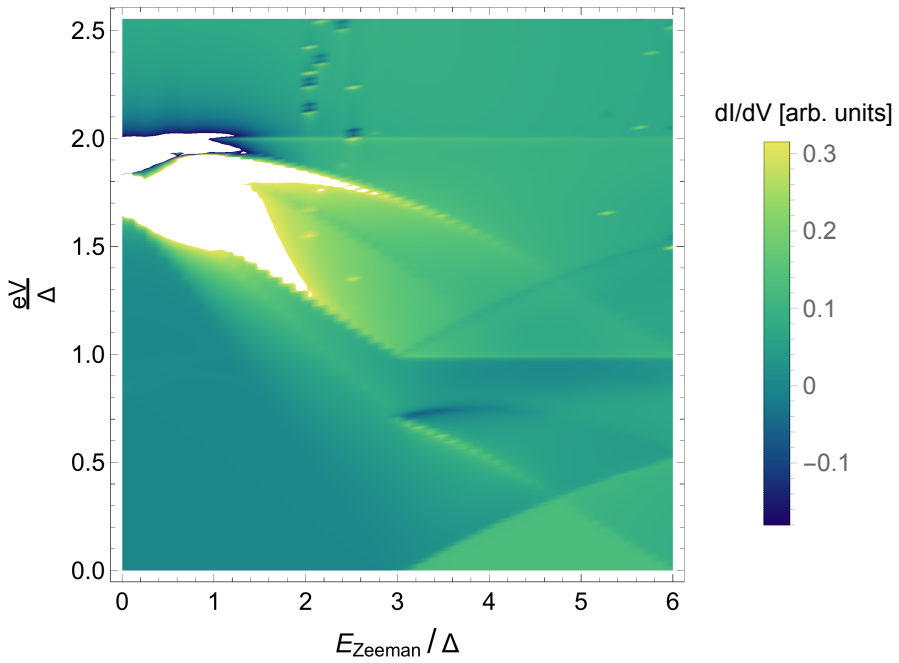

Figure 6.5.6: $\alpha = 0.42\text{eVÅ}$, $\tilde{\mu} = 1000\mu\text{eV}$, $\Delta = 235\mu\text{eV}$, $\gamma = 3\Delta$. Here we have a 2D conductance plot in arbitrary units, Zeeman-energy in the 2DEG on the x-axis and source-drain bias energy on the y-axis.

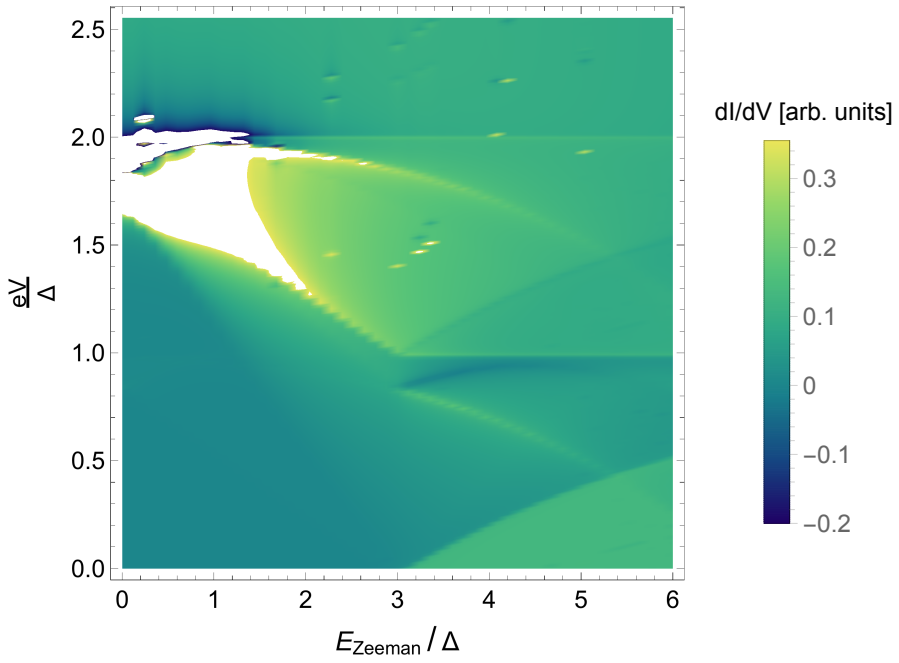

Figure 6.5.7: $\alpha = 0.59\text{eVÅ}$, $\tilde{\mu} = 1000\mu\text{eV}$, $\Delta = 235\mu\text{eV}$, $\gamma = 3\Delta$. Here we have a 2D conductance plot in arbitrary units, Zeeman-energy in the 2DEG on the x-axis and source-drain bias energy on the y-axis.

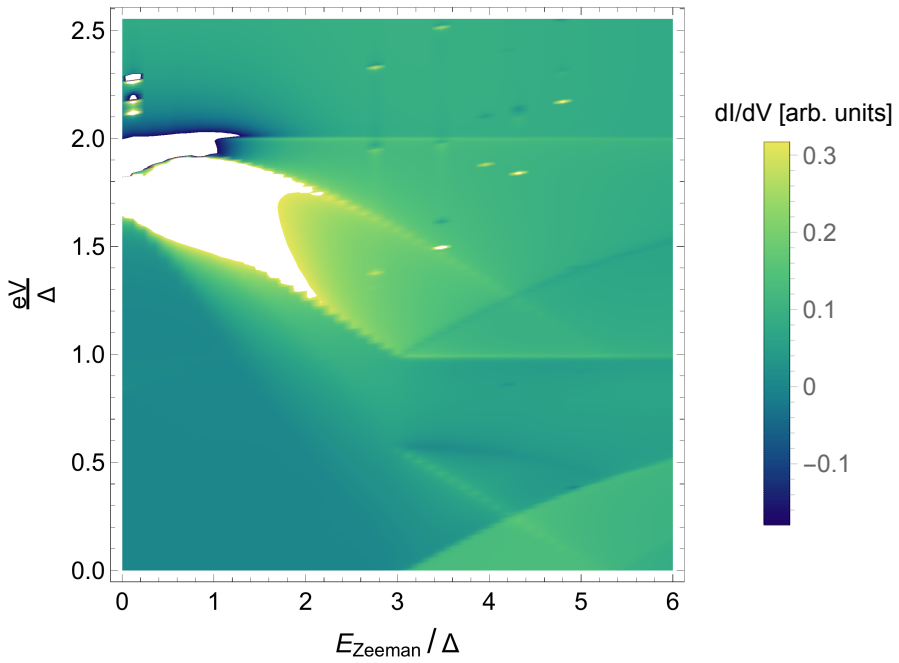

Figure 6.5.8: $\tilde{\mu} = 500\mu$eV, $\alpha = 0.59$eVÅ, $\Delta = 235\mu$eV, $\gamma = 3\Delta$. Here we have a 2D conductance plot in arbitrary units, Zeeman-energy in the 2DEG on the x-axis and source-drain bias energy on the y-axis.

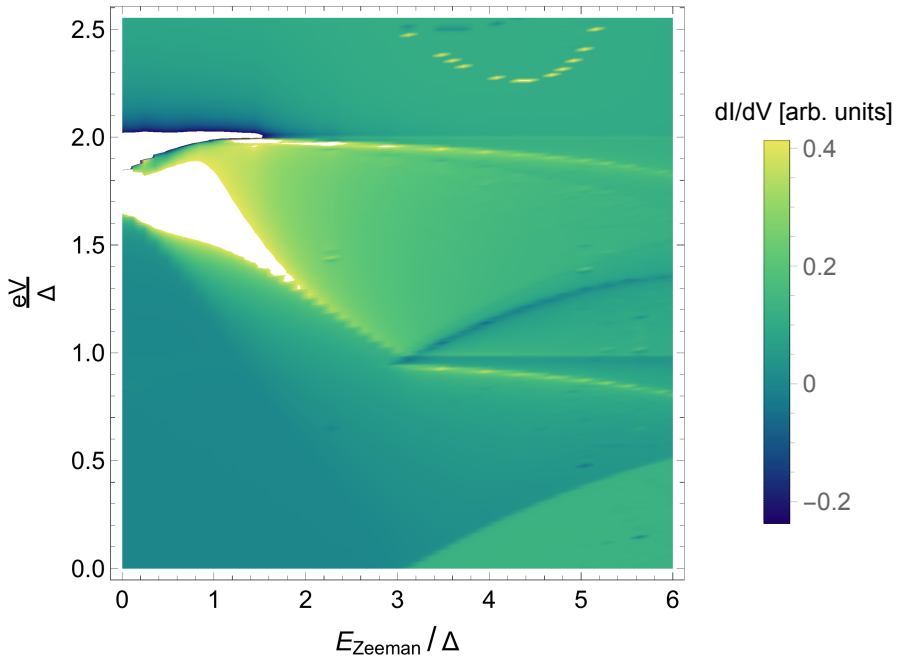

Figure 6.5.9: $\tilde{\mu} = 1800\mu$eV, $\alpha = 0.59$eVÅ, $\Delta = 235\mu$eV, $\gamma = 3\Delta$. Here we have a 2D conductance plot in arbitrary units, Zeeman-energy in the 2DEG on the x-axis and source-drain bias energy on the y-axis.

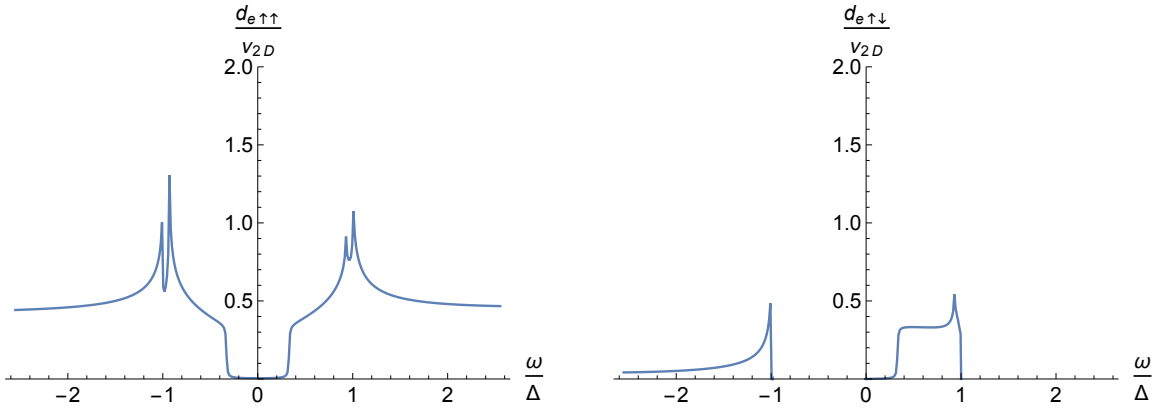

Figure 6.5.10: $E_{Zeeman} = \frac{3}{5}\gamma$, $\alpha = 0.59\text{eV}$, $\tilde{\mu} = 1000\mu\text{eV}$, $\Delta = 235\mu\text{eV}$, $\gamma = 3\Delta$. The spin-diagonal- and spin-off-diagonal-part of the electron density of states normalized to the 2D free electron density of states, as a function of energy.

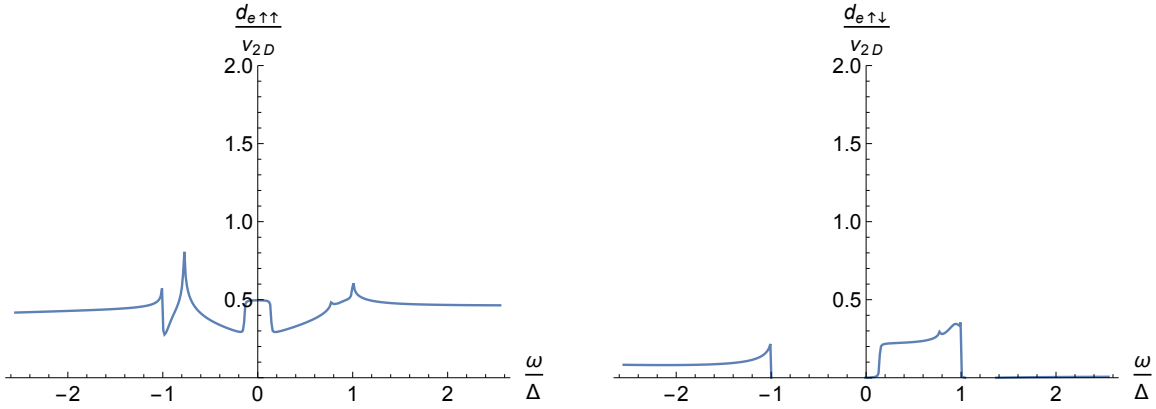

Figure 6.5.11: $E_{Zeeman} = \frac{6}{5}\gamma$, $\alpha = 0.59\text{eV}$, $\tilde{\mu} = 1000\mu\text{eV}$, $\Delta = 235\mu\text{eV}$, $\gamma = 3\Delta$. The spin-diagonal- and spin-off-diagonal-part of the electron density of states normalized to the 2D free electron density of states, as a function of energy.

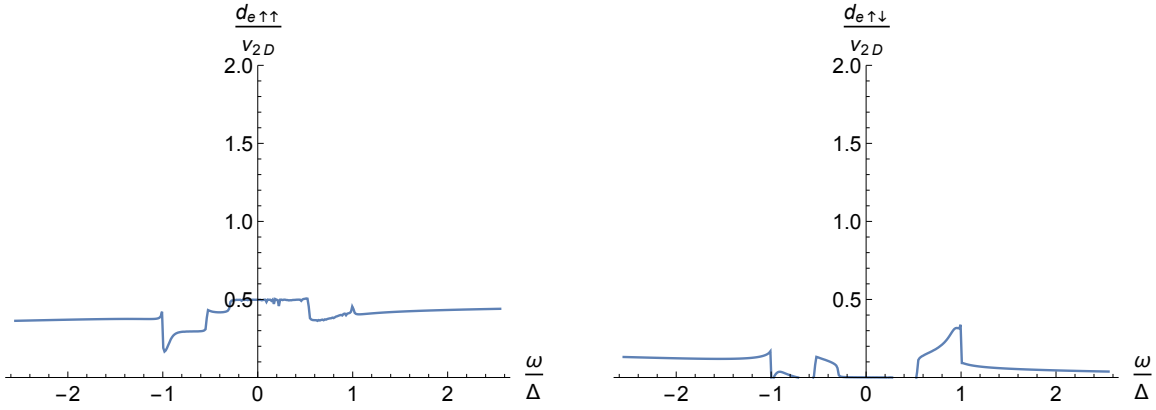

Figure 6.5.12: $E_{Zeeman} = 2\gamma$, $\alpha = 0.59\text{eV}$, $\tilde{\mu} = 1000\mu\text{eV}$, $\Delta = 235\mu\text{eV}$, $\gamma = 3\Delta$. The spin-diagonal- and spin-off-diagonal-part of the electron density of states normalized to the 2D free electron density of states, as a function of energy.

Chapter 7

Conclusion

In this thesis we performed theoretical investigations of a superconductor-2DEG junction. In chpt. 3 we built upon ref. [22] and studied the BdG equations including BCS superconductivity, effective mass and effective g-factor in the semiconductor and a delta-function potential to model a barrier between the two regions. We obtained the equation for the excitation spectrum of the system and derived the spectrum in the approximation that the wavenumber in the 2DEG is approximately that of the ground state of the infinite square well (AISW). We then went on to conduct some investigation into the proximity-induced gap in the 2DEG in this approximation, showing that the induced gap depends critically on the coupling-parameter ϵ_{g0}. Furthermore we analyzed the effective g-factor in this approximation for small magnetic fields, and concluded that $\epsilon_{g0} \to 0$ results in the wave-function being confined in the 2DEG, whereas for $\frac{\epsilon_{g0}}{\Delta} >> 1$ the relative wave-function probability weight in the 2DEG vanishes. We concluded this section with some numerical results for a set of concrete parameters chosen to exemplify the results derived so far.
We then went on to derive an energy-dependent self-energy in the 2DEG in a Green's function tunneling model where we integrate out the semi-infinite superconductor coupled to the 2DEG to obtain an effective Green's function in the 2DEG in chpt. 4. From this we obtained the excitation spectrum for the proximitized 2DEG. Via comparing the equations for the spectra we established a correspondence between the AISW-approximation in the wave-function model and the tunneling Green's model up to a shift in the chemical potential if we equate the parameters $\epsilon_{g0} = \gamma$ in chpt. 5, where gamma is related to the tunneling rate. This allowed us to immediately relate the results from the AISW-approximation to the proximitized 2DEG. Furthermore the result is useful because it extends the domain of applicability of the tunneling approximation in a Green's function model to any situation that can be effectively modeled by a wave-function AISW-approximation, and enables us in such a situation to find an estimate for the tunneling rate based on microscopic parameters.
In chpt. 6 we then built upon the tunneling Green's function model and applied it to tunneling spectroscopy of two proximitized 2DEGs. We analyzed the electron density of states (DOS) in the absence of SOI and calculated the conductance numerically. Here we found an asymmetry in the DOS for finite chemical potential, which can influence the conductance results. Finally we obtained numerical density of states and conductance results including Rashba spin-orbit interaction (SOI), and analyzed the effect of different strengths of the parameters γ, the chemical potential and the SOI strength on the conductance result and compared with experimental results. We showed that when the gap closes we get two conductance features at bias energy Δ and 2Δ, which corresponds well with experiment. We uncovered that the value of the chemical potential plays a role unless it is very large, and that it can lead to some non-linear conductance features like the ones observed in experiment at high bias voltage. Also we showed that the SOI strength can also influence these non-linear conductance features with increasing magnetic field, and that both chemical potential and SOI strength therefore contribute to these features.

We showed that if we assume an effective g-factor larger than what is regarded as probable (i.e. $g^* \sim 200$), we showed that we can get results that resemble experiment in many ways. We get an

induced gap of the right size, a conductance gap closing resembling experiment and can reproduce the features in experiment in a qualitative way. In conclusion we could not reproduce experiment for probable values of the parameters. However, we did uncover some general and interesting properties about the system that should be useful in analyzing future experiments, and hopefully this work can lay the foundation for further exploration into the analysis of tunneling spectroscopy of proximitized 2DEGs.

Further work into the problem could include: including SOI in the wave-function model and seek a correspondence with the Green's function tunneling model, or investigate further the reason for the problem with the size of the induced gap versus the size of the effective g-factor.

Chapter 8

Appendices

8.1 Appendix A

There are many layers of complexity in describing accurately the behaviour of solids. The first approximation one usually makes (see [24]) of the behaviour of solids in electric fields is to assume electrons moving freely, which describes the conduction in metals well. However, many solids are more complex than this simple model can describe. Thus we need some way to include the ion lattice's effect on the conduction electrons. One model that answers some qualitative questions about the lattice is the *nearly free electron model*. Here we assume a weak periodic potential originating from the periodic ion lattice, but still no electron-electron interaction except in a mean-field way. It will turn out that at the zone boundary of the Brillouin zone an energy gap can be formed.

Let us follow ref. [24] chpt. 7 and consider a one-dimensional lattice where the ions generate a periodic potential: $U(x) = U(x + a)$. Fourier analysis is useful:

$$U(x) = \sum_G U_G e^{iGx}. \tag{8.1}$$

Likewise we can write the wavefunction of our particle as a Fourier series (permitted by the boundary conditions of the lattice):

$$\psi(x) = \sum_k C(k) e^{ikx}. \tag{8.2}$$

We now want to solve the wave equation of an electron in the crystal, $\mathcal{H}\psi = \epsilon\psi$, where $\mathcal{H}$ is the Hamiltonian and ϵ is the energy eigenvalue. Rewriting everything in k-space we get the equation:

$$\sum_k \frac{k^2}{2m} C(k) e^{ikx} + \sum_G \sum_k U_G C(k) e^{i(k+G)x} = \epsilon \sum_k C(k) e^{ikx}. \tag{8.3}$$

For each Fourier component on both sides of the equation to have the same coefficient we need the following identity:

$$(\lambda_k - \epsilon) C(k) + \sum_G U_G C(k - G) = 0, \tag{8.4}$$

where $\lambda_k \equiv \frac{k^2}{2m}$. This is called *the central equation*. Assuming that we solve for all the C's in this equation, the wavefunction will have the form:

$$\psi_k(x) = \sum_G C(k - G) e^{i(k-G)x}, \tag{8.5}$$

which clearly fulfills the Bloch Theorem that any wavefunction in a periodic potential is the product of a plane wave and some periodic function with the potential periodicity.

Let us first consider a wavevector exactly at the zone boundary at $\frac{1}{2}G$, that is at π/a. Then we have:

$$k^2 = \left(\frac{1}{2}G\right)^2 = (k-G)^2. \tag{8.6}$$

Now as an approximation we retain only the coefficients $C(\frac{1}{2}G)$ and $C(-\frac{1}{2}G)$ in the central equation. Now for there to be any non-trivial solutions to the central equation (8.4) the energy must fulfill:

$$\epsilon_\pm = \lambda \pm U. \tag{8.7}$$

Now we assume a k which is only close to the boundary $\frac{1}{2}G$. With the same two-component approximation the wavefunction has the form:

$$\psi(x) = C(k)e^{ikx} + C(k-G)e^{i(k-G)x} \tag{8.8}$$

The central equation then has a solution if the energy satisfies:

$$\det\begin{pmatrix} \lambda_k - \epsilon & U \\ U & \lambda_{k-G} - \epsilon \end{pmatrix} = 0 \Leftrightarrow \tag{8.9}$$

$$\epsilon = \frac{1}{2}(\lambda_{k-G} + \lambda_k) \pm \sqrt{\frac{1}{4}(\lambda_{k-G} + \lambda_k)^2 + U^2}\,. \tag{8.10}$$

The two energy solutions describe two different energy bands. Now approximating the k as being sufficiently close to the zone boundary that we can Taylor expand the square root to first order, we get:

$$\epsilon_{\tilde{k}} \approx \epsilon_\pm + \frac{\tilde{k}^2}{2m}(1 \pm \frac{2\lambda}{U}), \tag{8.11}$$

where $\tilde{k} \equiv k - \frac{1}{2}G$, and $\lambda \equiv \frac{(1/2G)^2}{2m}$, i.e. the bandwidth. Here we see that a clear energy gap has emerged, and that the subsequent band bending leads to something which can be modeled as an effective mass:

$$m^*/m = \frac{1}{\frac{2\lambda}{U} \pm 1}. \tag{8.12}$$

Now in this model the effective mass depends on the energy gap and the bandwidth λ. This makes sense since the bandwidth determines the overall curvature of the band, while the band gap of course modifies how much the curvature changes close to the zone boundary.

8.2 Appendix B

Here we show some of the work on the way to test to which extent the first order perturbation result holds, i.e. for what range of B-field strengths can we still postulate that the slope of the energy with respect to the magnetic field depends on where the wavefunction lives *without a magnetic field applied*? In order to test this we will need to explicitly calculate an analytical expression for the following two quantities:

$$a_n \equiv \int_0^d |\psi_n(z,B)|^2 \,\mathrm{dz}; \qquad a_s \equiv \int_{-\infty}^0 |\psi_s(z,B)|^2 \,\mathrm{dz}. \tag{8.13}$$

We thus hypothesize the following formula for calculating the effective g-factor based on the Feynman-Hellmann theorem:

$$g^* = \frac{a_n}{a_n + a_s} g_n + \frac{a_s}{a_s + a_n} g_s. \tag{8.14}$$

So now we actually need to solve the coupled equations from (3.32) for the coefficients of the wavefunction. Simplifying the wavefunction down to only 4 unknown coefficients using the boundary condition:

$$\psi(d) = 0, \tag{8.15}$$

and seeing that we can rewrite the coefficients in equation (8.14) in terms of the ratio of a_n and a_s only:

$$\frac{a_n}{a_n + a_s} = \frac{a_n}{a_s} \frac{1}{1 + \frac{a_n}{a_s}} = \frac{1}{\frac{a_s}{a_n} + 1}, \tag{8.16}$$

we can actually reduce our task of only finding three coefficients, since the ratio a_n/a_s is independent of the normalization of the wavefunction. Since we have four equations with three unknowns, the last 'leftover' equation would then yield a constraint on the allowed energies.

So first of all we invoke the hard-wall boundary condition at $z = 0$. This yields:

$$A_+ e^{ik_z d} - A_- e^{-ik_z d} = 0 \Leftrightarrow \tag{8.17}$$

$$A_- = A_+ e^{2ik_z d}; \qquad H_- = H_+ e^{2ik_h d} \Rightarrow$$

$$\psi_k = e^{ik_{||} r_{||}} \left[A_+ e^{ik_z z} \begin{pmatrix} 1 \\ 0 \end{pmatrix} A_- e^{-ik_z z} \begin{pmatrix} 1 \\ 0 \end{pmatrix} + H_+ e^{ik_h z} \begin{pmatrix} 0 \\ 1 \end{pmatrix} + H_- e^{-ik_h z} \begin{pmatrix} 0 \\ 1 \end{pmatrix} \right] = \tag{8.18}$$

$$e^{ik_{||} r_{||}} \left[A_+ \begin{pmatrix} 1 \\ 0 \end{pmatrix} \left(e^{ik_z z} + e^{-ik_z (z-2d)} \right) + H_+ \begin{pmatrix} 0 \\ 1 \end{pmatrix} \left(e^{ik_h z} + e^{-ik_h (z-2d)} \right) \right] = \tag{8.19}$$

$$e^{ik_{||} r_{||}} \left[A_+ e^{ik_z d} \begin{pmatrix} 1 \\ 0 \end{pmatrix} \left(e^{ik_z (z-d)} + e^{-ik_z (z-d)} \right) + H_+ e^{ik_h d} \begin{pmatrix} 0 \\ 1 \end{pmatrix} \left(e^{ik_h (z-d) + e^{-ik_h (z-d)}} \right) \begin{pmatrix} 0 \\ 1 \end{pmatrix} \right] \equiv \tag{8.20}$$

$$e^{ik_{||} r_{||}} \left[A \begin{pmatrix} 1 \\ 0 \end{pmatrix} \sin(k_z (z-d)) + H \begin{pmatrix} 0 \\ 1 \end{pmatrix} \sin(k_h (z-d)) \right]. \tag{8.21}$$

Writing up the boundary conditions for these new wavefunctions yields:

$$-A \sin(k_z d) \begin{pmatrix} 1 \\ 0 \end{pmatrix} - H \sin(k_h d) \begin{pmatrix} 0 \\ 1 \end{pmatrix} = B_+ \begin{pmatrix} u \\ v \end{pmatrix} - B_- \begin{pmatrix} v \\ u \end{pmatrix}. \tag{8.22}$$

$$\frac{A k_z \cos(k_z d)}{2m_n} \begin{pmatrix} 1 \\ 0 \end{pmatrix} + \frac{H k_h \cos(k_h d)}{2m_n} \begin{pmatrix} 0 \\ 1 \end{pmatrix} - \frac{1}{2m_s} \left[(\kappa + i p_z) B_+ \begin{pmatrix} u \\ v \end{pmatrix} - (\kappa - i p_z) B_- \begin{pmatrix} v \\ u \end{pmatrix} \right] = U a \left[B_+ \begin{pmatrix} u \\ v \end{pmatrix} - B_- \begin{pmatrix} v \\ u \end{pmatrix} \right]. \tag{8.23}$$

Now we need to solve the coupled equations for the coefficients of the wavefunction. It is here that we can eliminate one of the coefficients by *not* demanding overall normalization of the total wavefunction, since this will not affect the ratio that we are interested in. Thus we find:

$$\frac{B_+}{A} = -i\frac{k_z m_s \cos(dk_z) + m_n(\kappa - ip + 2m_s U_a)\sin(dk_z)}{2m_n p u}; \tag{8.24}$$

$$\frac{B_-}{A} = -i\frac{k_z m_s \cos(dk_z) + m_n(\kappa + ip + 2m_s U_a)\sin(dk_z)}{2m_n p v}; \tag{8.25}$$

$$\frac{H}{A} = \frac{\frac{\sin(dk_z)}{\sin(dk_h)} - \frac{i(u^2-v^2)(k_z m_s \cos(dk_z)+m_n(\kappa+2m_s U_a)\sin(dk_z))}{\sin(dk_h)pm_n}}{2uv}. \tag{8.26}$$

From now on we will not mention that our coefficients are renormalized by A, but simply let $A \to 1$, since this will easen the notational burden.
Let us now move on to determining the coefficients a_n and a_s:

$$a_n \equiv \int_0^d \bar{\psi}_{2DEG} \cdot \bar{\psi}^*_{2DEG}\, \mathrm{dz} = \int_0^d \sin^2(k_z(z-d))\, \mathrm{dz} + \int_0^d |H|^2 \sin^2(k_h(z-d))\, \mathrm{dz} \tag{8.27}$$

$$= \frac{2dk_z - \sin(2dk_z)}{4k_z} + |H|^2 \frac{2dk_h - \sin(2dk_h)}{4k_h}.$$

For the second one it will be helpful to define:

$$\tilde{B_+} \equiv uB_+; \quad \tilde{B_-} \equiv vB_-; \quad \tilde{B}^*_+ = -\tilde{B}_-. \tag{8.28}$$

Before we calculate the integral in the superconductor it is time to try and simplify a bit. To do this we must remember the following:

$$u^2 \equiv \frac{1}{2}(1+\frac{\xi_p}{E_p}); \quad v^2 \equiv \frac{1}{2}(1-\frac{\xi_p}{E_p}); \quad uv = \frac{1}{4}\left(1+|\frac{\xi_p}{E_p}|\right) = \frac{1}{4}\left(1+|\frac{\sqrt{\Delta^2 - E_p^2}}{E_p}|\right) = \frac{1}{2}\frac{\Delta}{|E_p|}. \tag{8.29}$$

where $\xi_p^2 = \tilde{E}_p^2 - \Delta^2$. Since we are looking at subgap states $|\tilde{E}_p| < \Delta$, clearly ξ_p is imaginary, which means that:

$$u^2 = (v^2)^* = (v^*)^2 \Leftrightarrow u = \pm v^*. \tag{8.30}$$

This leads us to an interesting observation:

$$B^*_+ = +i\frac{k_z m_s \cos(dk_z) + m_n(\kappa + ip_z + 2m_s U_a)\sin(dk_z)}{2m_n p u^*} \tag{8.31}$$

$$= \mp i\frac{k_z m_s \cos(dk_z) + m_n(\kappa + ip_z + 2m_s U_a)\sin(dk_z)}{2m_n p v} \equiv \mp B_- \Rightarrow \tag{8.32}$$

$$|B_+|^2 = |B_-|^2; \quad B_+B^*_- = -B^2_+; \quad B_-B^*_+ = -B^2_- \tag{8.33}$$

Another thing that will be helpful is that from the definitions of u^2 and v^2, we can say that $u = \pm v^*$, with an unkown sign, but though with a definite sign. This allows us for example to rewrite:

$$1 + \frac{u^* v}{u v^*} = \frac{1}{u^2}. \tag{8.34}$$

Using exactly this we see that:

$$a_s \equiv \int_{-\infty}^{0} \bar{\psi}_s \cdot \bar{\psi}_s^* \, \mathrm{dz} = \int_{-\infty}^{0} e^{2\kappa z} \left[(|B_+|^2 + |B_-|^2)(|u|^2 + |v|^2) - \left(\frac{\tilde{B_+^*} \tilde{B_-} e^{2ipz}}{u^2} + c.c. \right) \right] \tag{8.35}$$

$$= \frac{1}{2\kappa}(|B_+|^2 + |B_-|^2)(|u|^2 + |v|^2) - \frac{1}{2(\kappa^2 + p^2)} \left\{ \frac{\tilde{B}_+ \tilde{B}_-^* (\kappa - ip)}{u^2} + c.c. \right\}.$$

Thus the ratio becomes:

$$\frac{a_n}{a_s} = \frac{\frac{2dk_z - \sin(2dk_z)}{4k_z} + |H|^2 \frac{2dk_h - \sin(2dk_h)}{4k_h}}{\frac{1}{2\kappa}(|B_+|^2 + |B_-|^2)(|u|^2 + |v|^2) - \frac{1}{2(\kappa^2 + p^2)} \left\{ \frac{\tilde{B_+} \tilde{B_-}^* (\kappa - ip)}{u^2} + c.c. \right\}}. \tag{8.36}$$

Bibliography

[1] A. W. Harrow, A. Hassidim, and S. Lloyd. "Quantum Algorithm for Linear Systems of Equations". In: *Phys. Rev. Lett.* 103 (15 2009), p. 150502. URL: http://link.aps.org/doi/10.1103/PhysRevLett.103.150502.

[2] M. Leijnse and K. Flensberg. "Introduction to topological superconductivity and Majorana fermions". In: *arXiv:1206.1736v2* (2012).

[3] V. Mourik et al. "Signatures of Majorana Fermions in Hybrid Superconductor-Semiconductor Nanowire Devices". In: *Science* 336.6084 (2012), pp. 1003–1007. ISSN: 0036-8075. eprint: http://science.sciencemag.org/content/336/6084/1003.full.pdf. URL: http://science.sciencemag.org/content/336/6084/1003.

[4] S. M. Albrecht et al. "Exponential protection of zero modes in Majorana islands". In: *Nature* 531.7593 (Mar. 2016), pp. 206–209.

[5] *Microsoft Spends Big to Build a Computer Out of Science Fiction*. New York Times. URL: http://www.nytimes.com/2016/11/21/technology/microsoft-spends-big-to-build-quantum-computer.html?_r=0.

[6] T. Karzig et al. "Scalable Designs for Quasiparticle-Poisoning-Protected Topological Quantum Computation with Majorana Zero Modes". In: *arXiv:1610.05289* (2016).

[7] F. Pientka et al. "Topological Superconductivity in a Planar Josephson Junction". In: *arXiv:1609.09482* (2016).

[8] M. Hell, M. Leijnse, and K. Flensberg. "Two-dimensional platform for networks of Majorana bound states". In: *arXiv:1608.08769* (2016).

[9] J. J. Sakurai and J. J. Napolitano. *Modern Quantum Mechanics*. 2nd ed. Pearson New International Edition, 2014.

[10] R. Winkler. *Spin-Orbit Coupling Effects in Two-Dimensional Electron and Hole Systems*. Springer-Verlag Berlin Heidelberg, 2003.

[11] J. D. Jackson. *Classical Electrodynamics*. 3rd ed. John Wiley & Sons, 1999.

[12] L. Petersen and P. Hedegård. "A simple tight-binding model of spin–orbit splitting of sp-derived surface states". In: *Surface Science* 459.1–2 (2000), pp. 49 –56. ISSN: 0039-6028. URL: http://www.sciencedirect.com/science/article/pii/S0039602800004416.

[13] H. Bruus and K. Flensberg. *Many-Body Quantum Theory in Condensed Matter Physics*. Oxford University Press, 2004.

[14] P. G. Gennes. *Superconductivity of Metals and Alloys*. Westview Press, 1966.

[15] A. Y. Kitaev. "Unpaired Majorana fermions in quantum wires". In: *Physics-Uspekhi* 44.10S (2001), p. 131. URL: http://stacks.iop.org/1063-7869/44/i=10S/a=S29.

[16] S. Tewari and J. D. Sau. "Topological Invariants for Spin-Orbit Coupled Superconductor Nanowires". In: *Phys. Rev. Lett.* 109 (15 2012), p. 150408. URL: http://link.aps.org/doi/10.1103/PhysRevLett.109.150408.

[17] J. D. Sau et al. "Generic New Platform for Topological Quantum Computation Using Semiconductor Heterostructures". In: *Phys. Rev. Lett.* 104 (4 2010), p. 040502. URL: http://link.aps.org/doi/10.1103/PhysRevLett.104.040502.

[18] Y. Oreg, G. Refael, and F. von Oppen. "Helical Liquids and Majorana Bound States in Quantum Wires". In: *Phys. Rev. Lett.* 105 (17 2010), p. 177002. URL: http://link.aps.org/doi/10.1103/PhysRevLett.105.177002.

[19] M. Kjaergaard. *Proximity Induced Superconducting Properties in One and Two Dimensional Semiconductors. Towards Topological States of Matter*. PhD at Center for Quantum Devices at University of Copenhagen., 2015.

[20] B. J. van Wees et al. "Quantized conductance of point contacts in a two-dimensional electron gas". In: *Phys. Rev. Lett.* 60 (9 1988), pp. 848–850. URL: http://link.aps.org/doi/10.1103/PhysRevLett.60.848.

[21] D. A. Wharam et al. "One-dimensional transport and the quantisation of the ballistic resistance". In: *Journal of Physics C: Solid State Physics* 21.8 (1988), p. L209.

[22] A. Volkov et al. "Proximity and Josephson effects in superconductor-two-dimensional electron gas planar junctions". In: *Physica C: Superconductivity* 242.3 (1995), pp. 261 –266.

[23] D. J. Griffiths. *Introduction to Quantum Mechanics*. 2nd ed. Pearson Education International, 2005.

[24] C. Kittel. *Introduction to Solid State Physics*. 8th ed. John Wiley & Sons, Inc., 2005.

[25] T. D. Stanescu, R. M. Lutchyn, and S. Das Sarma. "Majorana fermions in semiconductor nanowires". In: *Phys. Rev. B* 84 (14 2011), p. 144522. URL: http://link.aps.org/doi/10.1103/PhysRevB.84.144522.

[26] T. Schäpers. *Superconductor/Semiconductor Junctions*. Springer-Verlag Berlin Heidelberg, 2001.